| | |
|---|---|
| **Titre:** Title: | On the Coordination of Electric Water Heater Loads for Frequency Support and Load Following in Power Systems |
| **Auteur:** Author: | Amirali Delavaran Shiraz |
| **Date:** | 2024 |
| **Type:** | Mémoire ou thèse / Dissertation or Thesis |
| **Référence:** Citation: | Delavaran Shiraz, A. (2024). On the Coordination of Electric Water Heater Loads for Frequency Support and Load Following in Power Systems [Mémoire de maîtrise, Polytechnique Montréal]. PolyPublie. https://publications.polymtl.ca/59284/ |

**POLYTECHNIQUE MONTRÉAL**
affiliée à l'Université de Montréal

# On the Coordination of Electric Water Heater Loads for Frequency Support and Load Following in Power Systems

**AMIRALI DELAVARAN SHIRAZ**
Département de génie électrique

Mémoire présenté en vue de l'obtention du diplôme de *Maîtrise ès sciences appliquées*
Génie électrique

Août 2024

**POLYTECHNIQUE MONTRÉAL**
affiliée à l'Université de Montréal

Ce mémoire intitulé :

**On the Coordination of Electric Water Heater Loads for Frequency Support and Load Following in Power Systems**

présenté par **Amirali DELAVARAN SHIRAZ**
en vue de l'obtention du diplôme de *Maîtrise ès sciences appliquées*
a été dûment accepté par le jury d'examen constitué de :

**Jean MAHSEREDJIAN**, président
**Roland MALHAMÉ**, membre et directeur de recherche
**François BOUFFARD**, membre

# ACKNOWLEDGEMENTS

I would like to express my deepest gratitude to my thesis advisor, Prof. Roland Malhamé, whose guidance, expertise, and unwavering support were instrumental throughout the entire research process. His invaluable insights and constructive feedback have greatly enriched the quality of this thesis.

I am also grateful to Polytechnique Montréal for providing the essential resources and facilities that enabled the completion of this research work. Additionally, I would like to extend my heartfelt gratitude to Professors Mahseredjian and Bouffard for graciously accepting to be members of my thesis jury.

Furthermore, I extend my heartfelt appreciation to all the participants and contributors involved in this study. Their cooperation and willingness to share their expertise were indispensable in achieving the objectives of this thesis.

I would also like to thank my family for their encouragement, understanding and patience throughout this journey. Their love and support provided the motivation needed to overcome challenges and persevere until the completion of this thesis.

Lastly, I acknowledge the countless researchers, scholars, and pioneers whose work served as a foundation for this study. Their contributions have paved the way for advancements and innovations, inspiring future generations of researchers.

# RÉSUMÉ

Au cours des dernières années, les impacts environnementaux croissants des centrales à base d'énergies fossiles de production d'énergie, ainsi que les préoccupations concernant leur durabilité, ont conduit à l'exploration de solutions alternatives pour répondre à la demande croissante en électricité. Plutôt que de recourir à l'approche conventionnelle d'expansion des infrastructures existantes de production et de transmission d'énergie, il est devenu impératif de rechercher des stratégies innovantes capables de gérer efficacement la demande de pointe sans surcharger le réseau.

En effet, l'intégration des sources d'énergie renouvelable pricipalement de types solaire et éolien dans le réseau électrique nécessite une réévaluation des opérations traditionnelles du réseau et des mécanismes de contrôle. La nature intermittente ainsi que leur caractère décentralisé de ces sources présentent de nouveaux défis pour maintenir la stabilité du réseau et garantir un approvisionnement électrique fiable. Alors que le réseau évolue pour accueillir une part plus importante d'énergies renouvelables, des solutions innovantes et des stratégies adaptatives seront essentielles pour relever ces défis techniques et assurer la résilience du système électrique.

Les techniques de gestion de charge ont émergé comme une approche prometteuse dans cette entreprise, offrant un moyen efficace d'influencer l'utilisation de l'électricité par les consommateurs et de façonner le profil de charge. En ajustant stratégiquement les schémas de consommation d'électricité, les initiatives de gestion de charge visent à réduire la pression sur le système électrique pendant les périodes de demande de pointe et à stabiliser sa fréquence, augmentant ainsi la fiabilité du réseau.

Dans le but d'assurer la stabilité et la fiabilité du réseau, cette thèse explore l'utilisation efficace d'un modèle complet pour les chauffe-eau électriques regroupés équipés de configurations de contrôle de tension individuelles en tant que mécanisme de Demand Response (DR), inspiré par les algorithmes de contrôle de fréquence utilisés dans les systèmes électriques conventionnels. Nous avons acquis une compréhension approfondie de la relation dynamique entre les chauffe-eau électriques et le réseau en développant des équations aux dérivées partielles de Kolmogorov représentant la dynamique agrégée des chauffe-eau électriques contrôlés. Cette approche démontre la fraction de dispositifs actifs pouvant contribuer efficacement aux efforts de contrôle, permettant ainsi une surveillance précise de l'étendue de la contrôlabilité disponible à tout moment. Divers scénarios ont été examinés pour évaluer l'efficacité des chauffe-eau électriques dans l'atténuation des fluctuations de fréquence, ainsi

que la réponse aux pertes subites de génération, avec des comparaisons de performances réalisées par rapport aux approches conventionnelles, s'appuyant généralement uniquement sur la Frequency Regulation (PFR).

**Mots-clés:** Stabilité de fréquence, Réponse à la Demande, Chauffe-eau électriques, Contrôle de tension, Équations de Kolmogorov, Équations aux Dérivées Partielles, Régulation Primaire de Fréquence

# ABSTRACT

In recent years, the growing environmental impacts of traditional power generation plants and concerns about their sustainability have grown, which have led to the exploration of alternative solutions to meet the growing electricity demand. Rather than resorting to the conventional approach of expanding existing power generation and transmission infrastructure, it has become imperative to seek innovative strategies that can effectively manage peak demand without stressing the grid.

Indeed, the integration of renewable energy sources into the power grid necessitates a reevaluation of traditional grid operations and control mechanisms. The intermittent nature as well as the decentralized character of these sources present new challenges for maintaining network stability and ensuring reliable electrical supply. As the grid evolves to accommodate a higher share of renewables, innovative solutions and adaptive strategies will be essential to address these technical hurdles and uphold the resilience of the power system.

Load management techniques have emerged as a promising approach in this endeavor, offering an effective means to influence consumer electricity usage and shape the load profile. By strategically adjusting electricity consumption patterns, load management initiatives aim to reduce pressure on the electrical system during peak demand periods and stabilize its frequency, thereby increasing network reliability.

With the aim of ensuring grid stability and reliability, this thesis explores the effective use of a comprehensive model for grouped Electric Water Heaters (EWH) equipped with individualized droop control setups as a Demand Response (DR) mechanism, inspired by frequency control algorithms used in conventional power systems. We have gained a deep understanding of the dynamic relationship between electric water heaters and the grid by developing Kolmogorov partial differential equations representing the aggregated dynamics of controlled electric water heaters. This approach demonstrates the fraction of active devices that can effectively contribute to control efforts, thus enabling precise monitoring of the extent of controllability available at any given time. Various scenarios were examined to evaluate the efficacy of EWH in mitigating frequency fluctuations, with performance comparisons made against conventional approaches, typically relying solely on Primary Frequency Regulation (PFR).

**Keywords:** Frequency stability, Demand Response, Electric Water Heaters, Droop control, Kolmogorov equations, Partial Differential Equations, Primary Frequency Regulation

# TABLE OF CONTENTS

# LIST OF TABLES

# LIST OF FIGURES

# LIST OF SYMBOLS AND ABBREVIATIONS

| | |
|---|---|
| DR | Demand Response |
| EWH | Electric Water Heater |
| FFT | Fast Fourier Transform |
| HWC | Hot Water Consumption |
| LFC | Load-Frequency Control |
| NERC | North American Electric Reliability Corporation |
| PDE | Partial Differential Equations |
| PDF | Probability Density Functions |
| PFR | Primary Frequency Regulation |
| PSD | Power Spectral Density |
| SFR | Secondary Frequency Regulation |
| TCL | Thermostatically Controlled Loads |
| TFR | Tertiary Frequency Regulation |

# CHAPTER 1 INTRODUCTION

In recent years, the environmental impact of traditional power generation plants has become a growing concern, prompting the search for alternative solutions to meet the rising demand for electricity. Instead of expanding existing power generation and transmission systems, it is crucial to explore innovative approaches that can effectively address peak demand without overloading the grid. Load management techniques have emerged as a viable strategy to influence consumer electricity usage and shape the load profile, ultimately reducing the strain on the power system.

Electric Water Heaters (EWH) present an intriguing opportunity both as a Demand Response (DR) tool, and in support of ancillary services. This is due to their inherent thermal inertia, which can shield customers from the effects of fluctuating heating inputs typically required for frequency regulation. Furthermore, as EWHs utilize resistance heating elements as their energy source, voltage modulation can be achieved without encountering the compressor-related challenges faced by loads, such as air conditioners or refrigerators. The primary objective is to leverage EWHs both for frequency support under normal circumstances and as a rapid and temporary support line during situations such as dips in renewable energy due to solar or wind source intermittency, sudden significant increases in load, or unexpected losses of generation.

The main contribution of the thesis is a modeling methodology for large aggregates of EWHs whose individual power consumption is controlled via a frequency-driven droop control mechanism. The obtained model becomes the basis of a numerical exploration of the potential of EWHs when used for frequency support and temporary load following. In order to derive the model, we proceed in three steps. Firstly, we define the droop control mechanism for individual EWHs. Secondly, we incorporate the stochastic behaviour of hot water demand into the individual model. Thirdly, we consider a large group of synchronized EWHs regulated by a droop controller. Mathematical equations representing each EWH are developed, alongside the design of appropriate feedback mechanisms for the droop controller. This ensures that minor fluctuations in demand are managed effectively by distributing the load among the EWHs proportionally according to their capabilities. Subsequently, Kolmogorov equations are employed to predict the aggregated dynamic behavior of the EWHs over time. Leveraging Partial Differential Equations (PDE) derived from preceding stages, the dynamics of Thermostatically Controlled Loads (TCL) are determined, along with associated boundary conditions.

In effect, the master's thesis explores a decentralized control mechanism inspired by frequency support algorithms commonly used in conventional power systems, instead of commonly used centralized control mechanisms [4], [5], [6]. An important component of the thesis relates to the utilization of a large aggregate of EWHs to control power system modulation, frequency support and energy storage within power systems. Expanding upon the concept of droop control, this decentralized proportional control strategy traditionally utilized to regulate generators as the primary line of defense against frequency fluctuations in power systems, the thesis aims to adapt it for application to EWHs. By leveraging the thermal characteristics of EWHs, this adapted droop control mechanism seeks to achieve frequency regulation without compromising customer comfort, while also serving as a means to reserve extra energy during times of increased demand.

The research is divided into several chapters, each addressing different key aspects. Chapter 2 provides a thorough relevant literature review. This chapter lays the groundwork for our study, exploring the stability of power systems, frequency control principles, and the potential of demand side resources like EWHs to improve grid stability. Through this review, we aim to understand the challenges and opportunities of using EWHs to enhance power system performance.

In chapter 3, we delve into the concept of droop control, a fundamental principle in power system dynamics, examining its classical framework and constructing a simplified area model. Inspired by Kundur's analysis of power system [7], we explore the potential integration of EWHs into droop control strategies, aiming to establish them as effective DR mechanisms. Our focus lies in developing a comprehensive model for grouped EWHs with individualized droop control, contributing to the optimization of power system stability and performance.

Chapter 4 mainly discusses the stochastic modeling of the EWHs, under an assumption of uniform water temperature distribution within the tank. This assumption allows us to analyze water temperature dynamics and corresponding power requirements over time. Our aim is to understand the intricate heat transfer dynamics within EWHs and uncover their behavior and energy consumption patterns, providing valuable insights for energy management and conservation efforts. By utilizing the Kolmogorov PDEs characterization of the controlled aggregate, it becomes possible to determine the fraction of EWHs in the ON state at any given moment. This information is crucial for effective load modulation, as only the active EWHs can contribute to the control effort. Additionally, minimum heating rate limits for each EWH must be maintained to guarantee customer comfort.

Once an aggregate PDE-based simulator is established, Chapter 5 explores the impact of introducing droop control for EWHs in a primary frequency regulation mode within a power

system. The research investigates two scenarios: dealing with generation dips or load increases in the presence of conventional primary frequency control, and addressing issue of rapid compensation of frequency fluctuations. In particular, examining the behavior of water temperature probability densities and the oscillations in the number of ON devices, the thesis aims at assessing the effectiveness of EWHs under a new droop control scheme in mitigating frequency fluctuations. A potential solution to "cold load peak" phenomenon is also presented. It involves temporarily adjusting the temperature set point of the devices. The main idea of this solution is to investigate the effects of allowing the EWHs' water temperatures to fall all the way to a lower than normal temperature setpoint upon which the thermostat turns back ON.

# CHAPTER 2 Background and Literature Review

## 2.1 Power Systems Dynamics

Electric power systems usually need to address two main goals: to minimize costs and ecological impact while simultaneously ensuring high levels of reliability and service quality. To achieve this, power generation during the operation of these systems must continuously balance supply with demand while also maintaining frequency and voltage within the required technical limits, which is essential for the proper functioning of electrical devices.

Given that the majority of power generation currently relies on synchronous generators, it is crucial for these machines to maintain frequency synchronization. However, in the aftermath of significant system disruptions, these generators can lose synchronization and become "out of step," a circumstance that can result in power generation interruptions, the cascading shutdown of systems, and ultimately, widespread blackouts [7].

As previously noted, the matter of system stability has consistently held a prominent position in discussions. This concern can be segmented into various categories and subcategories, such as voltage stability and frequency stability. This research predominantly focuses on tackling the issues associated with frequency stability. Frequency stability, in essence, refers to the methods employed to maintain a consistent frequency when confronted with varying scenarios of mismatch between supply and demand.

### 2.1.1 Swing Equation

Synchronous machine controls play an essential role in maintaining frequency stability [7]. Consequently, it is very important to investigate the mechanisms through which synchronous machines achieve this stabilization, given that the same phenomena are addressed in this thesis.

In the context of the turbine-generator complex as implemented in this thesis, two opposing forces come into play: the mechanical torque $T_m$ and the electromagnetic torque $T_e$. When these two torques are not in perfect equilibrium, a net torque emerges, which can result in either acceleration or deceleration. To determine this net torque we can write [7]:

$$\Delta T = T_m - T_e \tag{2.1}$$

where

$\Delta T$: is the accelerating or decelerating torque in the turbine.

$T_m$: is the mechanical torque.

$T_e$: is the electromagnetic torque.

Now, based on Newton's second law of motion for rotational systems, we have:

$$J\frac{d(\Delta\omega)}{dt} = \Delta T$$

where:

$J$: is the combined moment of inertia of the generator and turbine, in $\text{kg} \cdot \text{m}^2$.

$\Delta\omega$: is the deviation of the rotor's angular velocity from the nominal angular velocity $\omega_0$. This can be written as:

$$\Delta\omega = \omega - \omega_0$$

where $\omega_0$ is the nominal angular velocity corresponding to the system's nominal frequency (50 Hz or 60 Hz).

$t$: is time, in seconds (s).

Now, following a disturbance $\Delta\omega$, which will lead to a corresponding $\Delta T$, we can analyze the effect of inertia on stabilizing the speed disturbance $\Delta\omega$. We can write:

$$J\frac{d(\Delta\omega)}{dt} = \Delta T \tag{2.2}$$

Letting $M = J$, we have:

$$\begin{aligned} &M\frac{d(\Delta\omega)}{dt} = \Delta T_m - \Delta T_e = \Delta P_m - \Delta P_e \rightarrow \\ &\frac{d(\Delta\omega)}{dt} = \frac{\Delta P_m - \Delta P_e}{M} \end{aligned} \tag{2.3}$$

where

$\Delta\omega$: is the deviation of the rotor's angular velocity from the nominal angular velocity $\omega_0$.

$P_m$: is the mechanical power.

$P_e$: is the electrical power.

$\Delta T_m$: is the deviation in mechanical torque.

$\Delta T_e$: is the deviation in electrical (electromagnetic) torque.

By emphasizing power rather than torque, a more relevant factor in the context of electrical systems analysis is considered. This is important for a comprehensive understanding of power systems. Equation (2.3), commonly known as the Swing Equation, serves as a fundamental expression within this field. Variations in mechanical power and electrical power required by generators impact the rotor's speed, which is directly related to grid frequency.

When abrupt changes in the system's active power demands occur, there is a delay before the mechanical power from prime movers can compensate for these shifts. For instance, if generators suddenly serve a higher load, the rotation speed of synchronous machines decreases. Considering that system frequency $f$ is directly linked to the rotation speed of these machines $\omega$, any reduction in machine speed results in a corresponding drop in system frequency. This behaviour is crucial to understanding system stability in electrical networks.

## 2.2 Frequency Control

Understanding a transmission network's stability requires distinguishing between the effects of various control actions on its active and reactive power. To maintain frequency stability, it may be advisable to set aside the impact of excitation controls, including reactive power controls, and concentrate solely on deviations in active power as there exist reasonable decoupling between active and reactive control loops [7]. In order to secure the operation of the electrical system, its frequency must remain within strict limits, typically within 0.01% deviation from its nominal value [8]. Since generation and consumption are deeply interconnected, it is vital to maintain a balance between them. The *Load-Frequency Control (LFC)* accomplishes these goals [5]. This control mechanism is traditionally provided by synchronous units in conventional power plants mostly in Europe, and it involves the following types of control:

| | |
|---|---|
| `Primary Frequency Regulation (PFR):` | It stabilizes the system frequency following a disturbance. Whenever frequency deviations exceed 20 mHz, the primary control is activated and carried out locally through proportional control loops (prime movers governing systems). The frequency containment reserve (FCR) is assigned to this kind of control [9]. |
| `Secondary Frequency Regulation (SFR):` | The objective of SFC is to maintain generation-consumption balance within each control area, as well as to maintain power flows interchanges between control areas at their scheduled levels. Following a disturbance, secondary control restores frequency to its nominal value. TSOs modify the active power set points through Automatic Generation Control (AGC) which is a form of integral control [9]. |
| `Tertiary Frequency Control`: | Tertiary is an automatic control action, activated manually by the Transmission System Operator (TSO) and is used to support the control area's secondary control. During a balanced system situation, the second reserve replaces the last, so there is a secondary reserve available when the next disturbance occurs [9]. Both control actions are allocated reserves known as Frequency Restoration Reserve (mFRR) and Replacement Reserve (RR). Additionally, it aims to modify operating points of synchronous generators to achieve the same output with better efficiency and less environmental damage. |

In North America, the approach to frequency control is governed by standards and guidelines set forth by the North American Electric Reliability Corporation (NERC). While the general principles of frequency control, such as the PFR, are similar to those in European systems, there are key differences in the implementation and structure of frequency regulation and contingency reserves.

After the immediate stabilization provided by PFR, North American systems use Automatic Generation Control (AGC) to fine-tune the frequency and return it to its nominal value of 60 Hz. This process is similar to the secondary frequency control in Europe but has notable differences in how it is executed.

- **AGC Functionality:** AGC in North America continuously monitors frequency deviations and issues control signals to selected generators to adjust their output. Unlike in European systems, where centralized control often dominates, North American AGC is more distributed, with greater emphasis on balancing authorities maintaining control

within their regions while coordinating across larger interconnections.

- **Regulation Reserves:** In North America, regulation reserves are specifically designated for AGC to correct small, continuous fluctuations in frequency. These reserves must be responsive and capable of adjusting output quickly to match the continuous load and generation balance changes. The structure of regulation reserves tends to be more distributed across different balancing authorities compared to the European model.

Contingency reserves in North America are structured similarly to tertiary control reserves in Europe, but the process of activation and the types of reserves differ.

- **Spinning Reserves:** Spinning reserves in North America are provided by online generators that can be dispatched rapidly to cover the loss of generation. The response time and deployment protocols follow NERC standards, which often emphasize quicker response times compared to European systems, particularly in larger interconnections like the Eastern Interconnection.
- **Non-Spinning Reserves:** Non-spinning reserves are brought online within a few minutes to restore balance after a large disturbance. These reserves can include demand response programs and offline generation resources. In North America, there is a growing emphasis on integrating DR into contingency reserves to enhance flexibility.
- **NERC Contingency Standards:** NERC standards require each balancing authority to maintain sufficient contingency reserves to cover its largest single contingency. These reserves must be deployed within 10 minutes, which contrasts with some European systems that may allow longer deployment times depending on the contingency severity.

In this thesis, our focus is solely on the analysis of the impact of PFR, as it represents the initial proportional control mechanism activated in response to imbalances in power demand and supply. Our objective is to leverage residential devices to aid in frequency regulation during the PFR phase. Hence, we only implement this phase on the grid we are about to describe.

### 2.2.1 Primary Frequency Control

As described earlier, governing systems provide frequency response to prime movers. As a result, this section will present some control schemes associated with prime movers and energy supply systems.

The fundamental configuration presented in this study entails a straightforward generator unit accompanied by a non-reheat steam turbine, as detailed in [7]. The graphical representation of the associated generator's layout is illustrated in Fig 2.1, while specific parameters concerning the turbine governor can be found in Table 2.1 [10].

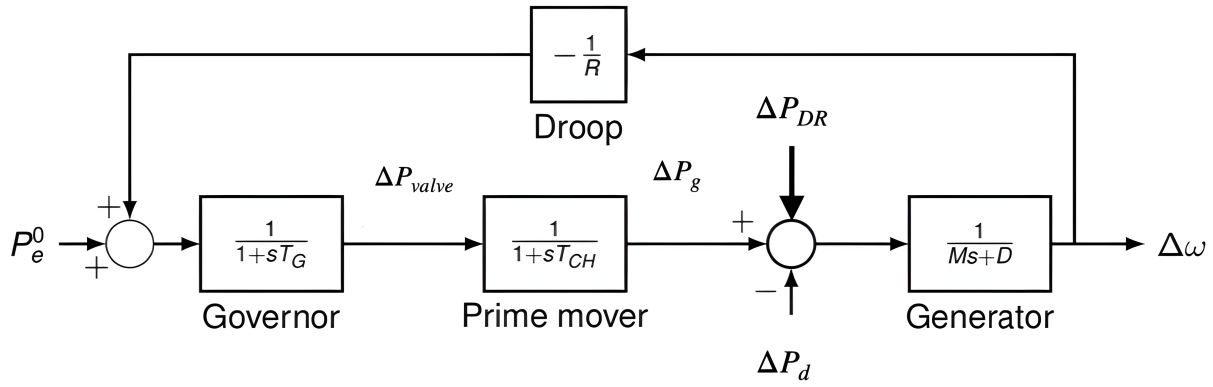


Figure 2.1 Block diagram of a typical reheat steam turbine generator.

| | |
|---|---|
| $\Delta f$: | frequency deviations from its nominal value 60 Hz. |
| $P_0^e$: | load reference. |
| $P_g$: | generated Power. |
| $P_d$: | power demand. |
| $P_{DR}$: | power from Demand Response (to be investigated further down). |
| $T_{ch}$: | steam chest time constant. |
| $T_G$: | governor time constant. |
| $M$: | generator's inertia Constant. |
| $R$: | droop constant. |
| $D$: | load damping factor, which is assumed to be 1 p.u indicating that a 1% change in frequency results in a corresponding 1% change in load. The damping parameter $D$ is chosen based on simulations that optimize the balance between fast frequency recovery and system stability. |

Fig 2.1 shows a transient droop compensation block. Due to the water inertia effect, a change in the gate position initially causes a turbine mechanical power change that is opposite to what was intended. Thus, the turbine reacts to a frequency event in the opposite way from

what it is intended to, as water flow lags gate positioning. Therefore, a transient droop compensator is included in the speed governor for stable control performance. As a result of this block of droop compensation, the governor's gain decreases for oscillatory high-frequency deviations, and increases for steady-state deviations [7].

It is evident from the diagram that this thermal unit functions as a closed-loop system. This system involves a controller that monitors component speed and compares it to a specified reference speed. Any deviation prompts the controller to signal the actuator. This adjusts the steam valve, modifying the speed until it aligns with the predetermined set point [11].

For instance, an increase in system load can lead to a mismatch between the mechanical power generated by the prime mover and the electrical power demanded by the synchronous generator. This mismatch results in a change in shaft speed. Steam valves are manipulated by the controller to align the mechanical energy supplied by the prime mover with the electrical power required.

### 2.2.2 Frequency Control Through Demand Side Resources

In the previous sections, we analyzed PFR, which was influenced by the rotating machines' inertia. As the demand for electricity has increased, a search for alternative solutions such as renewable resources to meet the increasing demand has become more important due to the environmental impact of traditional fossil fuel-based power generation plants.

Smart grid technology and growing renewable energy penetration offer many advantages and challenges when it comes to operating modern power grids in a reliable and economic manner. As renewable energy sources like wind and solar become more popular, carbon emissions, pollutants, and fossil fuel dependency can be reduced; however, such variable resources can increase power system uncertainty, resulting in additional balancing requirements for ancillary services (frequency response, regulation, load following). Several recent studies have found a strong correlation between ancillary service requirements and renewable energy installed capacity [12] [13] and, consequently, integration costs. Increasing renewable energy capacity typically requires additional balancing capability from conventional generators, due to expected errors and hourly variances [14]. Furthermore, when conventional generation is replaced by intermittent renewable sources, the frequency response capability of the power system is reduced, since there are fewer generators online during a forced generator outage.

Within smart grid technologies, DR control emerges as an effective approach to trim peak loads, diminish balancing needs, and deliver emergency assistance. With the right design and execution, DR can potentially offer all these benefits at a lower cost than other options [14].

Table 2.1 Turbine Governor Parameters

| **Parameter** | **Value** |
|---|---|
| $\mathrm{R}(\frac{pu}{pu})$ | 0.05 |
| $T_G(s)$ | 0.2 |
| $T_C(s)$ | 0.3 |
| $2H(s)$ | 10 |
| $D(pu)$ | 1 |

It is crucial to comprehend the characteristics and potential challenges associated with each DR control candidate to fully harness their benefits.

Consequently, frequency control mechanisms provided by demand side resources have been examined increasingly in recent years. Among the most promising candidates to perform such services are TCL devices, such as refrigeration systems, heat pumps, air conditioning systems, and electrical water heaters. The speed of response of these technologies is particularly impressive due to their "duty-cycle" based operation and ease of switching on/off during frequency events [15]. Furthermore, no major discomforts are caused to the end users if the consumption intensity of these loads is temporarily reduced, assuming their power input can be continuously controlled [16]. If the power consumption of numerous TCLs is properly managed, their aggregate response may be made to somewhat mimic the droop characteristic of conventional generation units [17].

In this thesis, the primary emphasis is on evaluating the influence of a particular DR control strategy on EWHs. EWHs are recognized as highly effective devices for integration into DR, boasting numerous advantages, some of which are highlighted in Table 2.2.

Table 2.2 Characteristics of Electric Water Heaters (EWHs)

| **Advantage** | **Description** |
|---|---|
| (1) | In comparison to other household appliances like washing machines, dryers, and refrigerators, EWHs consume relatively high amounts of power. It is estimated that EWHs consume about a third of the energy consumed by households; this contributes to the overall peak load of the household [18] |
| (2) | Since an EWH utilizes heating elements that function as resistors, there is no need for grid reactive support. This is an advantage over other types of TCLs, such as air conditioners which involves compressors, since it makes implementing different control strategies much less complex. |
| (3) | In the provision of balancing services, electric water heaters can serve as energy storage devices by heating water to the appropriate temperature range [14]. In addition to reducing peak loads, this capability makes it easier to trim the system's capacity for regulation. |

Several studies have explored the use of EWHs for load regulation. Notably, Hammerstrom and Kondoh investigated a centralized control model employing 10,000 EWHs to regulate the total power demand over a 24-hour control scheme [19]. Their model featured a conventional water heater with two heating elements, only one of which is active at any given time. Each water heater was equipped with a controller receiving three signals: $c_1$, $c_2$, and $t_{after}$. Here, $c_i$ determined the next on/off condition of the respective thermostat, while $t_{after}$ served as a time-keeping value to prevent frequent on/off cycles. During each time step, a central power system operator estimated both upward and downward reserve capacities for power regulation in the subsequent control time step, involving all controllable EWHs. If adjustments were needed to alter the total power consumption of EWHs, a signal was dispatched to each water heater controller to modify their consumption appropriately.

In another study, Sepulveda proposed a swarm based control scheme for Direct Load Control (DLC) of Distributed Electric Water Heaters (DEWH) [20]. The algorithm aims to optimize load profiles, decrease peak load demand, and enhance overall power system efficiency. It employs a Particle Swarm Optimization (PSO) based centralized controller that adjusts DEWHs' operation for peak shaving, load shifting, and valley filling. A fitness function proposed

((2.4)), evaluating the trade-off between aggregated peak load demand and water heater temperature, emphasizing customer satisfaction by giving higher weight to temperature control. The algorithm operates on a 15-minute evaluation cycle to achieve objectives over a 24-hour period.

$$F = \sum_{i=0}^{N}(|Td_i - Ta_i|.\omega_1 + |Pd - Pa_i|.\omega_2) \tag{2.4}$$

Where

| | |
|---|---|
| $N$: | number of water heaters. |
| $Td_i$: | maximum water temperature setpoint. |
| $Ta_i$: | estimated water temperature. |
| $Pd$: | desired aggregated load. |
| $Pa_i$: | water heater load. |
| $\omega_1$: | temperature weight factor. |
| $\omega_2$: | aggregated load weight factor. |

Pourmousavi and Nehrir, on the other hand, proposed an adaptive hill-climbing algorithm to control the load of aggregate EWHs for PFR [21]. It involves three control modes aiming at keeping frequency within a $\pm 0.05$ Hz. As a result of this control method, the dynamic load percentage can be adjusted immediately in response to frequency deviations, allowing for enhanced transient frequency response.

In another study Ali Haider, Will Stark, Ted. K.A. Brekken from Oregon State University also highlighted the possibility of using residential electric hot water heaters as distributed energy storage resources for frequency regulation in the electrical grid [22].

When grid frequency is high indicating excess generation relative to load, they propose storing energy in the lower element of the water heater while allowing the EWHs to coast during low frequency periods. With this approach, significant energy storage is achieved without compromising hot water availability for users since the temperature variation in the lower part of the tank is leveraged for energy storage.

It was shown in the study that with a simple enhancement, water heaters can regulate frequency by 5% without affecting the temperature of the water withdrawn by users.

This modification involves replacing the lower thermostat with an embedded controller and power converter at a low cost, enabling a greater variation in the temperature of the lower tank while maintaining a constant temperature in the upper tank. Electric water heaters are

controlled by proportional loops combined with upper and lower tank relays.

According to estimates, there are at least 500 MW/Hz of potential frequency regulation resource in the Pacific Northwest of the United States, with millions of electric hot water heaters.

An alternative droop-based control algorithm is discussed in a study by Jae Woong Shim, Gregor Verbi, Heejin Kim, and Kyeon Hur [23]. It involves multiple distributed Battery Energy Storage Systems (ESS) with state of charge (SOC) feedback to regulate grid frequency.

By integrating multiple ESS into the load frequency control, the proposed method enhances the functional roles of the existing generators.

As part of the study, the mathematical links between ESS, SOC, and power dynamics are elaborated, and the control performance for a group of ESS is evaluated using metrics such as the cutoff frequency, settling time, and the initial and final value theorems for grid operations. It also discusses the role of ESS frequency coordination as well as how generators and ESS can work in coordination with the SOC feedback.

As previously highlighted, effective frequency regulation necessitates the presence of backup storage systems, ready to address any discrepancies that may arise between energy production and demand. In the context of DR, it becomes crucial to recognize and leverage available resources. By acknowledging the importance of energy management strategies, the system can easily switch to alternative sources or storage solutions during times of peak demand or unexpected production shortfalls. Having a thorough understanding of available resources and integrating DR increases the grid's robustness and responsiveness, resulting in a more resilient and reliable system.

In recent years, various methods have been suggested to estimate the real-time capacity of DR, aiming to provide support to the electrical grid. For example Sheshyekani, Kiani and Dagdougui presented a control structure for the participation of aggregated TCLs in frequency regulation service [1]. The aggregation is performed using the State Space Model (SSM) of TCLs, a model inspired by a previous work [2] that applied SSM for real-time aggregation of electric vehicles (EVs). The dynamics of a TCL population is efficiently described using a state-bin transition model and is shown in Fig 2.2. This model divides the temperature dead-band into intervals, capturing the state distribution of TCLs with different set point-temperatures and dead-bands. Because different devices with different set-points and dead bands are involved, the first step would be normalizing the indoor temperature. The normalized temperature is used to locate the current state-bin of a TCL in the state space. The following form can be used to aggregate TCLs within the state space model

(SSM):

$$\begin{cases} x(k+1) = Ax(k) + bu(k) \\ y(k) = Cx(k) \end{cases} \tag{2.5}$$

The state vector x represents the fraction of TCLs in each state bin, and the input vector u updates this state vector at each time interval. The Markov transition matrix A, generated offline using the Hidden Markov Model, governs the transition probability of TCLs between state bins. The output vector y describes the aggregated TCLs' power, and the matrix b facilitates control actions. TCL output power is obtained by aggregating TCLs using a constant matrix, C. The State Space Model (SSM) predicts state transitions within a time interval, and a "collect-and-correct" procedure, involving measured temperatures and switch status, enhances prediction accuracy. The TCLs' regulation capacity in both responding modes is determined based on the SSM of aggregated TCLs.

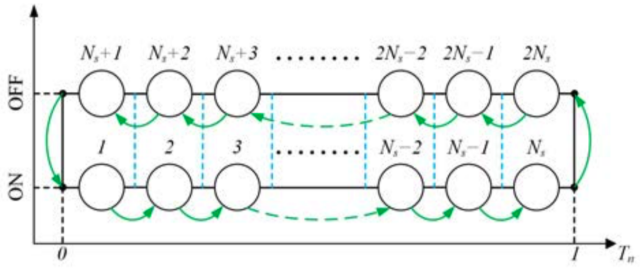


Figure 2.2 State space of aggregated TCLs [1] [2].

# CHAPTER 3 Frequency stability and Droop-Based Demand Response Control in Power Systems

In the intricate landscape of power system control, the concept of droop control has endured as a foundational principle, guiding the behavior of generators and shaping the dynamic equilibrium of energy networks. This chapter embarks on a journey to reexamine the classical notion of droop control, as explicated by Kundur [7]. Furthermore, we begin constructing a simplified area model that will serve as our simulation playground in the subsequent chapters, enabling us to probe the potential impact of EWHs operating under a droop control framework.

As previously discussed, the goal of this chapter is the establishment of a comprehensive model for grouped EWHs equipped with individualized droop control strategies. Our intention is to harness this setup as a DR mechanism. The concept of DR has been introduced to flexibly adjust power consumption on the demand side as dictated by specific circumstances. Implementation of DR has dual objectives from the perspective of the power system: first, to minimize the requirement for spinning reserves, and second, to concurrently maintain the stability of system frequency, ultimately improving the overall performance of the system.

## 3.1 Power system frequency response

The fundamental configuration presented in this study entails a straightforward generator unit accompanied by a non-reheat steam turbine, exactly as detailed in previous chapter 2.2.1. The graphical representation of the associated generator's layout was illustrated in Fig 2.1, while specific parameters concerning the turbine governor can be found in Table 2.1.

Utilizing Newton's second law within the context of the mentioned turbine system for frequency minor deviations calculation leads us to the following expression [7]:

$$\Delta P_g(t) - \Delta P_d(t) = 2H\frac{d\Delta f(t)}{dt} + D\Delta f(t) \tag{3.1}$$

The supply side sets aside a predetermined capacity to facilitate frequency droop control. Furthermore, the system integrates DR which, because of its fast electrical transients is expected to act as a swift power compensator in response to frequency changes. The interaction of factors like generator turbine inertia, droop value, and load damping coefficient results into frequency dynamics. This process can lead to a shift to a distinct equilibrium point. Given

the components of the generator, the system can contribute to PFR. PFR involves governor control, a mechanism that regulates the active power output of generation units and manages load consumption to promptly counter frequency fluctuations within seconds.

In this section, we conduct a series of simulations to analyze the system's responses for various scenarios, with the aim of ultimately including DR contribution in PFR.

In this scenario, the system operates in its steady state and relies solely on the benefits that are derived from synchronized generator-based PFR. As presented in Fig 3.1, during a typical operational day of the grid at its steady state, the frequency of the system is observed to stabilize at 60 $Hz$, while the generators operate at their nominal rate of 1 $p.u.$

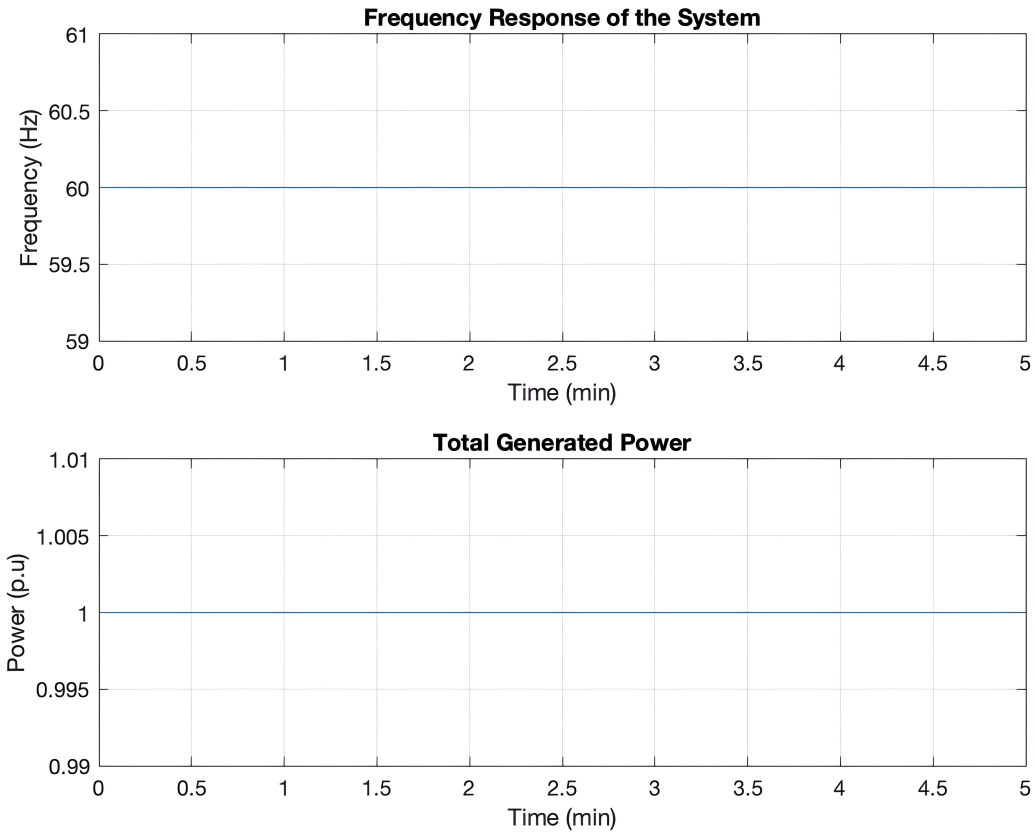


Figure 3.1 Upper: Frequency response of the system in steady state. Lower: with total power produced by the generators.

In another scenario, a perturbation in demand arises at $t = 2$ minutes, leading to a 3% increase. In this scenario, it is assumed that no PFR is available to assist in restoring the frequency back to its nominal value. As shown in Fig 3.2, at $t = 2$ minutes, the frequency begins to decline steadily due to the absence of a backup scheme like PFR to regulate power produc-

tion according to the new demand. Consequently, the total power produced by generators remains at its nominal value of 1 p.u.

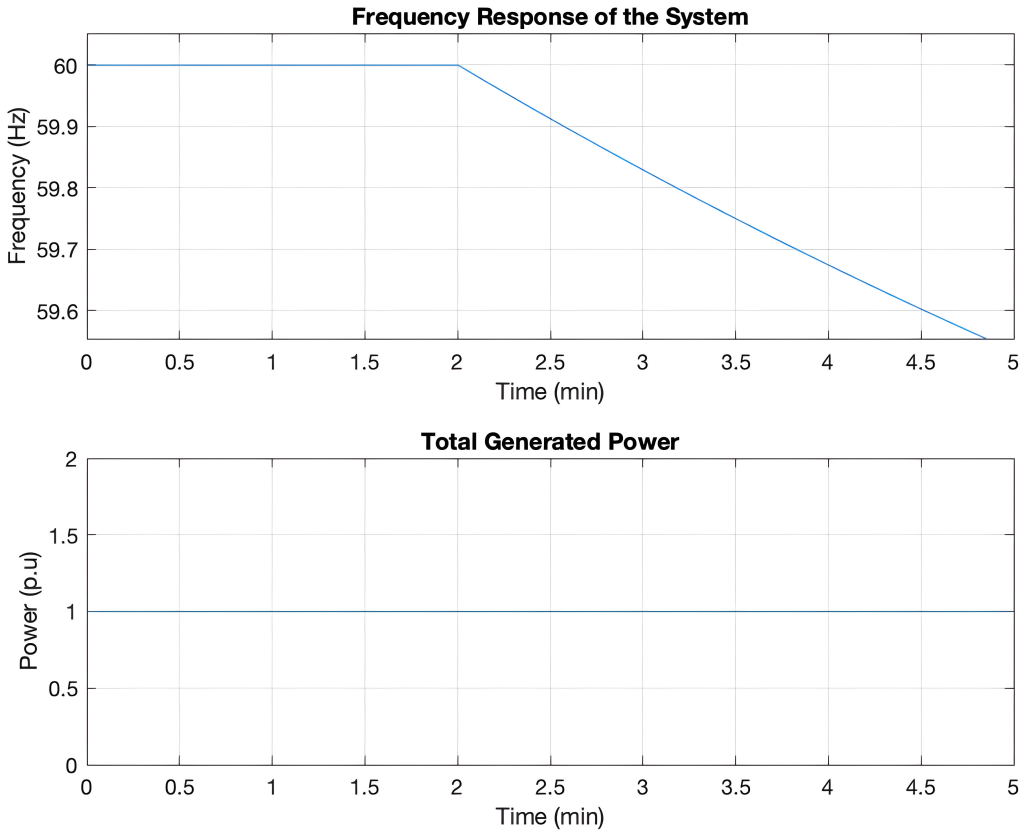


Figure 3.2 The responses of the system under 0.03% perturbation while there is no PFR implemented in the system. Upper: Frequency response of the system in steady state. Lower: with total power produced by the generators.

On the other hand, if PFR is implemented in the system, during the same occurrence of perturbation, it can be observed that the frequency can be regulated, preventing excessive dropping, as it is shown in Fig 3.3.

In Fig 3.3-Lower, it is evident that the implementation of PFR has led to an increase in production to fulfill the new power demand. Upon reaching steady state, a difference in frequency response is observable, attributable to the proportional control nature of PFR which leads to a steady state error. Typically, such errors are addressed by secondary and tertiary frequency controls, as explained in section 2.2 of chapter 2.

It is evident that we have achieved a reliable system, where the benefits of a PFR scheme aid in maintaining a balance between power production and demand. In the next section, we

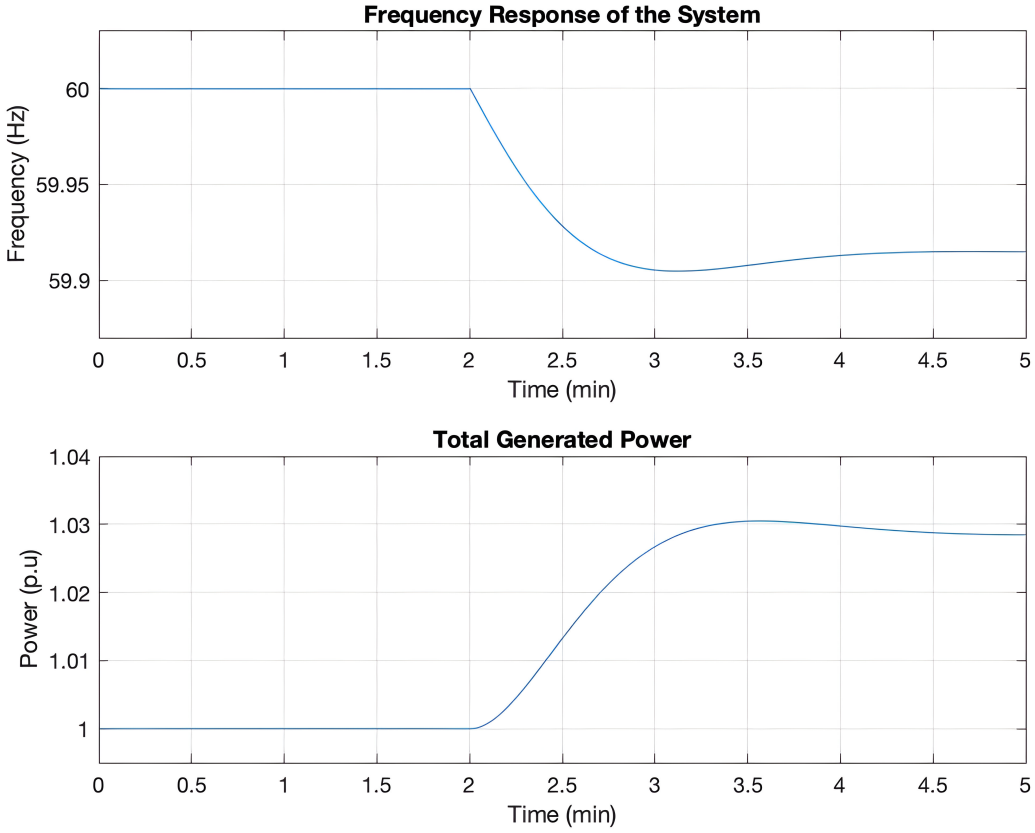


Figure 3.3 The responses of the system under 0.03% perturbation. Upper: Frequency response of the system in steady state. Lower: with total power produced by the generators.

apply the droop control concept used on synchronous generators for proportional frequency control to the EWHs, so as to make them part of the PFR action.

## 3.2 Droop-Based Demand Response Control Strategy

In section 2.2.2 of chapter 2, a thorough examination of various studies investigating control strategies in DR was provided. It was underscored that TLCs, particularly EWHs, have emerged as effective tools for facilitating these strategies.

EWHs are favored options within DR control strategies due to several compelling reasons:

1. **High Energy Consumption**: EWHs typically account for a substantial portion of household energy usage. By managing the operation of EWHs during peak demand periods, utilities can effectively regulate overall energy demand and alleviate strain on the grid.

2. **Thermostatic Control**: Equipped with thermostats to regulate water temperature, EWHs offer inherent control mechanisms that facilitate easy adjustment of heating cycles to align with demand response requirements.

3. **Thermal Energy Storage**: Serving as thermal energy storage devices, EWHs can heat water during off-peak hours when electricity is more abundant, economical or when excessive renewable energy is available, thus storing thermal energy for subsequent use. This capability contributes to load shifting and enhances grid stability.

4. **Flexibility in Operation**: EWHs possess large thermal masses and relatively slow temperature response times to demand changes, rendering them suitable for load shaping strategies. Their operation can be adjusted without significantly affecting user comfort.

5. **Consumer Acceptance and Comfort**: Interruptions in EWH operation, such as temporary adjustments in water temperature, are often less intrusive to users compared to other appliances. This factor enhances consumer acceptance of demand response programs based on EWHs.

While numerous studies have explored different algorithms for designing efficient DR schemes, we propose a droop-based model which could smoothly integrate DR within the prevailing and rather successful existing PFR grid approaches. Integrating droop control schemes into EWHs offers a promising approach to enhance their participation in DR programs, facilitating coordinated adjustments in power consumption while maintaining consumer comfort and grid stability. This section aims to develop an application of droop control schemes in

EWHs within the framework of demand response strategies in smart grids, establishing a robust control model to explore their effectiveness, feasibility, and potential impact on energy efficiency and grid reliability in subsequent chapters.

In our model the presented mechanism dynamically adjusts the power consumption of each EWH's heating element. This adjustment is based on the deviation of the grid frequency from the nominal frequency, along with relevant parameters such as the droop constant and the current heating element power.

Through conditional statements, the mechanism governs the power of the heating element in response to the magnitude of the frequency deviation. If the deviation exceeds predefined thresholds, the mechanism either increase or reduces the power of the heating element according to the sign of the frequency deviation.

It is important to note that the adjustment of the power of the heating element, proportional to the frequency deviation, is bounded by minimum and maximum thresholds. The minimal power constraint aiming at maintaining customer comfort and ensuring that there is always some energy stored in the EWHs during emergency scenarios, where immediate reduction of consumption is required. Specifically, the minimum bound has been established to help guarantee sufficient energy reserve within the EWHs, thus enabling them to respond promptly to grid stability concerns or other critical situations.

A code snippet (pseudo-code) is provided below to illustrate the concept of the droop scheme in Algorithm 1.

**Algorithm 1:** Update_HeatingRate

**Input :** $\Delta f(t)$, $R'$, $K_d$
**Output:** $R'_{new}$
**if** $\Delta f(t) < -K_d$ **then**
  $R'_{new} = R'/3$
**else if** $\Delta f(t) > K_d$ **then**
  $R'_{new} = R'$
**else**
  $R'_{new} = \frac{2R'}{3} + \frac{\Delta f}{K_d} \cdot \frac{R'}{3}$

Where

| | |
|---|---|
| $K_d$: | Nominal droop Constant for each EWH. It has been denoted as $K_d$ because, K represents a gain factor and the subscript d indicates that it is associated with droop control. |
| $R'$: | Power of heating element of each EWH. |

The chief advantage of this control scheme is its rapid response time (note that power consumption is controlled via voltage), enabling application within fractions of a second, a critical attribute in PFR. Moreover, its implementation is characterized by simplicity, avoiding the complexities associated with centralized control models ( [21] as an example) that require massive measurements and intricate communication systems.

A noteworthy drawback in decentralized models is the potential for aggregated load responses to result in excessive or insufficient power adjustments, stemming from the lack of centralized oversight. However, this droop-based model, effectively addresses this concern. By continuously tracking the fraction of active EWH thermostats—those capable of contributing to DR—we can mitigate the potential imbalances inherent to decentralized systems. A major specificity of the proposed control algorithm is that we can keep track of the number of ON devices which are at any moment the only ones capable of contributing to the control effort.

Since the on-off cycle of the water heater involves an electrical component, it is noteworthy to mention, we may have the flexibility to select the droop constant of EWHs to be as small as desired. However, is not desirable to induce excessively oscillatory power control actions at the level of EWHs. For further clarification of the suggested droop control mechanism, refer to Fig 3.4, which illustrates Algorithm 1.

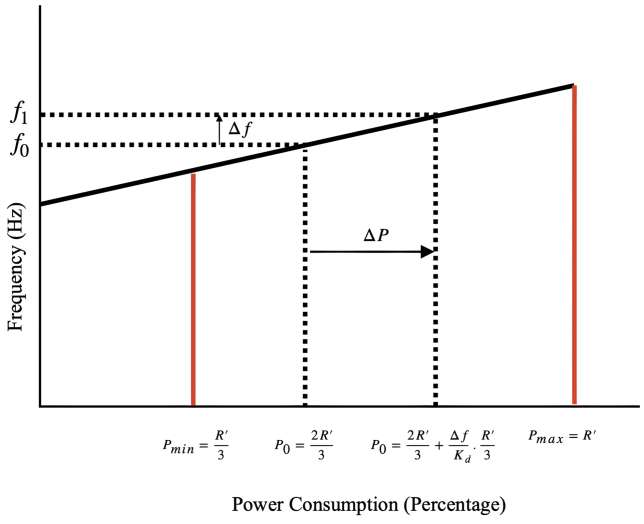


Figure 3.4 Droop Characteristic of the system used in EWHs.

Finally, a noteworthy aspect to underscore is our system's control of frequency deviation ($\Delta f$) across all devices. When grid perturbations lead to a frequency imbalance, it triggers individual responses from all EWHs, as depicted in Fig 3.4. In essence, each EWH independently fine-tunes its power consumption to counteract the imbalance. However, these devices operate without awareness of the collective efforts of all participating EWHs in regulating

the system. It is only their collective action on the frequency deviation $\Delta f$, which acts as a coordinating mechanism.

# CHAPTER 4 Physical Modeling of Electric Water Heaters: Characterizing Behavior

## 4.1 Establishing a model for individual and aggregate loads

In this section of the thesis, we focus on the stochastic modeling approach proposed for EWHs. Specifically, we consider the uniformity of water temperature within the tank as an assumption (mixed water in the tank). This assumption allows us to utilize a first-order heat transfer equation to determine the water temperature and corresponding power requirements at each time step. Through this modeling framework, we aim to analyze and understand heat transfer dynamics within EWHs. This will contribute to a comprehensive understanding of their behavior and energy consumption patterns which can be derived from:

$$\begin{aligned} R' m_t(t) - \dot{m}_L C_{pf}(T_d - T_{in}) - UA_r(T - T_a) \\ = C_{pf} M \frac{dT}{dt} \end{aligned} \tag{4.1}$$

| | |
|---|---|
| $M$: | water mass. |
| $C_{pf}$: | specific heat of water. |
| $U$: | loss coefficient of the tank. |
| $A_r$: | surface area of the tank. |
| $T_a$: | ambient temperature. |
| $T_d$: | customer's desired temperature of water. |
| $\dot{m}_L$: | water flow rate to the load. |
| $T_{in}$: | temperature of the inlet water. |
| $m_t$: | thermostat control boolean. |
| $R'$: | rate of energy input by the heating element. |

$R'$ is being controlled by the input voltage of the heater (V) and the size of the resistor used to produce heat ($R_s$).

$$R' = \frac{V^2}{R_s} \tag{4.2}$$

The model contains two types of state variables: (i) continuous state variables such as T (tank water temperature at time t) and (ii) discrete state variables such as $m_t$, which relate to the thermostat. Temperature dead band $[T_-, T_+]$, characterizes the dynamic behaviour of $m_t$. Thus when the tank temperature reaches $T_-$, $m_t$ switches to 1. Similarly, when the tank temperature reaches $T_+$, it will be switched to 0.
One of the complex steps in this procedure is modeling the customer's hot water usage due to its non-stationary behavior. Laurent and Malhamé [24] have argued that the stochastic demand process could be assumed to have piecewise constant statistics, with the statistics depending on the time of the day. Indeed, the nature of hot water extraction events, and thus their statistics, tend to be strongly correlated with the time of the day.

As proposed in [25], we consider the demand model as a Markovian jump process ($q(t)$) with two states of 0 and 1 while $A'$ is the energy extraction rate when the hot water demand state is ON. As indicated earlier, we consider a water extraction model with constant statistics. Also, we shall consider $T_d$ in (4.1) as a constant. This leads to a simplified EWH dynamic equation associated with a constant rate of energy extraction when hot water demand is ON. By simplifying (4.1) we have:

$$Rm_t(t) - Aq(t) - a(T - T_a) = \frac{dT}{dt} \tag{4.3}$$

In (4.3), $a$, $A(t)$ and $R$ are respectively, the thermal resistance of tank walls, the rate of energy extraction when water is in demand and the power rating of the heating element all expressed per unit of the tank thermal capacity. Furthermore, the two state Markov chain $q(t)$ is characterized by the (interval wise) time invariant transition rates $\alpha_0$ and $\alpha_1$ with the resulting switching probability equations:

$$Pr(q(t+h) > 0 | q = 0) = \alpha_1 h + o(h) \tag{4.4}$$

$$Pr(q(t+h) = 0 | q(t) > 0) = \alpha_0 h + o(h) \tag{4.5}$$

| | |
|---|---|
| $\alpha_0$: | probability of transition from water extraction state to non-extraction state. |
| $\alpha_1$: | probability of transition from no water extraction state to extraction state.. |
| $o(h)$: | $lim_{h\to 0}\frac{o(h)}{h} = 0$ and $h$ is the time step. |

The challenge of aggregation can be described as follows in the context of a homogeneous

control group consisting of M devices. In such a group, all M water heaters are assumed to share identical statistics and parameters. The total electricity of the M devices will be:

$$P(t) = R' \sum_{i=1}^{M} m_i(t) \tag{4.6}$$

$P(t)$: total power demanded by the group at t.

$m_i(t)$: state of $i-th$ EWH in the group.

However, (4.6) is a highly stochastic quantity. Malhamé [26], instead, proposes to consider the empirical mean $\bar{m}(t)$ instead of the individual $m_i(t)$. Under assumptions of independence of the individual EWH thermostatic states, $\bar{m}(t)$ converges as $M$ becomes large to the expectation of a generic $m_i(t)$. This convergence is almost everywhere (a.e.) by the strong law of large numbers. Thus:

$$\bar{m}(t) \triangleq \frac{1}{M} \sum_{i=1}^{M} m_i(t) \quad \underrightarrow{a.e} \quad E_w(m(t)) \tag{4.7}$$

In (4.7), $\bar{m}(t)$ is the so-called "aggregate" operating state and physically represents the average fraction of ON state devices of the group. It should also be mentioned that in the homogeneous case, $P(t)$ is proportional to $\bar{m}(t)$. $E_w(.)$ represents expectation operator conditional on ambient temperature.

### 4.2 Partial differential equations of load dynamics

If we consider the complete Markov process $\begin{bmatrix} T(t) \\ m(t) \\ q(t) \end{bmatrix}$, the probability density functions in below can be written with respect to the hybrid-state Markov process:

$$\begin{aligned} &f_{ij}(\lambda, t)d\lambda = P[\lambda \leq T(t) \leq \lambda + d\lambda, m(t) = i, q(t) = j] \\ &i, j = 0, 1 \end{aligned} \tag{4.8}$$

As discussed in (4.1), the load dynamics of a homogeneous group of EWHs are related to the fraction of ON devices through time. Therefore, if one determines the evolution of pdfs in (4.8), it could lead to an aggregate model of EWHs.

The following theorem is established in [26]:

**Theorem 1** *Hybrid state probability density functions $f_{ij}$ in* (4.8)*, satisfy the coupled systems of partial differential equations* (4.9)-(5.3) *for i=0, 1 and j=0,1 in regions a and b in Fig. 4.1, and* (4.11)-(4.12) *in region b in Fig. 4.1.*

$$\frac{\partial f_{11}(\lambda,t)}{\partial t} = \frac{\partial}{\partial \lambda}[r_{11}(\lambda,t) f_{11}(\lambda,t)] - \alpha_1 f_{11}(\lambda,t) + \alpha_0 f_{10}(\lambda,t) \tag{4.9}$$

$$\frac{\partial f_{10}(\lambda,t)}{\partial t} = \frac{\partial}{\partial \lambda}[r_{10}(\lambda,t) f_{10}(\lambda,t)] + \alpha_1 f_{11}(\lambda,t) - \alpha_0 f_{10}(\lambda,t) \tag{4.10}$$

$$\frac{\partial f_{01}(\lambda,t)}{\partial t} = \frac{\partial}{\partial \lambda}[r_{01}(\lambda,t) f_{01}(\lambda,t)] - \alpha_1 f_{01}(\lambda,t) + \alpha_0 f_{00}(\lambda,t) \tag{4.11}$$

$$\frac{\partial f_{00}(\lambda,t)}{\partial t} = \frac{\partial}{\partial \lambda}[r_{00}(\lambda,t) f_{00}(\lambda,t)] + \alpha_1 f_{01}(\lambda,t) - \alpha_0 f_{00}(\lambda,t) \tag{4.12}$$

*Where:*

$$r_{11}(\lambda,t) \triangleq a(\lambda - T_a) - R + A(t) \tag{4.13}$$

$$r_{10}(\lambda,t) \triangleq a(\lambda - T_a) - R \tag{4.14}$$

$$r_{00}(\lambda,t) \triangleq a(\lambda - T_a) + A(t) \tag{4.15}$$

$$r_{01}(\lambda,t) \triangleq a(\lambda - T_a) \tag{4.16}$$

The terms $r_{ij}$ for $i = 0, 1$ and $j = 0, 1$ in (4.13) to (4.16) are water cooling rates which can be interpreted as follows:

$r_{11}(\lambda,t)$: cooling rate of water in the tank when the EWH is ON and it is facing a water demand with water temperature of $\lambda$.

$r_{10}(\lambda,t)$: cooling rate of water in the tank when the EWH is ON and it is not facing a water demand with water temperature of $\lambda$.

$r_{01}(\lambda,t)$: cooling rate of water in the tank when the EWH is OFF and it is facing a water demand with water temperature of $\lambda$.

$r_{00}(\lambda,t)$: cooling rate of water in the tank when the EWH is OFF and it is not facing a water demand with water temperature of $\lambda$.

Furthermore, the following boundary conditions must hold for all t.
Conditions at infinity:

$$f_{11}(-\infty, t) = f_{10}(-\infty, t) = 0 \tag{4.17}$$

Probability conservation:
at $T_-$, for $j = 0, 1$:

$$\begin{aligned} &-r_{1j}(T_-, t) f^a_{1j}(T_-, t) + r_{1j}(T_-, t) f^b_{1,j}(T_-, t) \\ &+r_{0j}(T_-, t) f^b_{0j}(T_-, t) = 0 \end{aligned} \tag{4.18}$$

at $T_+$, for $j = 0, 1$:

$$r_{1j}(T_+, t) f^b_{1j}(T_+, t) + r_{0j}(T_+, t) f^b_{0j}(T_+, t) = 0 \tag{4.19}$$

Absorbing boundaries:
at $T_+$, for $j = 0, 1$:

$$0 \leq -r_{1j}(T_+, t) f_{1j}(T_+, t) \tag{4.20}$$

at $T_-$, for $j = 0, 1$:

$$0 \leq r_{0j}(T_-, t) f_{0j}(T_-, t) \tag{4.21}$$

And finally:

$$\begin{aligned} \bar{m}(t) &= \mathbb{E}_w[m(t)] \\ &= \int_{-\infty}^{\infty} [f_{11}(\lambda, t) + f_{10}(\lambda, t)]\, d\lambda \end{aligned} \tag{4.22}$$

Remark: Boundary conditions (4.20) to (4.21) exhibit an interesting characteristic in that they are natural boundary conditions (automatically satisfied) with the only possible exception (4.21), which is activated under specific circumstances. This activation occurs when $r_{11}(T_+, t)$ is positive, leading to the requirement that $f_{11}(T_+, t)$ must be zero as indicated by equation (4.20) since as a probability density function it cannot become negative.

The situation, $0 \leq r_{11}(T_+, t)$, arises when the power of the heating element is lower than the power loss associated with hot water extraction when $q(t) = 1$. All other inequalities in (4.20)-(4.21) are automatically satisfied and one does not really need to write them.

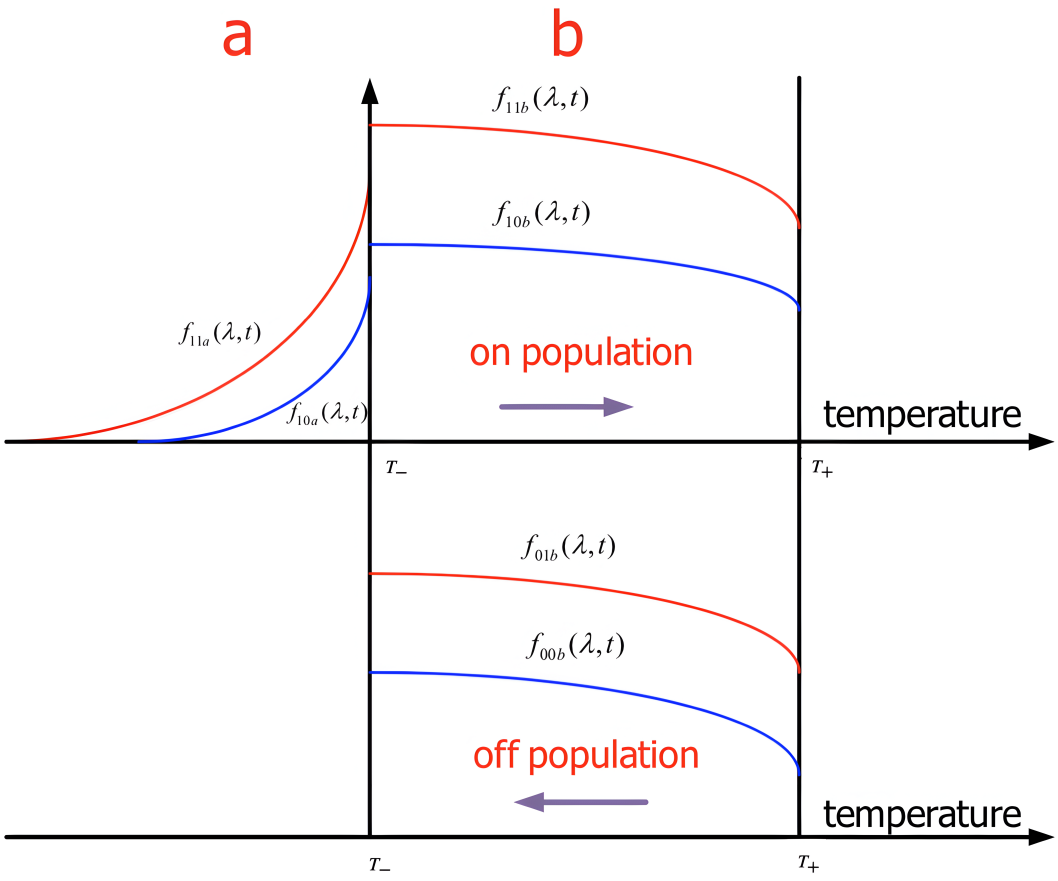


Figure 4.1 Illustration of dynamical system (4.9) to (4.12). $T_-$ and $T_+$ are lower and upper edges of the thermostats deadbands.

### 4.3 Identification of model parameters

For the purpose of this thesis, we have developed a model for a water heater using the configuration parameters outlined in Table 4.1.

Utilizing equations (4.1), (4.3), and the data provided in Table 4.1, we can derive the model parameters $a$ and $R$ as follows:

$$a = \frac{UA_R}{MC_{pf}} = 0.193 \times 10^{-4} \frac{1}{\text{min}} \tag{4.23}$$

$$R = \frac{R'}{MC_{pf}} = 0.2122 \frac{^\circ C}{\text{min} \cdot \text{W}} \tag{4.24}$$

Advancing towards the completion of our model, the determination of the remaining parameters—$A$, $\alpha_0$, and $\alpha_1$—in equations (4.4) and (4.5) is imperative. To achieve this, our focus turns to periods marked by constant demand, and we draw upon data pertaining to the average hourly Hot Water Consumption (HWC) of a typical English household, [3]. This data, visualized in Fig. 4.2, serves as a foundational reference. Guided by the insights derived from Fig. 4.2 and informed by the preceding work of Malhamé and Laurent [27], we present the compiled parameter values in Table 4.2.

To advance our model, we have examined the daily hot water usage of a residence in relation to its corresponding energy consumption [3].

Now, concerning the values in Table 4.2, we can determine the variables $A$ and $\alpha_1$, as follows:

Table 4.1 EWH Parameters

| **Parameter** | **Value** | **Unit** |
|---|---|---|
| $R'$ | 4.5 | kW $=\frac{kJ}{s}$ |
| $U$ | 8.75 | $\frac{J}{min^\circ C m^2}$ |
| $A_r$ | 2.8 | $m^2$ |
| Thermostat dead-band | 60-65 | °C |
| $T_a$ | 22 | °C |
| M | 304 | kg |

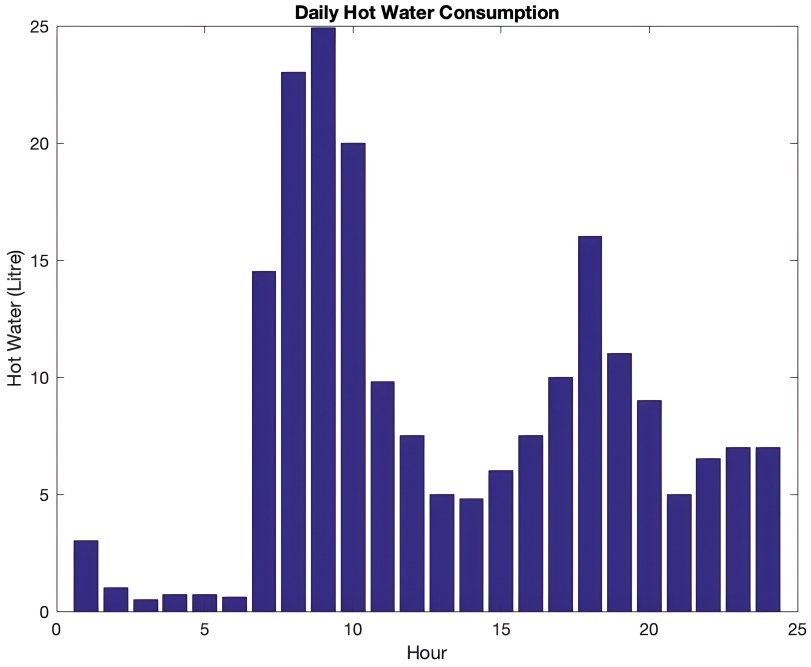


Figure 4.2 Hourly household hot water consumption [3].

Table 4.2 Hot Water Consumption Parameters

| **Parameter** | **Value** |
|---|---|
| Occupancy | 3 |
| Events | 21 |
| Daily Water Demand | 201 L |
| Daily Energy Extraction | 16.7 MJ |
| Water Flow Rate | 5 $\frac{L}{\text{min}}$ |

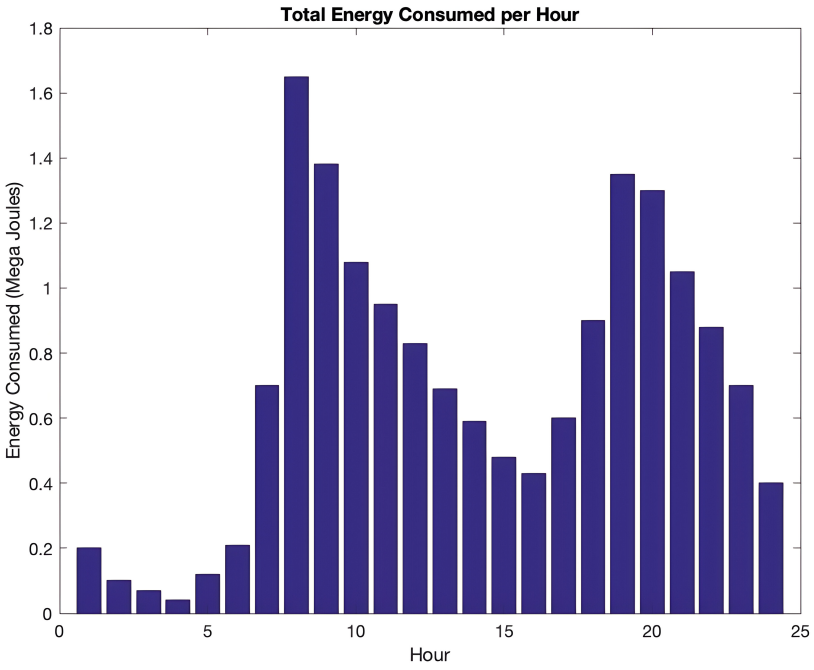


Figure 4.3 Daily energy consumption of a dwelling with respect to hot water usage in 4.2 [3].

$$A = \frac{\text{Energy Extracted Daily}}{\text{Time Length Spanned by events in a day}} \cdot \frac{1}{\text{Tank Water Thermal Capacity}} = 0.3266 \frac{^{\circ}C}{\text{min}} \tag{4.25}$$

$$\alpha_1 = \frac{1}{\text{Duration of a Water Event}} = \frac{21 \times 5}{201} = 0.52 \text{ min}^{-1} \tag{4.26}$$

Additionally, an hourly rate of energy extraction can be calculated based on the information presented in Figures 4.2 and 4.3, as illustrated in Figure 4.4.

In [26], Malhamé calculated an expression for the fraction of ON devices under the assumption that $A(t)$ remains constant, and $r_{11}$ is negative. The second assumption indicates that the EWH can provide enough power to warm the water even when the demand state is ON, meaning that the boundary condition in (4.20) is inactive. To derive the expression, we first introduce $\theta$. It can be comprehended that since $[T_- T_+]$ is usually a small interval, $r_{ij}(T, t)$ can be assumed fixed at $T = \frac{T_- + T_+}{2}$. Then we define:

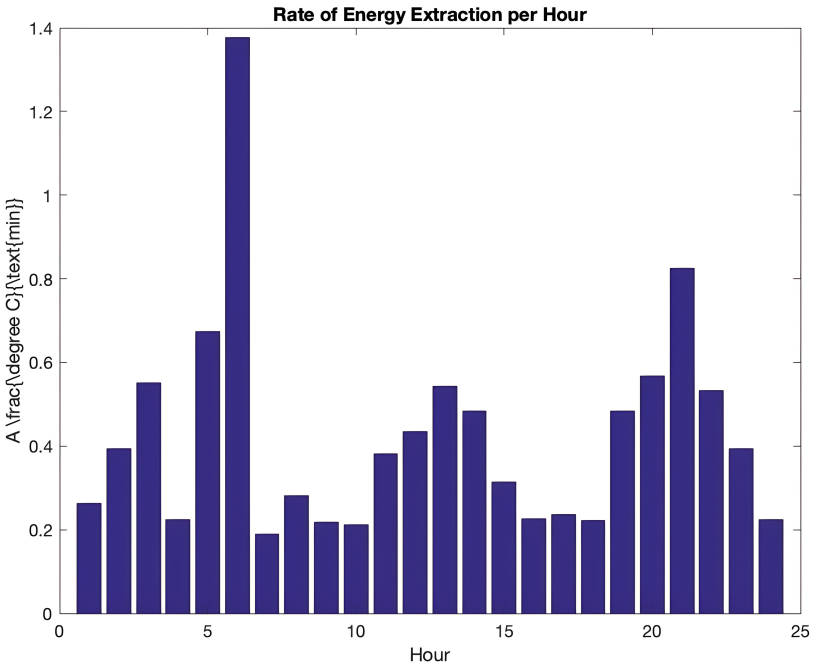


Figure 4.4 Hourly rate of energy extraction based on 4.2 and 4.3.

$$\theta_1^{-1} = -\left[\frac{\alpha_0}{r_{10}} + \frac{\alpha_1}{r_{11}}\right] \tag{4.27}$$

$$\theta_0^{-1} = \left[\frac{\alpha_0}{r_{00}} + \frac{\alpha_1}{r_{01}}\right] \tag{4.28}$$

As mentioned earlier, Malhamé in [12] showed that $\bar{m}$, the steady-state fraction of devices when $r_{11} \leq 0$ and for $\Delta \equiv T_+ - T_-$, can be calculated with:

$$\bar{m} = \left(\frac{\alpha_1}{\alpha_1 + \alpha_0}\right)\left[\frac{-\frac{\Delta}{r_{10}}}{-\frac{\Delta}{r_{10}} + \frac{\Delta}{r_{00}}}\right] + \left(\frac{\alpha_0}{\alpha_1 + \alpha_0}\right)\left[\frac{-\frac{\Delta}{r_{11}}}{-\frac{\Delta}{r_{11}} + \frac{\Delta}{r_{10}}}\right] \tag{4.29}$$

Now we can determine $\alpha_0$ using equation (4.29) and previous calculations in equations (4.25) and (4.26). It should be mentioned that we compute $m_s$, the fraction of on-state devices in the steady state, by dividing the hourly load in Fig. 4.3 by the maximum power of EWHs, 4.5 kW. The corresponding results have been provided in Table. 4.3.

Table 4.3 Average power demand by EWH and respective values of parameters $m_s$ and $\alpha_0$

| Hours | Load (kW) | $m_s$ | $\alpha_0\,(\text{min}^{-1})$ |
|---|---|---|---|
| 0 | 0 | 0 | 0 |
| 1 | 0 | 0 | 0 |
| 2 | 0.018 | 0.04 | 0 |
| 3 | 0.033 | 0.007 | 0.001 |
| 4 | 0.26 | 0.058 | 0.009 |
| 5 | 1.14 | 0.252 | 0.042 |
| 6 | 0.746 | 0.166 | 0.028 |
| 7 | 0.699 | 0.155 | 0.025 |
| 8 | 0.916 | 0.204 | 0.034 |
| 9 | 0.494 | 0.11 | 0.017 |
| 10 | 0.521 | 0.116 | 0.018 |
| 11 | 0.7 | 0.157 | 0.025 |
| 12 | 0.467 | 0.104 | 0.016 |
| 13 | 0.369 | 0.082 | 0.013 |
| 14 | 0.43 | 0.096 | 0.015 |
| 15 | 0.57 | 0.127 | 0.02 |
| 16 | 0.628 | 0.14 | 0.023 |
| 17 | 0.683 | 0.151 | 0.025 |
| 18 | 0.729 | 0.162 | 0.026 |
| 19 | 0.692 | 0.154 | 0.025 |
| 20 | 0.509 | 0.113 | 0.018 |
| 21 | 0.396 | 0.088 | 0.014 |
| 22 | 0.236 | 0.052 | 0.008 |
| 23 | 0.147 | 0.033 | 0.005 |

## 4.4 Numerical Solution

The development of joint density dynamics for EWH states was discussed in the previous section. An numerical framework is now presented for computing the evolution of the model. Furthermore, a Monte Carlo simulation of aggregate dynamics is implemented to validate our numerical analysis. This simulation will serve as the basis for comparing and mutually validating the two methodologies, providing a mutual validation of results.

### 4.4.1 Discretization of the Markov chains

According to the previous section, equations (4.9)-(4.12) can be expressed as follows:

$$\frac{\partial}{\partial t}f(x,t) = \frac{\partial}{\partial x}[A(x,t)f(x,t)] + Bf(x,t) \tag{4.30}$$

Where $A(x,t)$ is the cooling rate matrix and $B$ is the transition matrix associated to the Markov chain, which are defined based on (4.13)-(4.16) and (4.4)-(4.5):

$$f(x,t) = \begin{bmatrix} f_{00}(x,t) \\ f_{01}(x,t) \\ f_{10}(x,t) \\ f_{11}(x,t) \end{bmatrix} \tag{4.31}$$

$$A(x,t) = \begin{bmatrix} r_{00}(x) & 0 & 0 & 0 \\ 0 & r_{01}(x) & 0 & 0 \\ 0 & 0 & r_{10}(x,t) & 0 \\ 0 & 0 & 0 & r_{11}(x,t) \end{bmatrix} \tag{4.32}$$

$$B = \begin{bmatrix} -\alpha_o & \alpha_1 & 0 & 0 \\ \alpha_o & -\alpha_1 & 0 & 0 \\ 0 & 0 & -\alpha_o & \alpha_1 \\ 0 & 0 & \alpha_o & -\alpha_1 \end{bmatrix} \tag{4.33}$$

In Equation 4.32, $r_{00}$ and $r_{01}$ remain time-independent, as the sole time-dependent factor relates to the water demand, as expressed in equations 4.13 to 4.16. Given $N(t)$ as the population distribution vector of the Markov chain at time $t$, and referring to matrix $B$ in 4.33, one can express:

$$\frac{dN}{dt} = BN(t) \tag{4.34}$$

If we express the sampled version of $N(t)$ at a fixed time step $\Delta t$, it takes the form:

$$N(t + \Delta t) = e^{\Delta t M} N(t) \tag{4.35}$$

For small $\Delta t$ and considering small values for matrix $B$, a first-order approximation can be derived:

$$e^{\Delta t M} N(t) = \mathbb{I}_2 + \Delta t B \tag{4.36}$$

Now, we can derive a discretized approximation of the continuous-time Markov chain:

$$\begin{aligned} Pr(q(t + \Delta t) > 0 | q(t) = 0) &= \alpha_1 \Delta t \\ Pr(q(t + \Delta t) = 0 | q(t) > 0) &= \alpha_0 \Delta t \end{aligned} \tag{4.37}$$

### 4.4.2 Numerical Solution of Fokker-Plank Evolution Using the Lax-Wendroff Method

This section discusses the numerical solution to Kolmogorov Equation given in (4.30). One can derive the following from (4.30):

$$\begin{aligned} &\frac{\partial}{\partial t} f(x,t) = \frac{\partial}{\partial x}[A(x,t) f(x,t)] + B f(x,t) = \\ &\frac{\partial A(x,t)}{\partial x} f(x,t) + A(x,t) \frac{\partial f(x,t)}{\partial x} + B f(x,t) \end{aligned} \tag{4.38}$$

The Lax-Wendroff scheme provides a numerical difference method for this system [28] [29] using the following approximations for a function $f(m,n)$, denoted as $f_m^n$:

$$\frac{\partial}{\partial x} f_m^n = \frac{f_{m+1}^n - f_{m-1}^n}{2\Delta x} \tag{4.39}$$

$$\frac{\partial^2}{\partial x^2} f_m^n = \frac{f_{m+1}^n - f_m^n + f_{m-1}^n}{\Delta x^2} \tag{4.40}$$

The temperature discrete step size is denoted by $\Delta x$. Taylor's expansion is now applied to the second order approximation:

$$f_m^{n+1} = f_m^n + k \frac{\partial}{\partial t} f_m^n + \frac{1}{2} k^2 \frac{\partial^2}{\partial t^2} f_m^n \tag{4.41}$$

Here, $k$ denotes the time step. Substituting equation (4.41) into equation (4.38), we derive:

$$\begin{aligned} f_m^{n+1} =& f_m^n + k\left[\frac{\partial A_m^n}{\partial x} f_m^n + A_m^n \frac{\partial f_m^n}{\partial x} + B f_m^n\right] + \\ & \frac{1}{2}k^2 \frac{\partial}{\partial t}\left[\frac{\partial A_m^n}{\partial x} f_m^n + A_m^n \frac{\partial f_m^n}{\partial x} + B f_m^n\right] = \\ & f_m^n + k\left[\frac{\partial A_m^n}{\partial x} f_m^n + A_m^n \frac{\partial f_m^n}{\partial x} + B f_m^n\right] + \\ & \frac{1}{2}k^2[\frac{\partial^2 A_m^n}{\partial x \partial t} f_m^n + \frac{\partial A_m^n}{\partial x}\frac{\partial f_m^n}{\partial t} + \frac{\partial A_m^n}{\partial t}\frac{\partial f_m^n}{\partial x} + \\ & A_m^n \frac{\partial^2 f_m^n}{\partial x \partial t} + B\frac{\partial t f_m^n}{\partial t}] \end{aligned} \tag{4.42}$$

As a result of using (4.38) again on (4.42), and by simplifying it, we obtain the following equation:

$$\begin{aligned} f_m^{n+1} = & f_m^n + k\frac{\partial}{\partial x} A_m^n f_m^n + k A_m^n \frac{\partial}{\partial x} f_m^n + k B f_m^n \\ & + \frac{1}{2}k^2\left[3A_m^n \frac{\partial A_m^n}{\partial x}\frac{\partial f_m^n}{\partial x} + \frac{\partial A_m^n}{\partial t}\frac{\partial f_m^n}{\partial x}\right. \\ & + {A_m^n}^2 \frac{\partial^2 f_m^n}{\partial x^2} + A_m^n \frac{\partial B}{\partial x} f_m^n + (A_m^n B + B A_m^n)\frac{\partial f_m^n}{\partial x} \\ & + A_m^n \frac{\partial^2 A_m^n}{\partial x^2}\frac{\partial f_m^n}{\partial x} + (\frac{\partial A_m^n}{\partial x})^2 \frac{\partial f_m^n}{\partial x} \\ & \left. + B(B + 2\frac{\partial A_m^n}{\partial x})\frac{\partial f_m^n}{\partial x} + \frac{\partial^2 A_m^n}{\partial x \partial t}\frac{\partial f_m^n}{\partial x}\right] \end{aligned} \tag{4.43}$$

Considering the context discussed in Section 4.1 and Algorithm.1, where $A(x,t)$ is assumed to be dependent on both temperature and time during specific time intervals and $B$ remains constant while not being temperature-dependent, we have $\frac{\partial}{\partial t}A_m^n = \frac{\partial}{\partial t}R'^n$, $\frac{\partial}{\partial x}A_m^n = a$ and

$\frac{\partial}{\partial x}B = \frac{\partial}{\partial t}B = 0$. Therefore, the equation simplifies to:

$$\begin{aligned} f_m^{n+1} = f_m^n + kaf_m^n + kA(x,t)\frac{\partial}{\partial x}f_m^n + kBf_m^n \\ + \frac{1}{2}k^2\left[3A_m^n a\frac{\partial f_m^n}{\partial x} + \frac{\partial}{\partial t}R'^n\frac{\partial f_m^n}{\partial x}\right. \\ + {A_m^n}^2\frac{\partial^2 f_m^n}{\partial x^2} + A_m^n\frac{\partial B}{\partial x}f_m^n \\ + (A_m^n B + BA_m^n)\frac{\partial f_m^n}{\partial x} \\ \left. + (a)^2\frac{\partial f_m^n}{\partial x} + B(B+2a)\frac{\partial f_m^n}{\partial x}\right] \end{aligned} \tag{4.44}$$

Thus, equation (4.44) presents the numerical updating step for equations (4.9) to (4.12), with $\frac{\partial}{\partial x}f_m^n$ defined in (4.39) and $\frac{\partial^2}{\partial x^2}f_m^n$ in (4.40). Thus, solving a system analogous to Equation (4.38) becomes achievable using the previously computed matrices:

$$f_m^n = \begin{bmatrix} f_{00}(m,n) \\ f_{01}(m,n) \\ f_{10}(m,n) \\ f_{11}(m,n) \end{bmatrix} \quad B = \begin{bmatrix} -\alpha_o & \alpha_1 & 0 & 0 \\ \alpha_o & -\alpha_1 & 0 & 0 \\ 0 & 0 & -\alpha_o & \alpha_1 \\ 0 & 0 & \alpha_o & -\alpha_1 \end{bmatrix}$$

$$A_m^n = \begin{bmatrix} r_{00}(m) & 0 & 0 & 0 \\ 0 & r_{01}(m) & 0 & 0 \\ 0 & 0 & r_{10}(m,n) & 0 \\ 0 & 0 & 0 & r_{11}(m,n) \end{bmatrix}$$

### 4.4.3 Boundary Conditions

As discussed in Section 4.2, specific boundary conditions are imposed in accordance with the Kolmogorov equation. The initial focus is on addressing the absorbing boundaries outlined in (4.20) and (4.21). It is worth noting that (4.21) is considered logically inactive, as previously indicated in Section 4.2. Conversely, with reference to (4.20) and Table 4.3, this boundary condition may necessitate setting:

$$f_{11}(T_+,t) = 0 \quad \text{if} \quad 0 \le r_{11}(T_+,t) \tag{4.45}$$

In this scenario, the probability current of $f_{11}$ moves from right to left rather than left to right which will also affect the probability conservation boundary conditions in (4.18) and (4.19). In accordance with (4.18) and (4.19), at the lower temperature dead band $T_-$, all probability current flowing out of $f_{00}(T_-, t)$ and $f_{01}(T_-, t)$ will enter $f_{10}(T_-, t)$ and $f_{11}(T_-, t)$, respectively. Similarly, at the upper temperature dead band $T_+$, all probability current escaping from $f_{10}(T_+, t)$ and $f_{11}(T_+, t)$ will enter $f_{00}(T_+, t)$ and $f_{01}(T_+, t)$, respectively. This behavior is illustrated as follows:

$$f_{10}(T_-, t + \Delta t) = f_{10}(T_- - \Delta x, t) - \frac{r_{00}(T_-, t)}{r_{10}(T_-, t)} \cdot f_{00}(T_-, t) \tag{4.46}$$

$$f_{00}(T_+, t + \Delta t) = -\frac{r_{10}(T_+, t)}{r_{00}(T_+, t)} \cdot f_{10}(T_+, t) \tag{4.47}$$

$$f_{01}(T_+, t + \Delta t) = -\frac{r_{01}(T_+, t)}{r_{11}(T_+, t)} \cdot f_{01}(T_+, t) \tag{4.48}$$

For $f_{11}$ based on the sign of $r_{11}$, this probability will be computed as follows:

$$f_{11}(T_-, t + \Delta t) = f_{11}(T_-, t) - \frac{r_{01}(T_-, t)}{r_{11}(T_-, t)} \cdot f_{01}(T_-, t) \tag{4.49}$$
$$\text{if} \quad r_{11}(T_+, t) \leq 0$$

$$f_{11}(T_- - \Delta x, t + \Delta t) = f_{11}(T_- - \Delta x, t) - \frac{r_{01}(T_-, t)}{r_{11}(T_-, t)} \cdot f_{01}(T_-, t) \tag{4.50}$$
$$\text{if} \quad 0 \leq r_{11}(T_+, t)$$

### 4.4.4 Validation of Lax-Wendroff Scheme via Simulations

To validate the accuracy of the evolution equations and the proposed numerical simulation approach, we compare the outcomes with Monte Carlo simulations, as illustrated in Fig 4.6. The behavior observed in the Kolmogorov simulation closely aligns with the Monte Carlo results, with the latter being contingent on the size of the sample used (which amounted to 100,000 in the aforementioned simulation). As the Monte Carlo sample size increases, the alignment between the two simulations is expected to improve. It is important to note, however, that the computational time required for the Monte Carlo simulation significantly exceeds that of the PDE-based difference approximation.

In Algorithm 2, the Monte Carlo simulation's logic is fully described, with i) $x(i, j)$ representing the temperature of the $j - th$ house at time step $i$, ii) $q(i, j)$ as the binary demand state variable of house $j$ at time step $i$, and iii) $m(i, j)$ as the binary heating element state variable of the $j - th$ house at time step $i$. The evolution equations and the proposed nu-

merical simulation approach were applied using two distinct schemes, characterized by the sign of $r_{11}$ as previously outlined, which are summarized in Table 4.4 ($0<r_{11}$) and Table 4.5 ($r_{11} \leq 0$) [27].

| | |
|---|---|
| $\alpha_0 \frac{1}{min}$ | 0.042. |
| $\alpha_1(\frac{1}{min})$ | 0.61. |
| $R(\frac{^\circ C}{min.W})$ | 0.2122. |
| $a(\frac{1}{min})$ | 0.002. |
| $A(\frac{^\circ C}{min})$ | 0.81. |
| $T_a(^\circ C)$ | 22. |
| $T_-(^\circ C)$ | 60. |
| $T_+(^\circ C)$ | 65. |
| $T_D(min)$ | 500. |

Table 4.4 Parameter Values for Simulation 1

| | |
|---|---|
| $\alpha_0 \frac{1}{min}$ | 0.021. |
| $\alpha_1(\frac{1}{min})$ | 0.2. |
| $R(\frac{^\circ C}{min.W})$ | 0.4046. |
| $a(\frac{1}{min})$ | 0.002. |
| $A(\frac{^\circ C}{min})$ | 0.28. |
| $T_a(^\circ C)$ | 22. |
| $T_-(^\circ C)$ | 60. |
| $T_+(^\circ C)$ | 65. |
| $T_D(min)$ | 500. |

Table 4.5 Additional Parameter Values for Simulation 2

In both examples, the results in Fig. 4.6 clearly indicate a close correlation between Monte Carlo simulations and Kolmogorov evolution-based simulations.

The error in the total fraction of the ON state in these examples are just 2% and 1.5% respectively, underscoring the precision of our model when compared to the actual behavior of the aggregated EWHs.

**Algorithm 2:** Monte Carlo Simulation Algorithm

```
for i = 1 to T do
    for j = 1 to House Numbers do
        if x(i,j) < T_- then
            m(i+1,j) = 1;
        end
        else if T_+ < x(i,j) then
            m(i+1,j) = 0;
        end
        else
            m(i+1,j) = m(i,j);
        end
        if q(i,j) == 0 then
            if randon_number < α_0 · dt then
                q(i+1,j) = 1;
            end
            else
                q(i+1,j) = 0;
            end
        end
        else if q(i,j) == 1 then
            rand_num = rand(1);
            if rand_num < α_1 · dt then
                q(i+1,j) = 0;
            end
            else
                q(i+1,j) = 1;
            end
        end
        x(i+1,j) = x(i,j) − a · (x(i,j) − xa) · dt − q(i,j) · A · dt + R · m(i,j) · dt;
    end
end
```

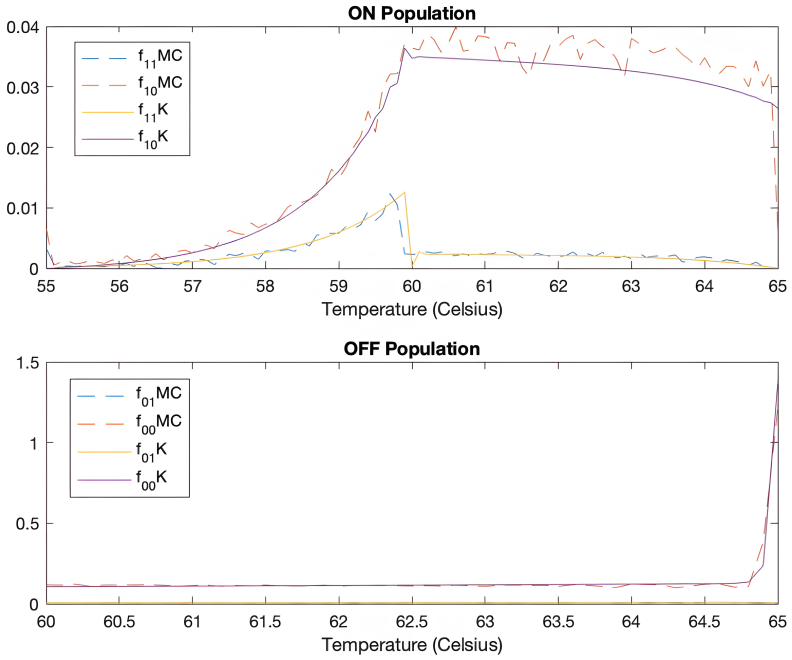


Figure 4.5 ON and OFF state density functions calculated by Kolmogorov equations and Monte Carlo simulation with respect to the parameters specified in Table 4.4 ($r_{11}(x_+, t) > 0$) when the system reaches steady state.

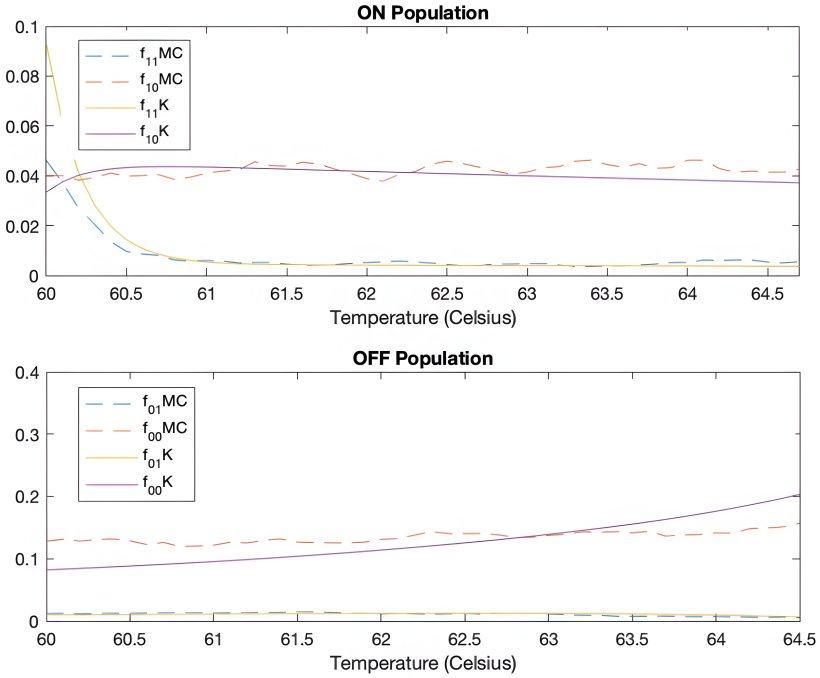


Figure 4.6 ON and OFF state density functions calculated by Kolmogorov equations and Monte Carlo simulation with respect to the parameters specified in Table 4.5 ($r_{11}(x_+, t) \leq 0$) when the system reaches steady state.

# CHAPTER 5 Enhancing Primary Frequency Regulation: Analyzing the Effects of Different EWH Control Schemes Implementation

In this chapter, we leverage the model derived in Section 4.4 to investigate the potential utilization of EWHs as a demand response energy storage solution in response to various electricity demand perturbations. We consider a Non-reheat Steam Power Plant which consists of 10 similar single typical large generator unit as previously described, boasting a nominal capacity of 1000 MW in total. Currently, each generator operates under a 90 MW load, with our chosen reference power set at $P_{basis} = 900MW{:=}1p.u.$

Additionally, EWHs account for approximately 30% of average domestic demand loads [30]. The group of EWHs is considered homogeneous and the EWHs are rated at 4.5 KW. Furthermore, about 30% of the total load is attributed to domestic consumption [17]. While we assume that only 33% of these EWHs are enlisted for Demand Response, the findings can be extrapolated to accommodate larger DR participation rates. Thus, around 3% of the total load consists of EWHs engaged in Demand Response. Throughout the conducted experiments, the collective EWHs were employed with the following set of parameters as they have been defined and detailed in section 4.3: $A = 0.81\frac{^\circ C}{min}$, $\alpha_1 = 0.52\frac{1}{min}$, $\alpha_2 = 0.041\frac{1}{min}$, $a = 0.193 \times 10^{-4} min^{-1}$ and $R = 0.2122\frac{^\circ C}{min.W}$. Furthermore, all EWHs have been configured to operate within a thermostat deadband ranging from $60^\circ C$ to $65^\circ C$ and ambient temperature of $22^\circ C$.

In Fig. 5.1, the frequency is observed to remain constant at 60 Hz, indicating an assumed initial perfect balance between power generation and power demand. Additionally, Fig. 5.2 illustrates the percentage of ON EWHs, under normal thermostatic control, settling to a steady state of approximately 47.8%. Finally, in Fig. 5.3, the total power generated in the power system and the contribution of aggregated EWHs, planned to be used in DR in future, are depicted, amounting to around 0.03 p.u when everything is in balance, as discussed earlier.

In the forthcoming experiments, we will utilize the system characterized by the aforementioned properties. By demonstrating EWHs' capacity to serve as an alternative source of frequency regulation capacity, the investigation aims to determine how effectively EWHs can participate in DR programs. There could be significant environmental benefits to this operational shift, including the reduction of CO2 emissions. As an additional benefit, this transition is aligned with environmental sustainability goals and offers the added benefit of permitting synchronous machines to perform a wide variety of alternative functions. By

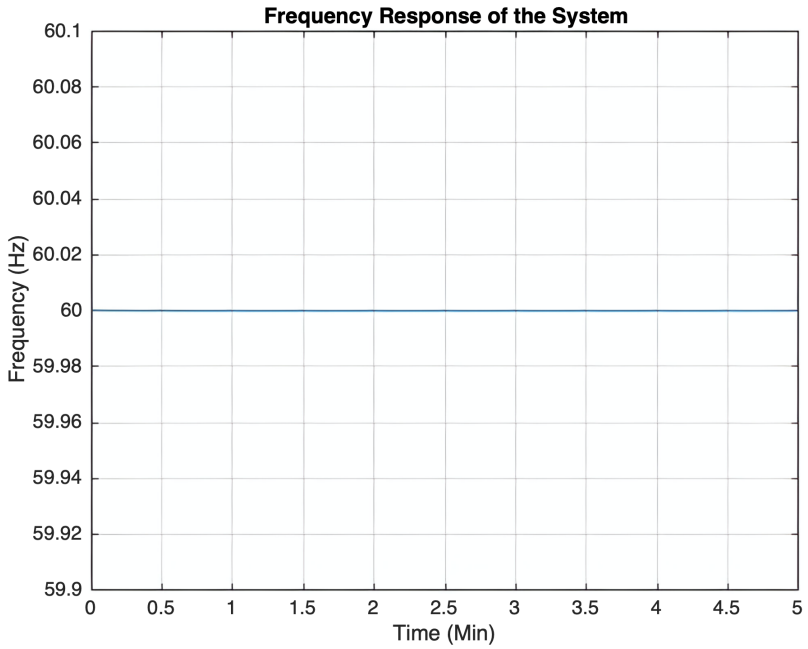


Figure 5.1 Frequency response of the system, showing the the balance in generated power and total demand.

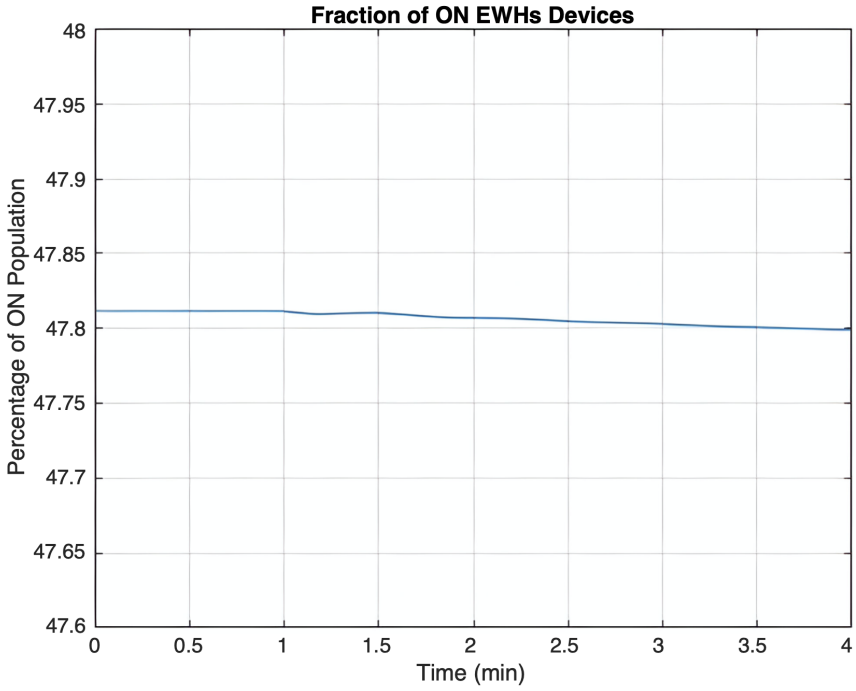


Figure 5.2 Percentage of ON population of EWHs over time, illustrating the dynamic behavior of EWHs.

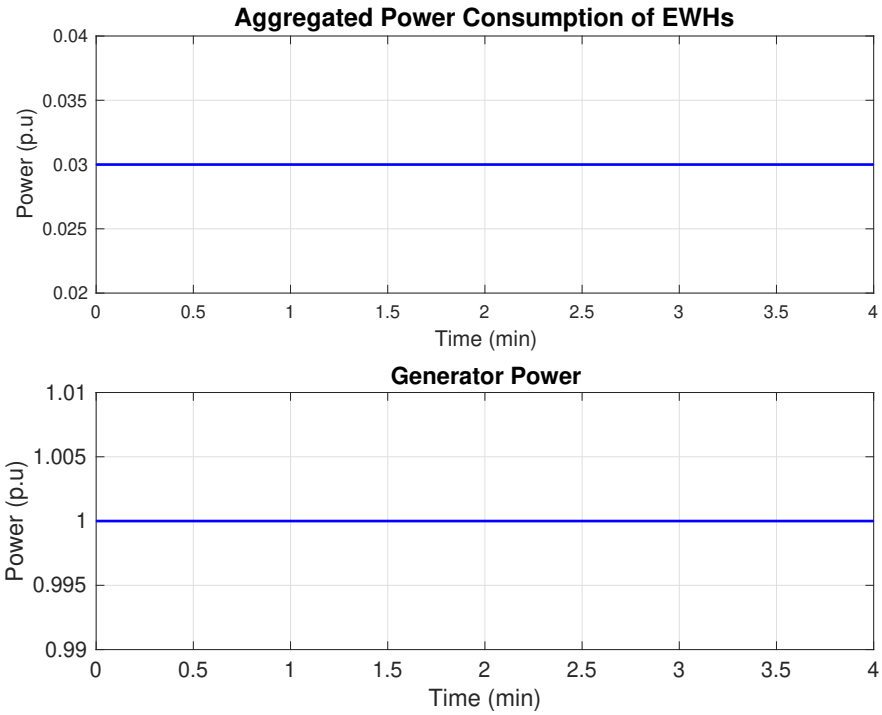


Figure 5.3 Upper: Aggregated power consumption of EWH with an offset of 0.03. Lower: Total power generated from the power system for primary frequency regulation during a Demand Response (DR) scenario.

reallocating resources strategically, the energy system becomes more flexible and efficient, improving its ability to adapt to unforeseen events.

When exploring the potential of a large group of EWHs to substitute for synchronous machines in primary frequency regulation functions, it is important to try to simulate as closely as possible realistic load perturbations that an actual power system has to smooth out to keep frequency within tight bounds. For this purpose, based on a frequency excursions data set obtained from [31], we construct synthetic load perturbations which when applied to our simulated power system would produce similar frequency oscillations under primary frequency regulation.

## 5.1 Fourier-Based Synthetic Candidate Load Perturbations Extraction from Real Frequency Data

In this context, we have employed real-time frequency data, visualized in Fig. 5.4, which represents the grid's frequency response to a perturbations in a 5-minute period from [31]. These frequency variations will subsequently be ascribed through transfer function inversion to candidate load perturbation trajectories. The latter will then serve as the basis for assessing the effectiveness of DR as a source of primary frequency regulation under normal-like conditions.

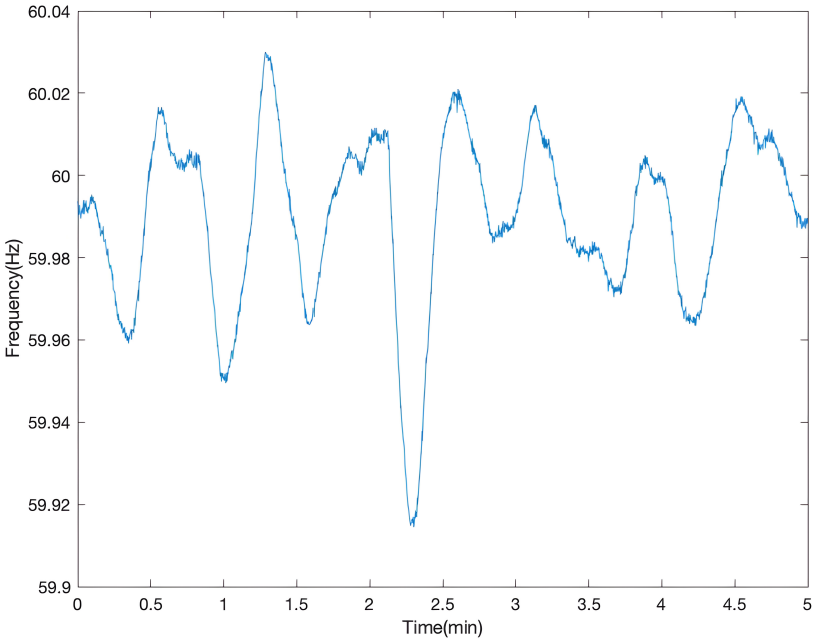


Figure 5.4 Temporal Evolution of the Frequency for a Physical Generator

The first step is to recreate the load oscillations that caused the frequency perturbation in Fig 5.4 so that we can apply them in future experiments. In order to achieve this, we initiate a comprehensive Fourier spectrum analysis, examining the composition of sinusoidal components that collectively form the specified signal. To begin, the signal's frequency content and spectral characteristics must be thoroughly analyzed. This is followed by the determination of the appropriate amplitudes associated with each sinusoidal component. This process ensures a thorough understanding of the signal's harmonic structure, facilitating precise amplitude assignments to effectively reconstruct the load oscillatory trajectory behind the signal under consideration.

The analysis involved computing the Fast Fourier Transform (FFT) of the signal, resulting in the Power Spectral Density (PSD) plot in Fig 5.5. The PSD plot provides a visual representation of the signal's frequency content, revealing the magnitudes of different frequency components present in the signal. The x-axis of the plot represents the frequency in Hz, while the y-axis represents the Power, indicating the contribution of each frequency component to the overall signal power.

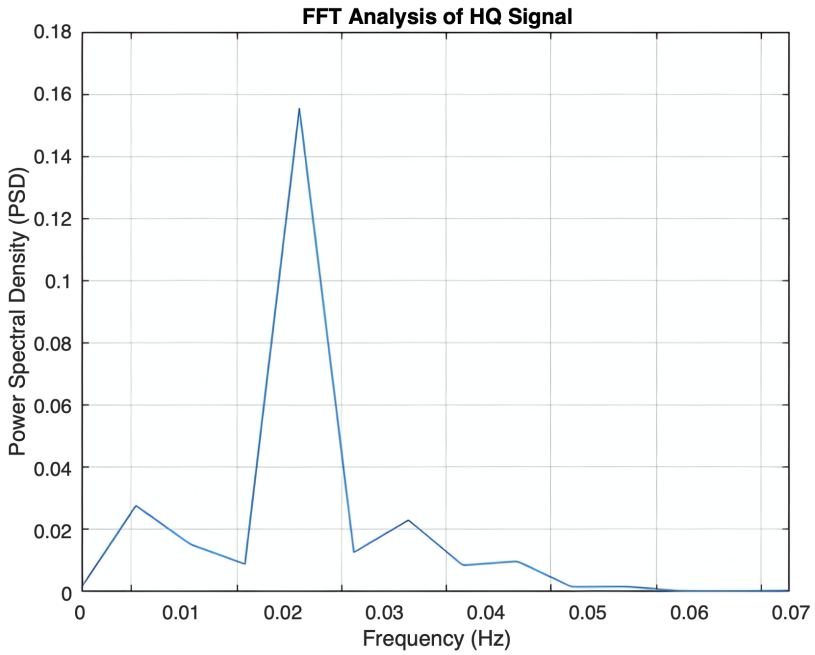


Figure 5.5 FFT Analysis of the Main Perturbation Signal. The plot illustrates the Power Spectral Density (PSD) of the signal, revealing frequency components and their magnitudes.

Based on the information presented in Figure 5.5, it can be assumed that the initial signal was mainly composed of approximately four distinct sinusoidal components with frequencies of 0.001039, 0.001534, 0.02598, 0.03118 adn 0.03638 Hz. After experimenting with various amplitudes, an optimized approximation for the perturbation input has been determined, as illustrated in Fig 5.7. Furthermore, in Fig 5.6, the resemblance between the frequency response of the main signal and the response of the newly constructed signal is evident. Also, in Figure 5.8, it is evident that the FFT diagram of the frequency response for the constructed signal in Figure 5.7 highlights the same frequencies with relative magnitudes.

Having identified reasonably realistic test load perturbations, we now proceed to design a droop controller for the EWHs to produce the hoped for primary frequency regulation action.

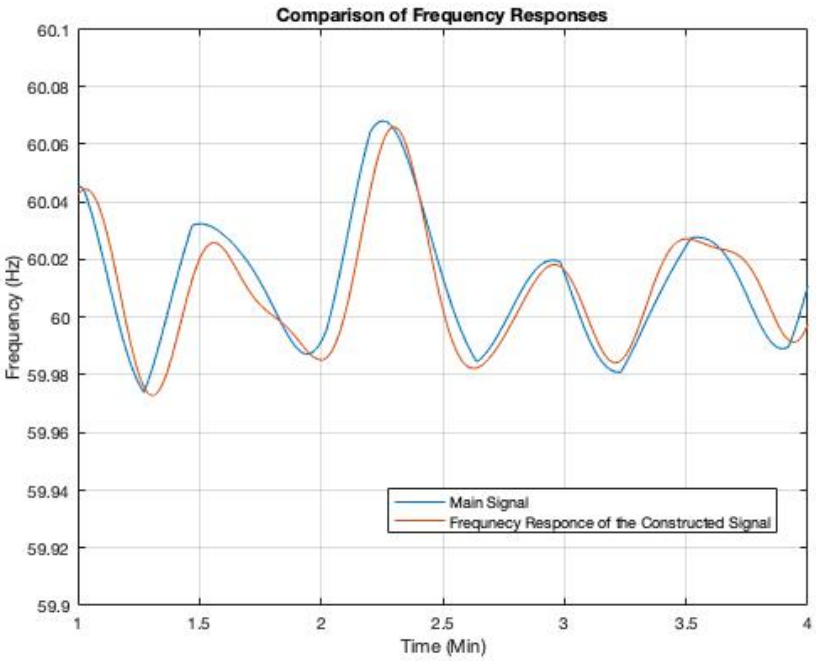


Figure 5.6 Comparison of the frequency responses between the main signal and a constructed signal based on FFT analysis. The blue curve represents the frequency response of the main signal (5.4), while the red curve depicts the response obtained by constructing a signal from FFT analysis of the main signal. The plot is limited to the frequency range of interest, and amplitude values are scaled accordingly.

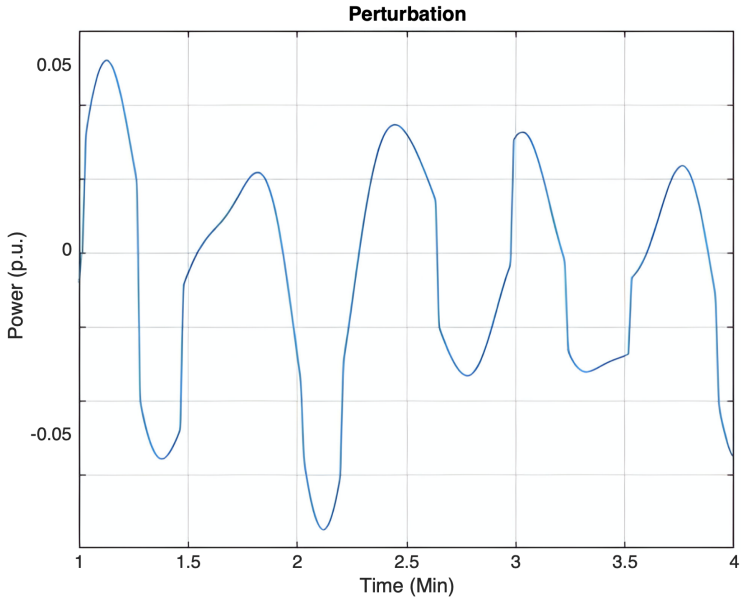


Figure 5.7 Perturbation signal, constructed from the FFT analysis of the main in signal in 5.4

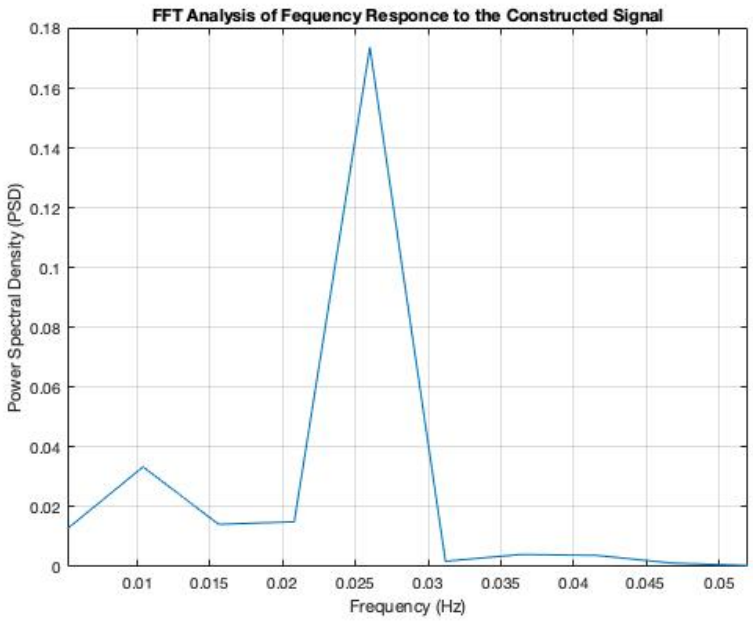


Figure 5.8 FFT Analysis of the Constructed Signal. The plot illustrates the Power Spectral Density (PSD) of the signal, revealing frequency components and their magnitudes. The analysis provides insights into the signal's frequency composition and spectral characteristics.

## 5.2 Exploring the Impact of the Choice of EWHs Droop Constant

In our model, we implement the droop technique in the heating elements of each EWH to dynamically adjust their power consumption based on the requirements for frequency regulation, as discussed in section 3.2 in chapter 3. This approach empowers individual EWHs to monitor local frequency deviations and modulate their power consumption accordingly. This strategy not only ensures responsiveness but also facilitates seamless matching of power demand.

The chief advantage of this control scheme is its rapid response time which is partly due to its decentralized nature, enabling application within fractions of a second, a critical attribute in PFR. Moreover, its implementation is characterized by simplicity, avoiding the complexities associated with centralized models that require complex communication systems. This essentially reproduces the significant advantage of primary frequency regulation as a decentralized control scheme.

An essential aspect to underline is that frequency deviation ($\Delta f$) is a signal widely observed in the power system and that will be observed across all devices. When grid perturbations lead to a frequency imbalance, it triggers individual responses from all EWHs. In essence, EWHs fine-tune their power consumption globally to counteract the imbalance.

Given that the water heating mechanism of EWHs is electric, this allows fast changes in power. This permits great flexibility in the setting of the droop constant of EWHs which could be very small value. However, through simulations, it becomes evident that the droop constant cannot be arbitrarily small. This limitation arises because multiple generators or EWHs contribute to the frequency regulation signal, and the characteristics of the power system area significantly influence the outcomes. In essence, the proportional control nature of the system implies that being too aggressive in setting a small droop constant may induce oscillatory behavior, even in classical PFR.

To identify an optimal value for the EWHs droop constant, extensive simulations were conducted where a 0.015 p.u constant perturbation has been added to the system at $t = 2min$, leading to the selection of a value of 0.00001 for the droop constant of each EWH. This value strikes a balance, being sufficiently small to ensure rapid responsiveness of the EWHs while avoiding excessive aggressiveness in their consumption behavior to track the load. Indeed, as shown in Fig 5.9, when the droop constant for EWHs is set to values smaller than 0.00001, the devices tend to act as overly aggressive proportional controllers. This results in rapid chattering of EWH power consumption to follow very small frequency deviations, which is unnecessary.

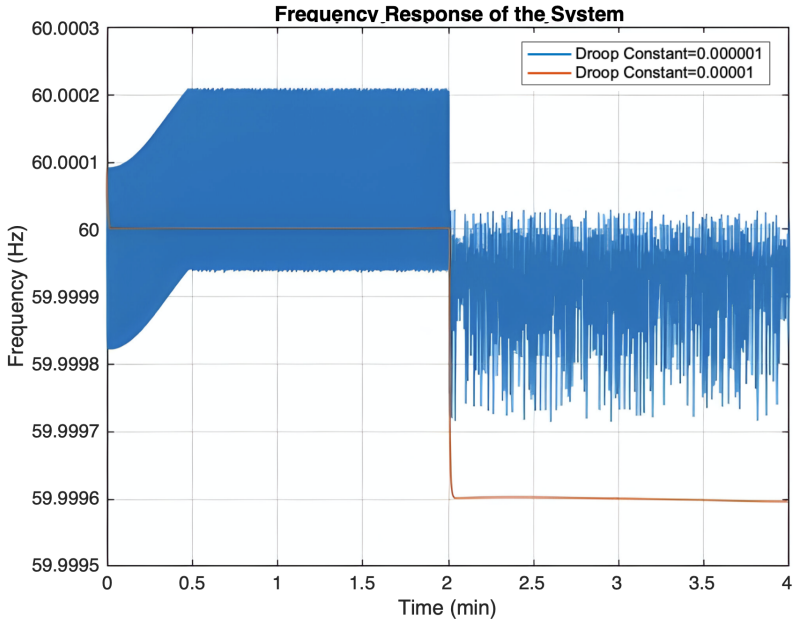


Figure 5.9 A comparison of two EWH droop constants. The droop constant represented by the blue color range is smaller, acting as an overly aggressive proportional controller.

Considering previous observations, a small droop constant becomes necessary when demand and supply in the system remain and substantially out of sync for a prolonged period of time. It is noteworthy that the determination of a "high" value in this context is contingent upon the proportionality of the aggregate EWHs' contribution to the system. For instance, in Fig. 5.9, the perturbation magnitude amounted to half of the total EWHs consumption, corresponding to $0.03p.u.$ In the presence of perturbations of such magnitude, the droop constant governs the operation of each device, possibly compelling them to operate at either minimum or maximum consumption levels. As illustrated in Fig. 5.10, the droop mechanism effectively induces a rapid reduction in consumption to the minimum level for each device.

In previous experiments, droop constant values set to small values have been effective in mitigating big perturbations. However, it may not be suitable to address all perturbations. For instance, when confronted with oscillatory or minor perturbations, employing larger droop constants could potentially offer greater smoothness.

As an illustrative case, we employed the perturbation signal constructed in the previous section (Fig 5.7), setting the droop constants to 0.00001 and 0.001 respectively. As anticipated, the system featuring the smaller droop constant exhibited slightly improved frequency regulation (Fig 5.11). However, as evidenced in Fig 5.12, the droop mechanism within each individual EWH device operated similarly to an aggressive proportional controller, causing

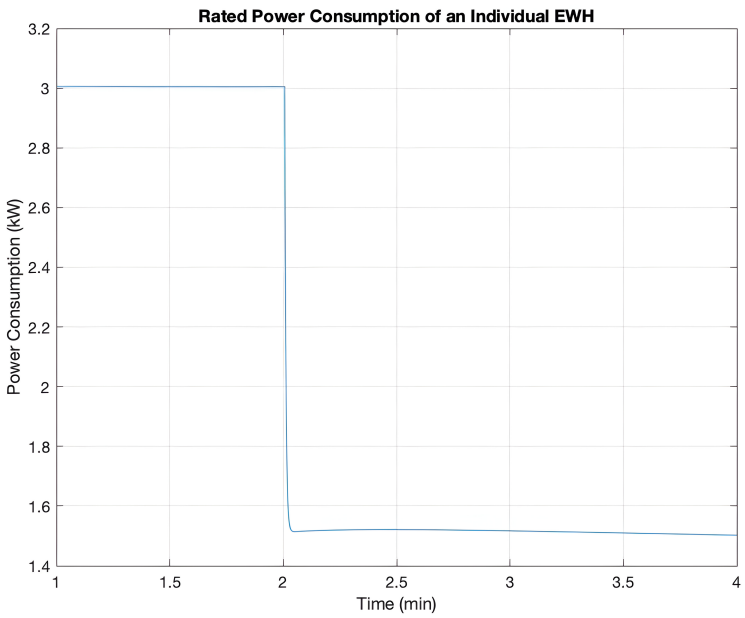


Figure 5.10 Power consumption of individual EWH devices in response to a $0.015p.u$ perturbation. The droop mechanism within each device is evident, causing a reduction in consumption to its minimum level due to the significant magnitude of the perturbation.

each device to alternately consume minimum or maximum power at each time step. Conversely, in the system with the larger droop constant, although there was a slightly inferior frequency regulation outcome (with mean frequency of 60.003 against 60.001 with smaller droop constant), it effectively mitigated the devices' tendency to switch between minimum and maximum power consumption levels aggressively, as illustrated in Fig 5.12.

In conclusion, this study has demonstrated that in scenarios characterized by significant and continuous perturbations necessitating comprehensive support from DR, smaller droop constants prove advantageous. These smaller constants enhance system responsiveness, enabling quicker adjustments to meet demand fluctuations. Conversely, in situations involving oscillatory perturbations requiring frequent changes in device consumption rate, larger droop constants offer utility. Such values allow for smoother device operation by moderating aggressive shifts between minimum and maximum power consumption levels.

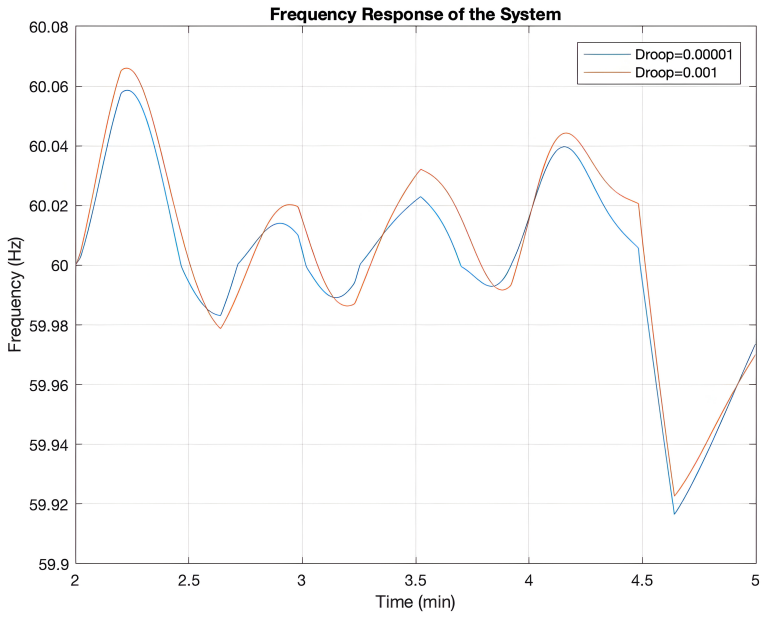


Figure 5.11 Frequency response of two systems with different droop constants to an oscillatory perturbation, as depicted in Fig 5.7.

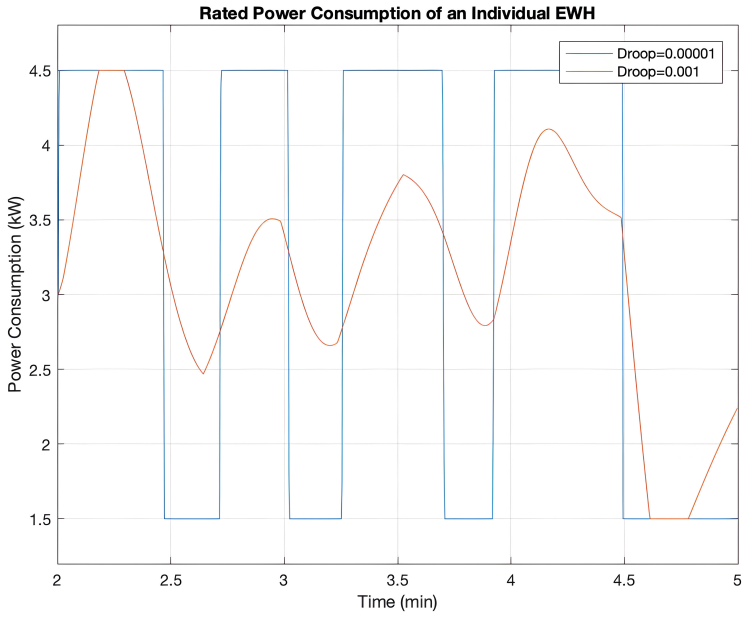


Figure 5.12 Power consumption of individual EWH devices in response to an oscillatory perturbation, as depicted in Fig 5.7, showing how droop mechanism is working. The system in blue, employing a smaller droop constant prompts the devices to swiftly alternate between maximum and minimum consumption levels, displaying aggressive behavior. Conversely, the system represented by the orange line operates more smoothly under the same conditions.

## 5.3 Exploring EWH with Droop Control as Alternatives for Area-Wide Frequency Deviation Responses

In this section, we delve into an investigation of the capacity of groups of EWHs organized under a droop control mode. Our focus is on their ability to effectively respond to area-wide frequency deviations. The goal is to explore whether these organized groups of EWHs can not only mimic but also serve as faster responding substitutes for groups of dedicated synchronous machines utilized for Automatic Generation Control (AGC). This inquiry is motivated by the potential of leveraging distributed EWHs in grid support services for frequency regulation in power systems.

To achieve this, three scenarios have been designed to simulate various frequency regulation situations, aiming to explore the impact of EWHs on frequency restoration.

- **Sudden Increase or Decrease in Demand:** Investigate changes in demand ranging from 0.015% to 0.05%.
- **Synthetic Real-Time Like Perturbation Data:** Investigating the system's response under the perturbation generated in Section 5.1.

### 5.3.1 Sudden Increase or Decrease in Demand

In this simulation, we explore the response of EWHs to multiple sustained changes in demand, namely 0.015%, 0.03% and 0.05% p.u. The objective is to evaluate the EWHs' capacity to adjust their consumption to balance fluctuations in demand. As evident in Fig 5.13 ($0.015\% p.u$ load change), the system employing DR shows significantly improved frequency regulation compared to the system without DR and just benefiting from PFR. To explore the limitations of EWHs in assisting the grid with frequency regulation, additional simulations were conducted with varying sizes of perturbations ($\Delta P_l$).

In Figure 5.14, in the simulation with $\Delta P_l = 0.03$, although the devices could adjust their consumption to address the power loss, the perturbation was significant enough to require a quicker reaction time to minimize the error in the frequency response. This can be observed in Figure 5.17, where the droop mechanism causes the EWHs to operate at their minimum power consumption rate more rapidly when facing a larger perturbation. However the rapid increase in the fraction of ON populations over time can be seen, in Fig. 5.15. To understand this behavior, it is crucial to examine the response of EWHs during this process. When the surge in demand prompts EWHs to decrease their power consumption, the heating rate of ON devices decreases and the water temperature in ON devices initiates a decline. In the

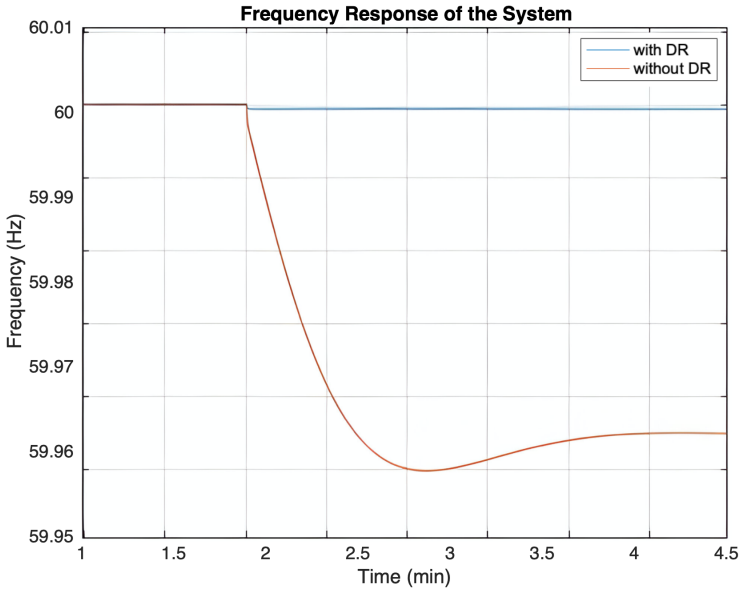


Figure 5.13 A comparison of the system's response to a 0.015 p.u perturbation with only the utilization of EWHs as DR. In both cases PFR has been used by the generation units.

meantime, devices that were OFF, cool down enough to join the ON population. As a result, over time, more devices join the ON population, yet they are unable to reach the upper thermostat deadband temperature $T_+ = 65°\text{C}$. This inability is a result of the droop-control induced reduction in power consumption of the devices, aimed at slowing down frequency decrease. In Fig 5.16, it appears that for $\Delta P_l = 0.03$, EWHs, as a result of droop-control action, have adjusted their consumption to the *minimum droop power setting*. This is due to the combined effects of the relatively important sizes of the load perturbations together with the high sensitivity of the droop controller as designed.

An intriguing observation derived from this experiment is highlighted in Fig 5.16, where a sudden surge in demand prompted EWHs to lower their power consumption, effectively entering a state of power starvation. Operating below their nominal power rates, it can be predicted that over time, an escalating number of EWHs will transition to the ON state. This arises from the necessity to maintain water temperature within acceptable temperature ranges. Furthermore, these units remain unable to enter the OFF state due to their commitment to DR activities.

The integration of these new EWHs into the ON state will lead to a higher overall power consumption by the aggregated EWHs, consequently reducing the available capacity for meaningful DR contributions. However, this effect may be challenging to detect in this simulation, as based on Fig 5.15, there is only a 1.8% increase in the ON state density layer,

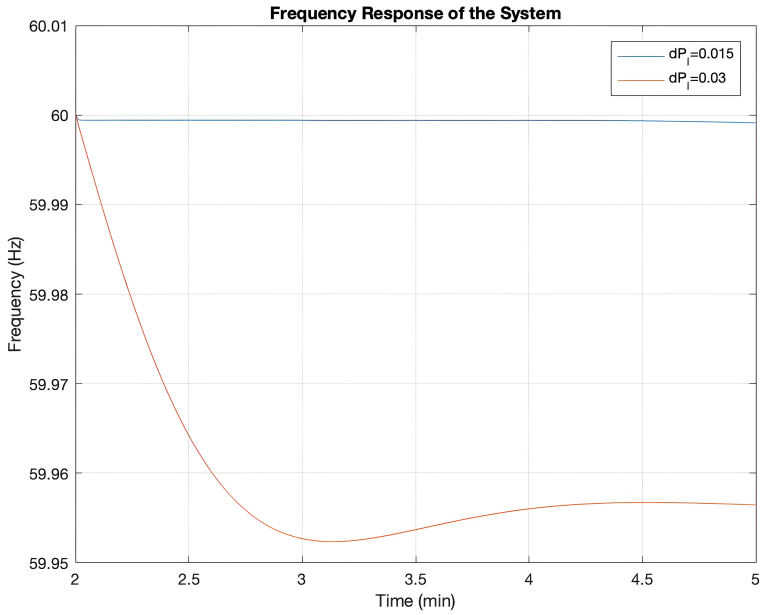


Figure 5.14 Combined frequency response of the power system with PFR and DR under three different load perturbation sizes at t=2 minutes.

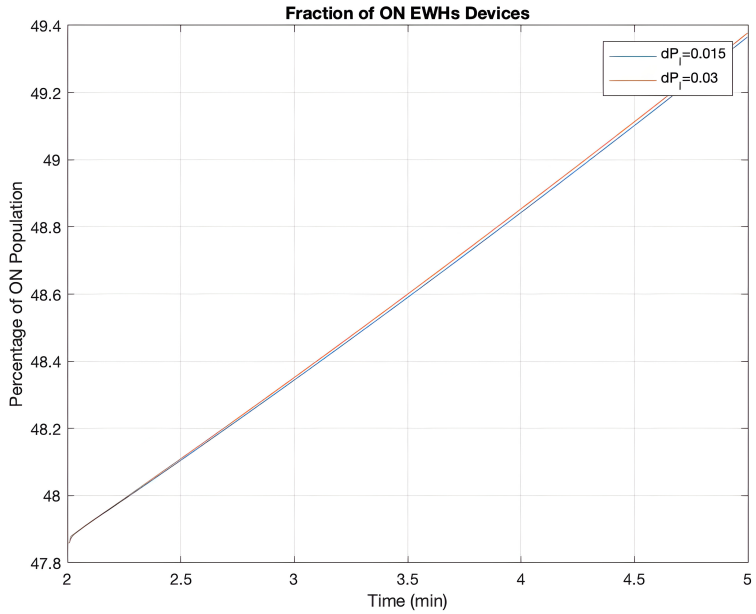


Figure 5.15 Dynamic behavior of the fraction of ON-State EWHs under distinct load perturbations at t=2 minutes.

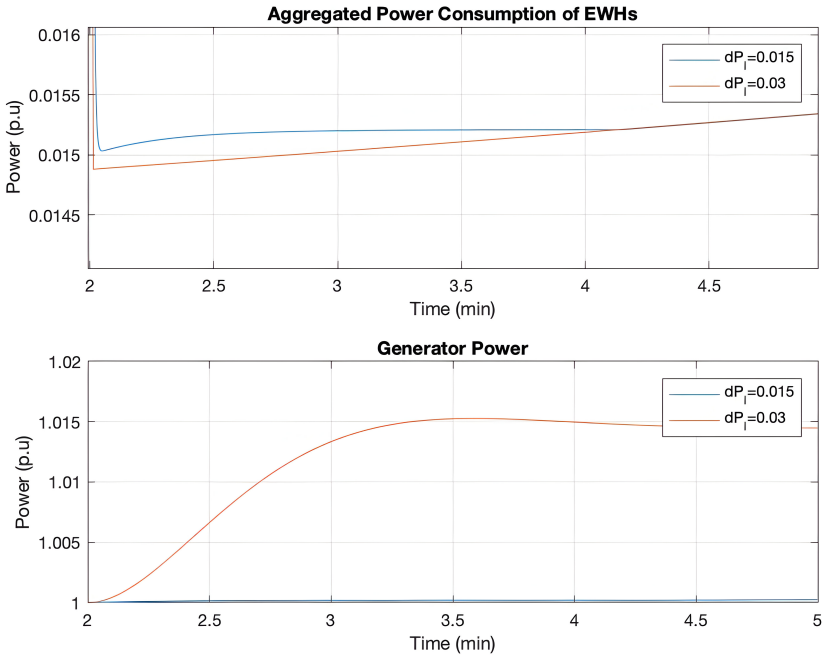


Figure 5.16 Upper: Power consumption of aggregated EWHs under three distinct load perturbations. Lower: Total power generated by generators for the same set of perturbations.

which is too subtle to be noticeable in aggregated power consumption of EWHs illustrated by Fig 5.16.

This effect is demonstrated through a simulation conducted in the same setting, where the results are presented in Fig 5.18 to Fig 5.20. The simulation involves a consistent increase in demand ($\Delta P_l$) of 0.015 p.u added to the grid at $t = 1$ min. Fig 5.18 illustrates that the droop system in EWHs operates to make each device function at its lowest power consumption level, represented by $R' = 1.5$ KW in our simulation due to Algorithm 1. As mentioned earlier, this leads to a higher number of ON devices, as evident in Fig 5.19. The total fraction of ON devices increases from 47.8 to almost 53% in less than 10 minutes. This rise in ON devices results in reduced power leverage for frequency regulation. In Fig 5.20, it is observed that the frequency remains nearly stable until approximately $t = 3$, after which it suddenly begins to decline.

Consequently, the findings underscore the need for caution when adjusting EWHs power consumption set points. While they prove to be effective tools in mitigating sudden perturbations, the persistency of their contribution is limited in time. Indeed, as time progresses, their capacity to dynamically reduce or increase total consumption is influenced, thus bringing to light the importance of strategic considerations in managing these set points and time

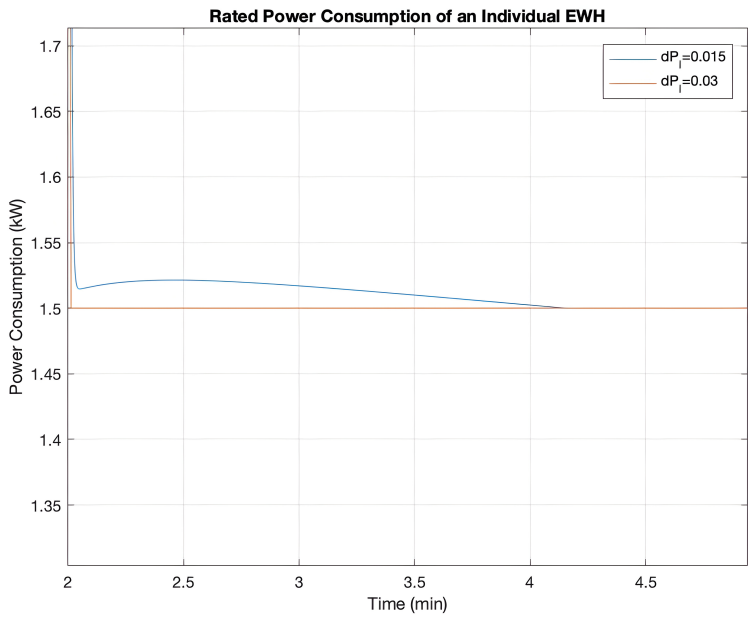


Figure 5.17 Power consumption of each EWHs in relation to its droop characteristic and frequency deviation signal under multiple perturbations. This figure illustrates how the droop mechanism in each individual device adjusts the power consumption to meet the DR requests.

of operations.

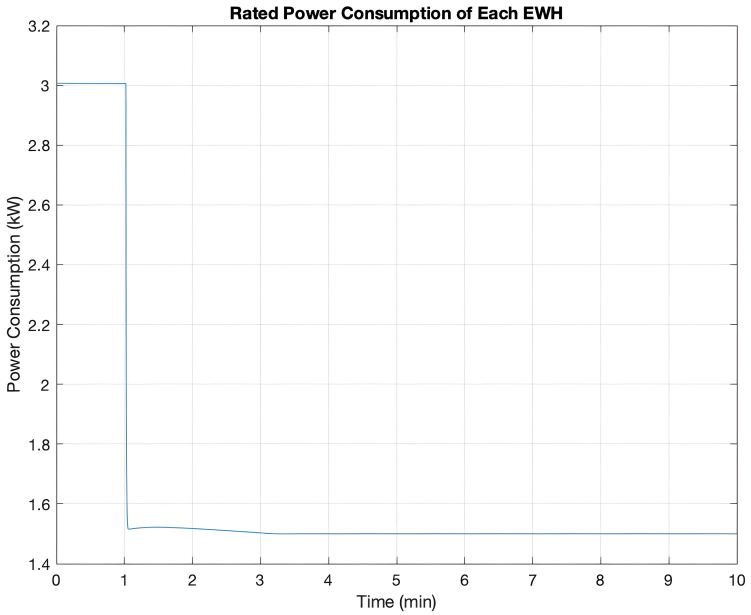


Figure 5.18 Power consumed by each EWH in response to a 0.015 p.u perturbation introduced to the grid at $t = 1$. The impact of the droop system implemented in each device is evident, as it prompts the EWHs to decrease their power consumption in reaction to the perturbation.

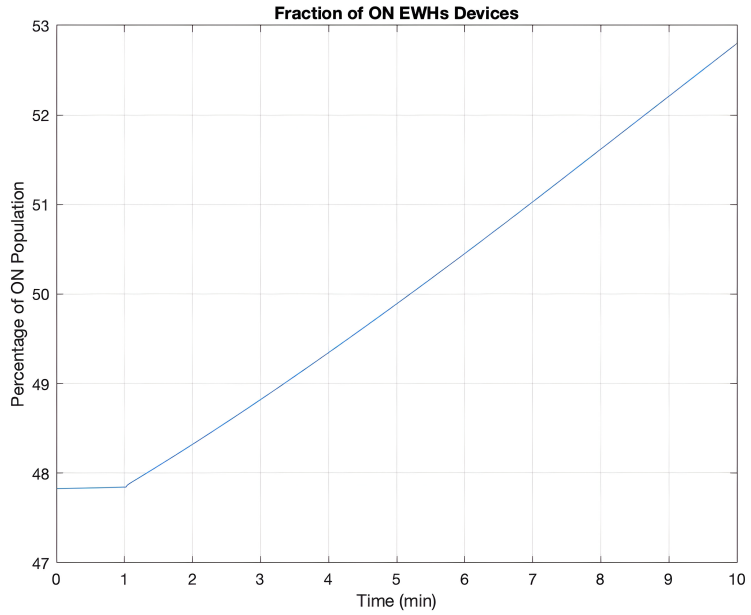


Figure 5.19 Evolution of the fraction of ON devices over time. The increasing trend is notable, indicating that the EWHs, having experienced a period of deprivation, are progressively transitioning to the ON state.

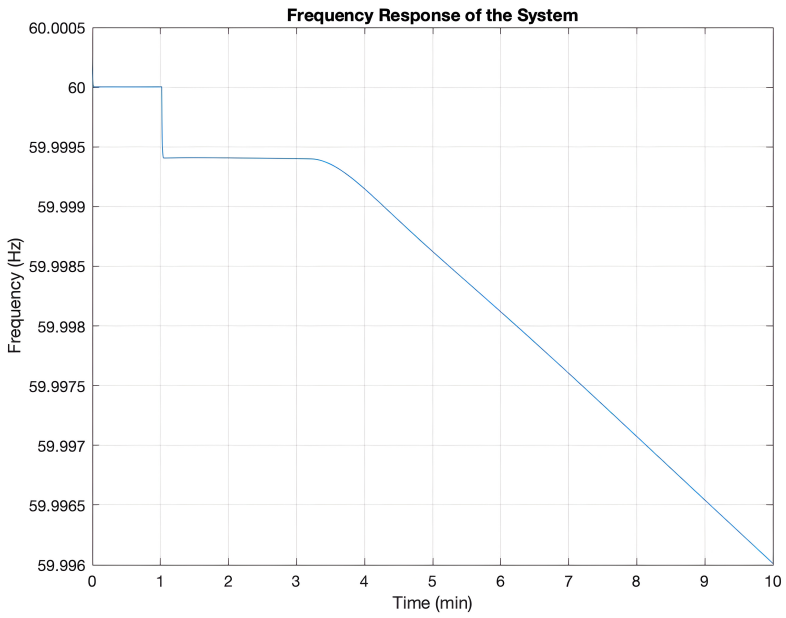


Figure 5.20 Grid frequency response to a 0.015 p.u perturbation. The rise in the number of ON devices, induced by the power starvation resulting from the droop system in each device, causes the frequency, which remained relatively stable for a while, to drop at $t = 3$.

### 5.3.2 Synthetic Real-time Like Perturbation Data

In this subsection, we conducted a simulation to analyze the system's response to the synthetic real-time like data constructed in Section 5.1. The purpose of this study is to evaluate the effectiveness and capabilities of DR achieved with droop control of EWHs and frequency regulation of generator units. Here as discussed earlier in section 5.2, the droop constant for EWHs has been set to 0.001, to prevent the devices to act too aggressively.

As shown in Fig 5.21, the use of DR , in conjunction with existing synchronous machine-based PFR, has significantly improved the frequency response of the system to perturbations, with the mean frequency under DR being 60.006 and standard deviation of $6.5 \times 10^{-4}$ compared to 60.018 and standard deviation of $9.8 \times 10^{-4}$ without DR. This improvement is achieved by adjusting the power consumption of all EWHs via droop control. The impact on the population of ON devices is displayed in Fig 5.22. One advantage of load induced sinusoidal frequency perturbations is their oscillatory behavior, which helps prevent sudden and continuous increases or decreases in the number of ON-state devices, as observed in Fig 5.15. Furthermore, in Fig 5.23, it appears that the introduction of DR, by helping to limit the size of frequency oscillations has in turn resulted in smaller magnitude power oscillations for generators, thus helping to reduce the associated wear and tear on these machines. In Figure 5.24, the impact of the droop mechanism in each individual EWH on the device's power consumption to meet frequency regulation requirements is evident. The system, benefiting from DR, exhibits an oscillatory behavior in power consumption to align with frequency perturbations.

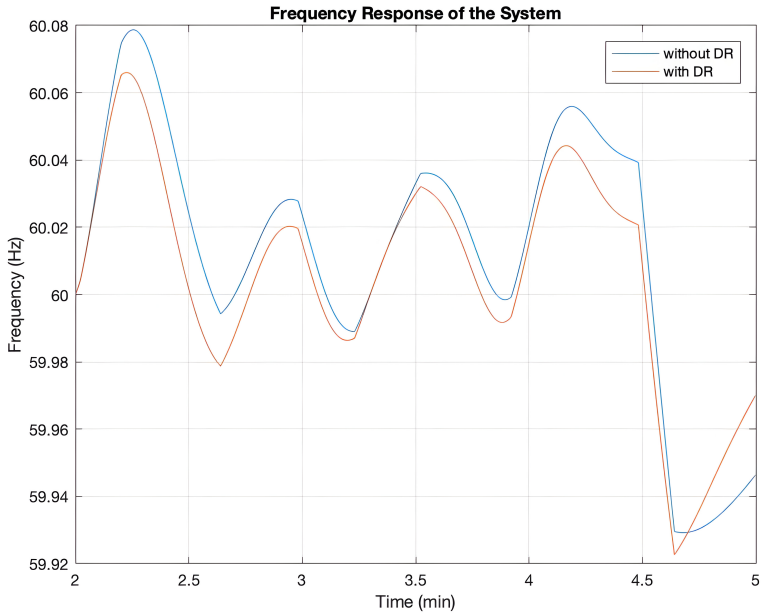


Figure 5.21 Frequency response of the power system with and without DR under the perturbation in 5.1. It can be clearly seen that using DR has helped the generators to regulate frequency more conveniently

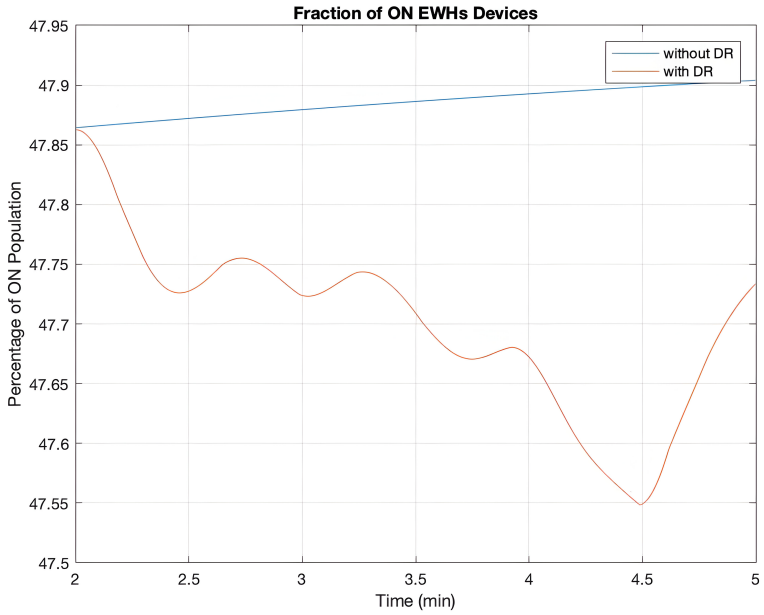


Figure 5.22 Dynamic behavior of the fraction of ON-State EWHs under sinusoidal perturbations. The fraction of ON devices is observed to be influenced by the sign and magnitude of the perturbation but the absolute magnitude of the fraction oscillations remains small.

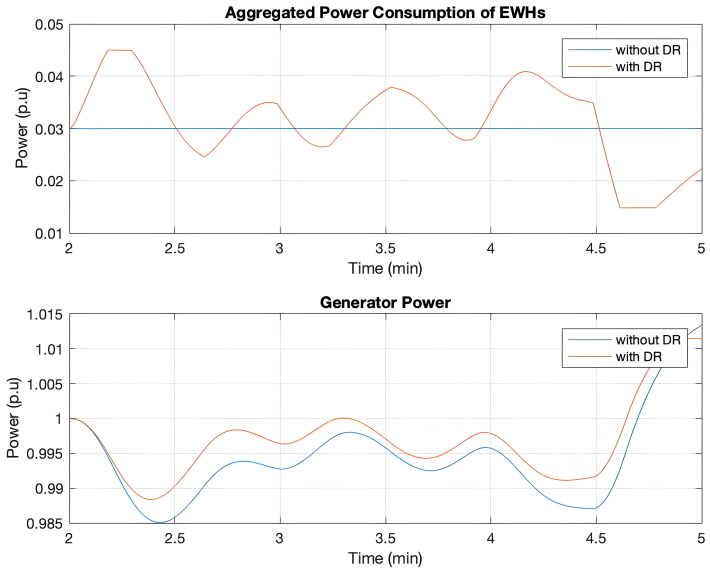


Figure 5.23 A figure illustrating the efficiency of DR, showcasing how it reduces pressure by adjusting the total power consumption of the devices. Upper: Power consumption of aggregated EWHs under oscillatory perturbations. Lower: Total power generated by synchronous units under the same conditions.

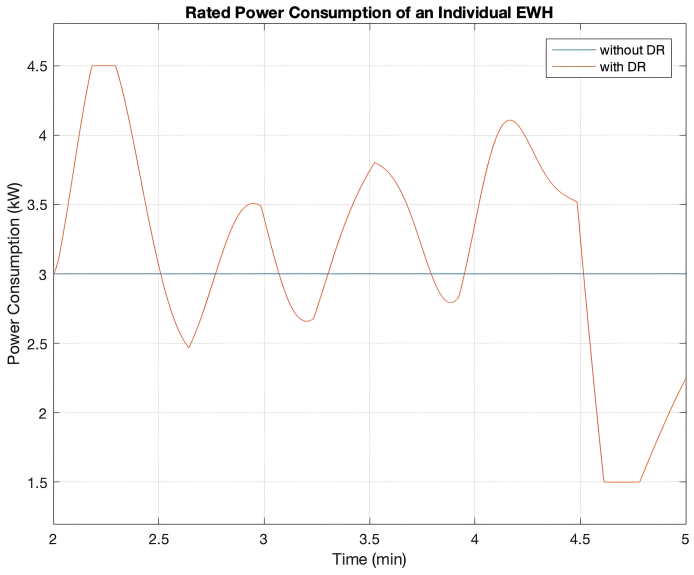


Figure 5.24 A figure showcasing the power consumption of each individual EWH, both with and without DR. The illustration reveals that the implementation of DR affects the droop mechanism within each device, thereby adjusting consumption rates to aid in system frequency regulation.

## 5.4 Time-Dependent Analysis for Hot Water Extraction Rate

It is important to note that the range of power changes that can be achieved at any one time with a group of EWHs acting as a DR tool is a direct function of the number of devices in the group which are in the ON state. The latter will be directly impacted by hot water extraction statistics which vary according to the time of the day. More water extraction is correlated with a higher fraction of ON devices. On the other hand, more water demand means higher rates of power consumption are needed to maintain acceptable water temperatures. This affects the permissible lower power bound in the droop controller during such periods and thus may create limits on the permissible ranges of power fluctuations for DR purposes. Thus, the equation is a complex one. In this context, conducting tests at various times throughout the day becomes essential, given as discussed, the strong dependency of system performance on the temporal statistics of hot water extraction rates.

Understanding the fluctuations in hot water demand across different periods is crucial for implementing effective strategies. Our exploration will look into the temporal dynamics of hot water extraction, shedding light on how performance metrics may vary throughout the day. Furthermore, the choice of droop power thresholds, a critical parameter in system control, could be chosen in relation to these temporal statistics. Finally, it may turn out that some amount of control beyond purely reactive droop control may be useful in putting the devices in the most useful initial conditions given for example an anticipated upcoming period of elevated water demand.

During the ensuing simulation, the energy extraction rate $A$ has been configured at $0.32\frac{^{\circ}C}{min}$, aligning with the time of day characterized by an average demand for hot water, as indicated in Figure 4.4.

As is demonstrated in Fig 5.25 , given the lower demand for hot water, there are fewer devices in the ON state compared to the simulation where $A = 0.81$, as the fraction of ON devices has dropped from 47.8% with $A = 0.81$ to 14.8% with $A = 0.32$. As mentioned earlier, this aspect is crucial, as the total power range available for DR is highly dependent on the number of ON devices. The total aggregated power consumption by EWHs has significantly decreased to approximately 0.01 p.u. This reduction can be attributed to the diminished contribution of devices in DR which is a result of mentioned decrease in hot water demand, as evidenced by Fig 5.26.

To investigate the correlation between the number of ON devices and the system's capability to regulate frequency, two distinct types of perturbations have been applied. The first involves a continuous sudden generation decrease with an amplitude of $0.015\,p.u.$ The second one

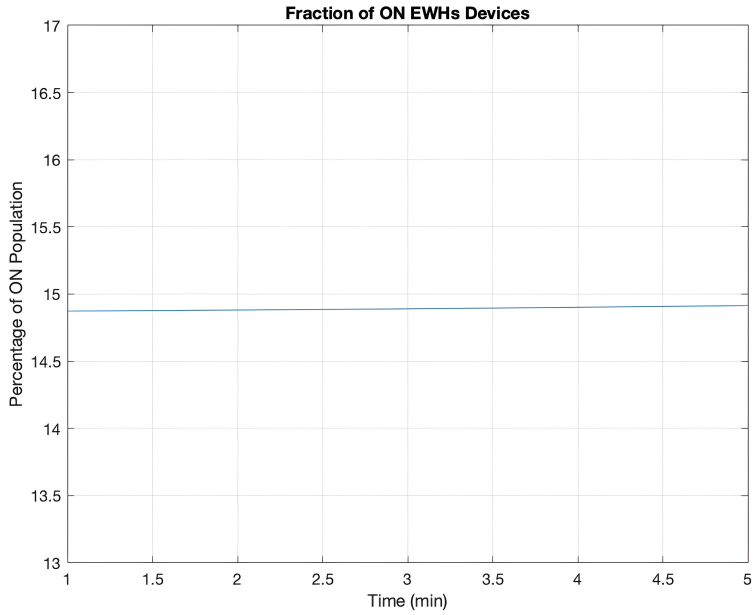


Figure 5.25 Fraction of ON devices with the rate of energy extraction is $A = 0.32\frac{^{\circ}C}{min}$. Low hot water demand leads to smaller number of devices contributing to frequency regulation.

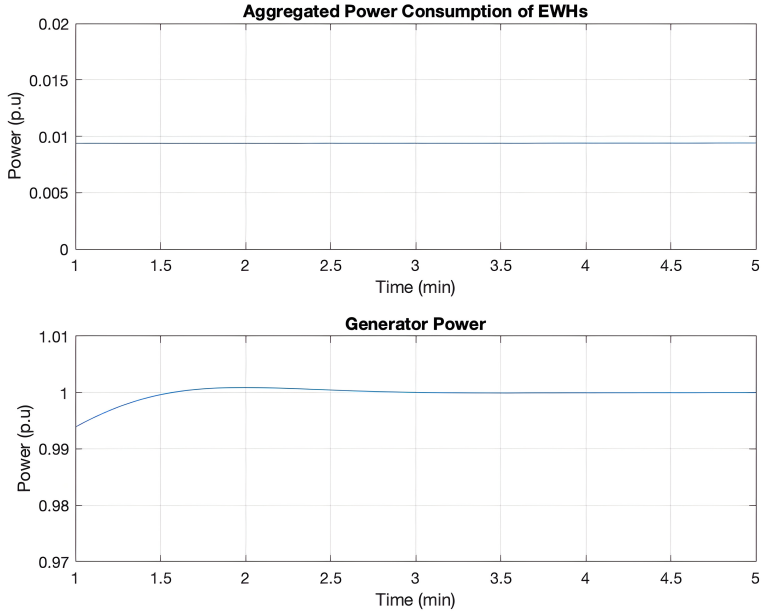


Figure 5.26 EWHs consume less power when hot water demand decreases from $A = 0.81\frac{^{\circ}C}{min}$ to $A = 0.32\frac{^{\circ}C}{min}$, which leads to less power available in DR. Upper figure: Power Consumption of EWHs. Lower figure: Power Generated in Generation Units.

corresponds to the synthetic real-system like perturbation depicted in Figure 5.7.

### 5.4.1 Sudden Loss of Generation

In this scenario, we assumed a sudden loss of generation, possibly resulting from a malfunction in a generator.

In Fig. 5.27, it can be observed that in the simulation with $A = 0.32$, while EWHs continue to assist PFR in achieving improved frequency response, their impact is limited due to a reduced population available for adjusting their consumption, as illustrated in Fig. 5.28. This contrasts with the significant effect they demonstrate in the simulation with $A = 0.81$.

This is further evident in Fig. 5.29, where the total change in power consumption of EWHs through their droop scheme is almost 0.005 p.u, significantly less than the power reduction observed in the same figure with $A = 0.81$, which is 0.015 p.u.

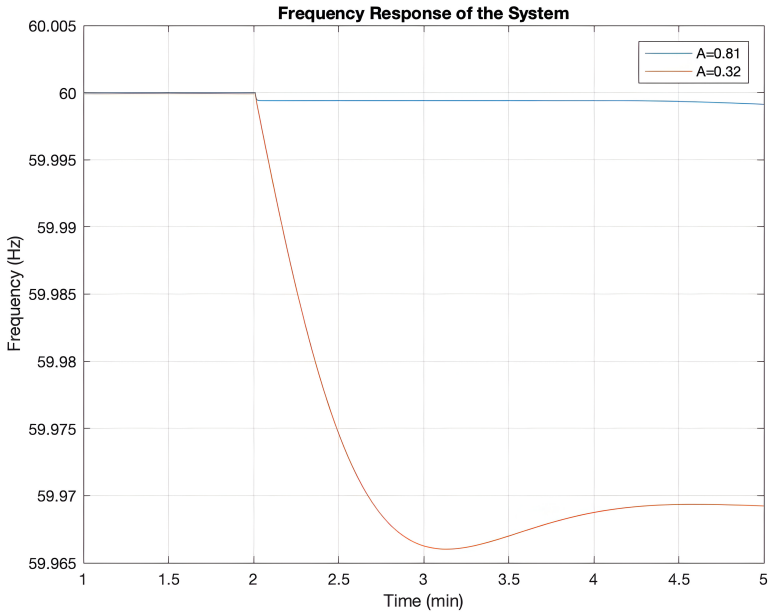


Figure 5.27 A comparison of the system's response to a 0.015 p.u perturbation with the utilization of both EWHs as DR and PFR, when the rate of energy extraction is $A = 0.81\frac{^{\circ}C}{min}$ and $A = 0.32\frac{^{\circ}C}{min}$.

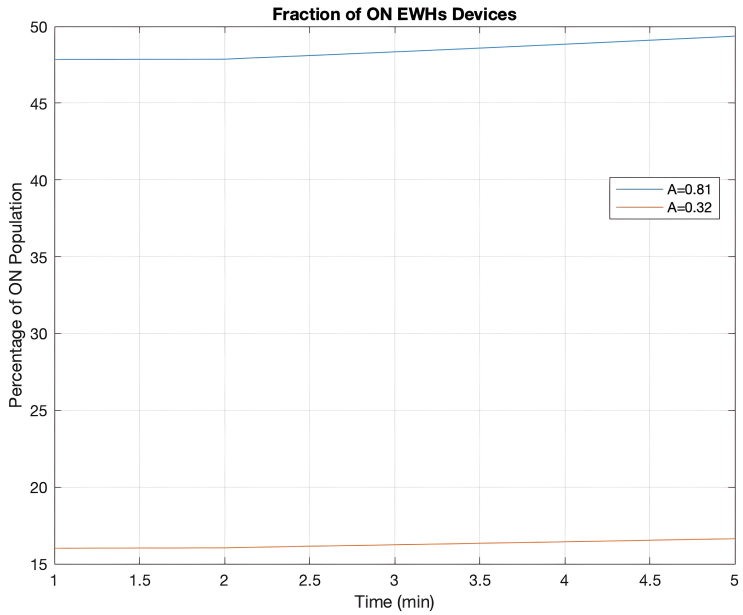


Figure 5.28 A comparison of the system's ON devices behaviour to a 0.015 p.u perturbation with the utilization of both EWHs as DR and PFR, when the rates of energy extraction are respectively $A = 0.81\frac{^{\circ}C}{min}$ and $A = 0.32\frac{^{\circ}C}{min}$.

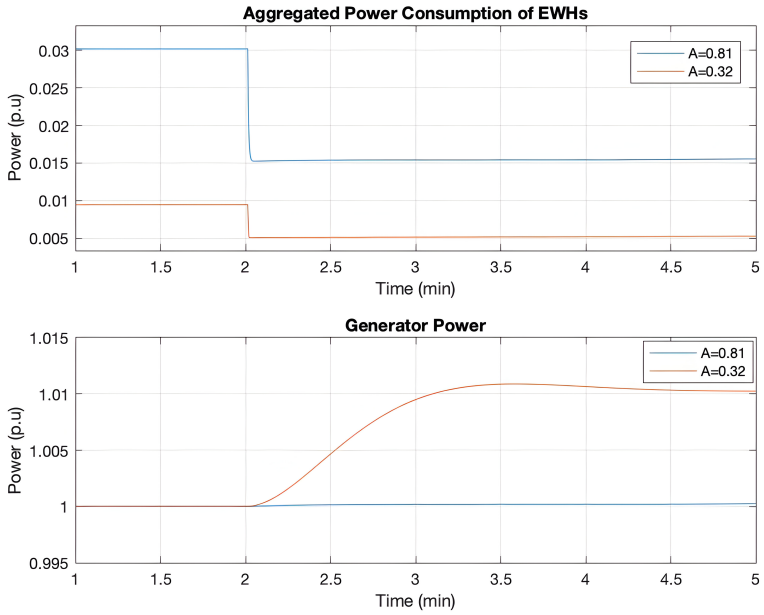


Figure 5.29 Lower demand in hot water consumption could lead to less power availability in EWHs to use as DR. Upper figure: Power Consumption of EWHs. Lower figure: Power Generated in Generation Units.

### 5.4.2 Synthetic Real-time Like Perturbation Data

In this scenario, the real-time mimic perturbation, as constructed in the previous section, has been applied to the system to observe the effect of hot water demand on DR ability in regulating the frequency.

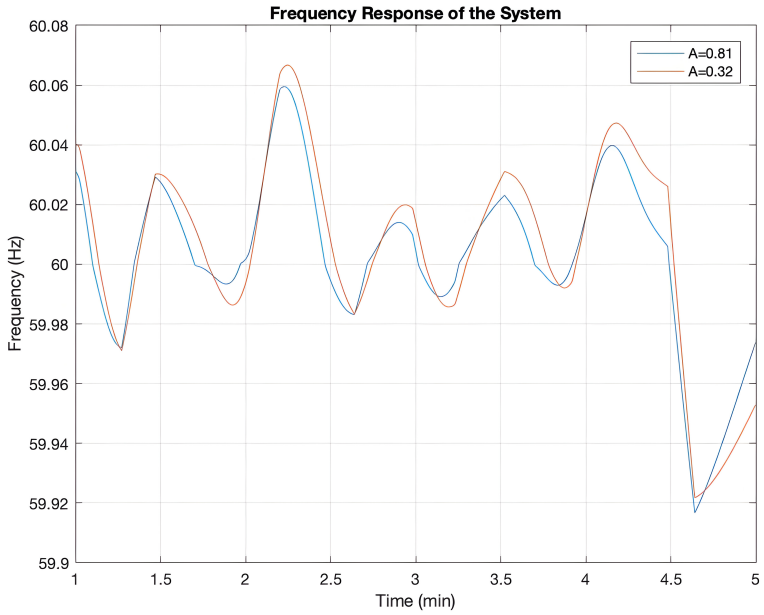


Figure 5.30 A comparison of the system's response to a real-time perturbation with the utilization of both EWHs as DR and PFR, when the rate of energy extraction is $A = 0.81\frac{^{\circ}C}{min}$ and $A = 0.32\frac{^{\circ}C}{min}$.

Once again, in Fig. 5.30, it can be observed that while the use of DR when $A = 0.32$, continues to assist the generators in regulating the frequency, its effectiveness is not as significant as it is in the scenario with more ON devices available ($A = 0.81$), as shown in Fig. 5.21. The blue frequency response of the system shows smoother rises and drops than the orange frequency response. This phenomenon is a result of the increased power storage available to EWHs, enabling them to better align with demand, as clearly depicted in Fig 5.32.

These simulations underline the importance of the number of EWHs in ON state present at any given time. For frequency regulation to be effective, the number of ON devices must be adjusted as it plays a key role in providing sufficient power. Furthermore, the simulations highlight the substantial correlation between the time of day (hot water usage) and the aggregated power available from EWHs. This being said, we note that even when the number ON devices is low, DR can remain satisfactory for oscillatory load or generation perturbations.

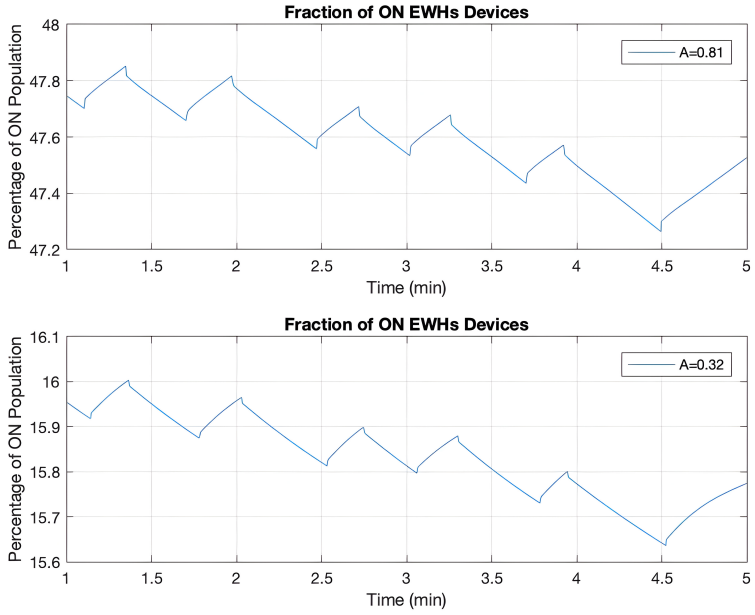


Figure 5.31 A comparison of the system's ON devices behaviour to a real-time perturbation with the utilization of both EWHs as DR and PFR, when the rate of energy extraction is $A = 0.81\frac{^{\circ}C}{min}$ and $A = 0.32\frac{^{\circ}C}{min}$.

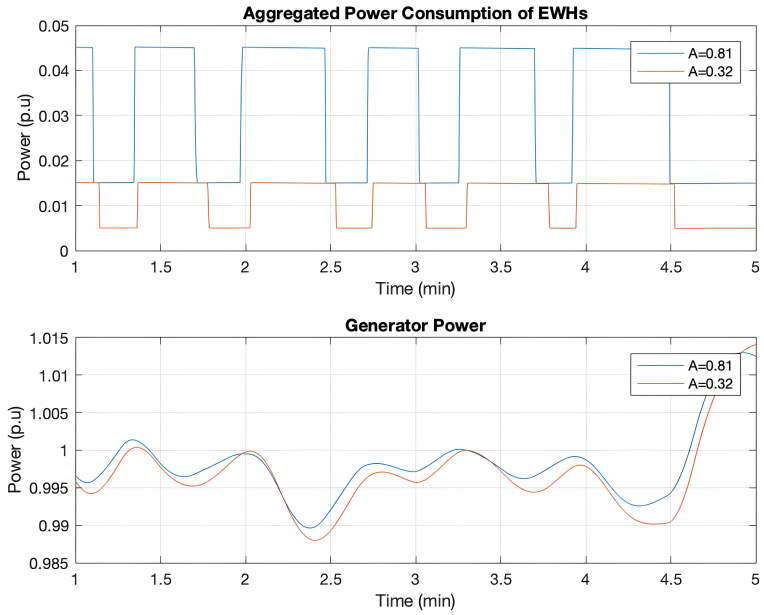


Figure 5.32 Lower demand in hot water consumption could lead to less power availability in EWHs to use as DR. Upper figure: Power Consumption of EWHs. Lower figure: Power Generated in Generation Units.

## 5.5 Exploring Extended Heating Modes and Temperature Thresholds

Ensuring a balance between electricity generation and consumption is a critical aspect of power systems. However, this equilibrium can be disrupted by various factors. A notable example is the "cold load peak," a phenomenon within the energy sector that primarily manifests in electricity demand patterns.

The term "cold load peak" refers to a significant surge in electricity demand during periods characterized by low ambient temperatures, typically occurring in cold weather conditions.

In scenarios where the power grid experiences a significant sustained imbalance between production and demand, EWHs may face challenges in restoring the equilibrium between generation and load needed to bring frequency back to nominal. To address this, a potential solution involves temporarily adjusting the temperature set point of the devices. This modification is particularly advantageous when EWHs are utilized in a load reduction mode. The purpose of this study is to investigate the effects of allowing the EWHs' temperatures to fall all the way to a lower temperature setpoint when the thermostat is ON. When they reach this new lower temperature setpoint, $T_{sp}$, the heating elements are operated at maximum capacity in a new density layer for the aggregate PDE model. This additional ON density layer, designated as $m = 2$, with distinct heating rules is illustrated in Fig 5.33. While the implementation of load-following applications is recognized as a potential application using EWHs, the primary focus here is on efficiently including the above modification within the existing droop control operating mode.

### 5.5.1 Partial Differential Equations with Respect to the New Layer

The probability density functions for the new ON probability density layer, can be written with respect to the hybrid-state Markov process in a manner similar to the formulations for the other two density layers as discussed earlier in section 4.2:

$$f'_{1j}(\lambda, t)d\lambda = P[\lambda \leq T(t) \leq \lambda + d\lambda, m(t) = 1, q(t) = j] \tag{5.1}$$
$$j = 0, 1$$

For the new ON probability density layer $m = 2$, the partial differential equations governing load dynamics could be derived similarly to those governing the other two layers as shown in equations (4.9) through (4.12) but with some adjustments.

$$\frac{\partial f'_{11}(\lambda,t)}{\partial t} = \frac{\partial}{\partial \lambda}[r'_{11}(\lambda,t)f'_{11}(\lambda,t)] - \alpha_1 f'_{11}(\lambda,t) + \alpha_0 f'_{10}(\lambda,t) \tag{5.2}$$

$$\frac{\partial f'_{10}(\lambda,t)}{\partial t} = \frac{\partial}{\partial \lambda}[r'_{10}(\lambda,t)f'_{10}(\lambda,t)] + \alpha_1 f'_{11}(\lambda,t) - \alpha_0 f'_{10}(\lambda,t) \tag{5.3}$$

Where:

$$r'_{11}(\lambda,t) \triangleq a(\lambda - T_a) - R + A(t) \tag{5.4}$$

$$r'_{10}(\lambda,t) \triangleq a(\lambda - T_a) - R \tag{5.5}$$

It should be noted, since devices in the first ON state layer with $m = 1$ are allowed to reduce their power consumption, thereby lowering their temperature to reach a new setpoint, this induces the density fluxes for $f_{11}$ and $f_{10}$ to move from right to left. In contrast, the density fluxes for $f'_{11}$ and $f'_{10}$ move from left to right. This directional inconsistency arises as devices in the second ON density layer, $m = 2$, operate at full power, aiming to restore the water tank's temperature to a safe level, ultimately bringing it back to $T_-$. The density fluxes that pass from this point enter density layer $m = 1$ after passing through $T_-$.

Additionally, the following boundary conditions must hold for all t, generally similar to those in section 4.2:

Conditions at infinity:

$$f'_{11}(-\infty,t) = f'_{10}(-\infty,t) = 0 \tag{5.6}$$

Probability conservation:
at $T_{sp}$, for j = 0,1:

$$r'_{1j}(T_{sp},t)f'^{b}_{1j}(T_{sp},t) + r_{1j}(T_{sp},t)f^{a}_{1j}(T_{sp},t) = 0 \tag{5.7}$$

at $T_-$, for j = 0,1:

$$-r_{1j}(T_-,t)f^{b}_{1j}(T_-,t) + r_{1j}(T_-,t)f^{c}_{1,j}(T_-,t) + r_{0j}(T_-,t)f^{c}_{0j}(T_-,t) - r'_{1j}(T_-,t)f'^{c}_{1j}(T_-,t) = 0 \tag{5.8}$$

Also other absorbing boundaries are added to the ones before in (4.20) and (4.21):
at $T_{-}$, for j = 0,1:

$$0 \leq -r'_{1j}(T_{-}, t) f'_{1j}(T, t) \tag{5.9}$$

at $T_{sp}$, for j = 0,1:

$$0 \leq r'_{1j}(T_{sp}, t) f'_{1j}(T_{sp}, t) \tag{5.10}$$

And finally:

$$\begin{aligned} \bar{m}(t) &= \mathbb{E}_w[m(t)] \\ &= \int_{-\infty}^{\infty} [f_{11}(\lambda, t) + f_{10}(\lambda, t) + f'_{11}(\lambda, t) + f'_{10}(\lambda, t)]\, d\lambda \end{aligned} \tag{5.11}$$

Remark: The boundary conditions (5.9) and (5.10) also reveal an intriguing feature which was observed before in section 4.2, in which they mainly represent natural boundary conditions, inherently satisfied without explicit enforcement. However, an exception arises in the specific scenario outlined by condition (5.9). This condition becomes active when $r'_{11}(T_{-}, t)$ attains a positive value. Consequently, in accordance with equation (5.9), it follows that $f'_{11}(T_{-}, t)$ must also be zero. This requirement stems from the nature of $f'_{11}(T_{-}, t)$ as a probability density function, prohibiting it from taking negative values. The logic here mirrors that of condition (5.9), ensuring consistency in the treatment of probability density functions under varying circumstances.

An illustration for understanding the regions and the way probability density functions look like has been provided in Fig 5.33.

### 5.5.2 Utilizing New Temperature Settings

There are some important remarks we should pay attention to in utilizing this algorithm, such as how long it takes for the devices in layer $m = 1$ to reach $T_{sp}$. This has a direct relation with how the power consumption of the devices drops, as managed by the droop system in each EWH. If the power rate drops in a way that the temperature decreases rapidly, it not only fails to assist the grid in power conservation but also accelerates the transition of devices to layer $m = 2$. In $m = 2$, each device requires full power consumption to restore the water temperature.

In Fig 5.34, for instance, we used the EWHs with the same settings as described in Table 4.4

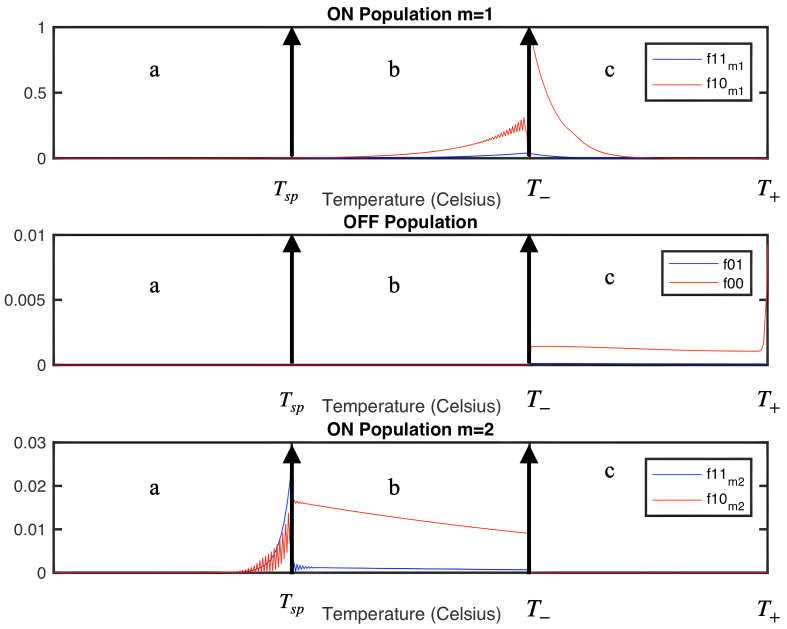


Figure 5.33 Illustration of the dynamical system (4.9) to (4.12) along with equations (5.2) to (5.4). $T_{sp}$ represents the temperature setpoint adjusted to lower the power consumption of the EWHs, aimed at conserving energy to further compensate generation deficit. Devices in $m = 1$ mode are operating with significantly lower power consumption, causing the water temperature to decrease to $T_{sp}$. Meanwhile, devices in $m = 2$ are functioning at maximum power to elevate the water temperature back to $T_-$ at which point, they switch back ti $m = 1$ mode.

but with $A = 0.32\frac{^\circ C}{min}$ to mimic the average energy extracted in an hour based on Fig 4.4 in chapter 4. Then the devices have lowered their setpoint temperature to $T_{sp} = 55^\circ C$ to analyze the EWHs' performance. During this time, the devices in layer $m = 1$ have reduced their power consumption to 10% of their normal power consumption, as was set in Algorithm 1 when the frequency is stable, $\frac{1}{10}R'$.

The total power consumed by the EWHs, denoted as $P_{EWH}$, is determined based on the total number of devices belonging to each layer, as calculated by (5.11). Initially, in steady state, the total power consumption of the EWHs was approximately 0.01 p.u. Upon implementing the new algorithm, this consumption instantly drops to 0.0015 p.u. In essence, this signifies that the EWHs are now saving 0.0085 p.u or 85% of their initial consumption, which can be redirected towards DR during periods of severe grid demand.

An important observation is that, after a 20-minute interval, it is anticipated that $P_{EWH}$ may increase as more devices transition to the ON layer $m = 2$, compelling them to operate at their

fully rated power, $R'$. However, even beyond this time frame, $P_{EWH}$ remains at 0.0023 with only a fraction of 0.05% of the devices operating at full power. This observation suggests that EWHs can effectively reduce their power consumption without causing significant discomfort to the end-users.

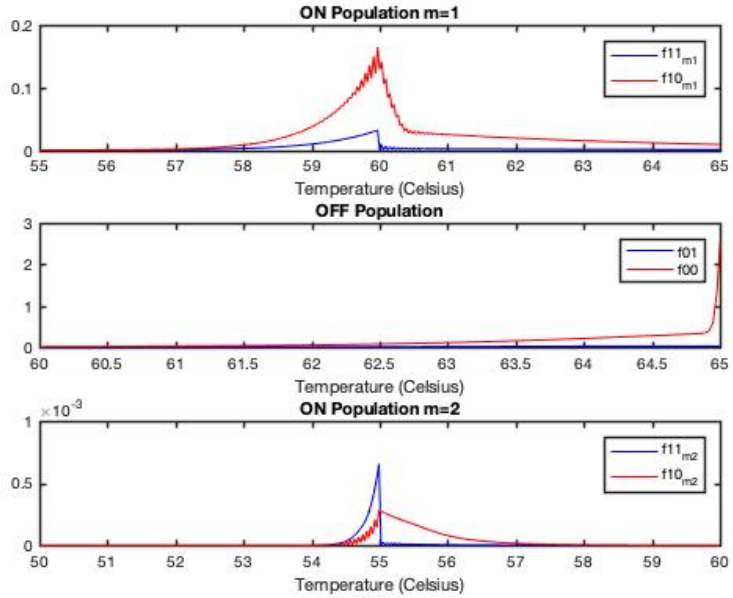


Figure 5.34 Illustration of the probability density functions updated by the Kolmogorov equations after 20 minutes of adjusting the EWHs setpoint temperature to $T_{sp} = 55°C$. The EWHs have fulfilled a shared energy demand, simulated by setting $A = 32\frac{°C}{min}$.

In another experiment, this control scheme was tested during a different time of the day characterized by a higher water demanded , aiming to observe variations in the results. This surge in demand was simulated by setting $A = 81\frac{°C}{min}$. Also $P_{EWH}$ is 0.03 p.u when the grid is at steady state. As illustrated in Fig 5.1, the increased demand led to more devices being in the ON state. Consequently, by adjusting their working rates downward, it is anticipated that $P_{EWH}$ will experience a more significant reduction.

An intriguing observation in this experiment is that despite a substantial reduction in the initial total power consumption of the devices ($P_{EWH} = 0.005$ p.u), signifying an 83% reduction in power consumption available for contribution in DR, the water temperature is dropping at a faster rate due to the heightened demand for hot water. As depicted in Fig 5.35, it is evident that there is an increased presence of devices in the ON density layer $m = 2$, which is around 30%. This has a notable impact on $P_{EWH}$ since more devices are operating at their full power rate. At $t = 20$ minutes, $P_{EWH}$ is 0.032 p.u, indicating that the devices are

consuming even more energy compared to their initial state.

It can be concluded that when the water demand is low, there is less power available to contribute to DR, but the system remains operational for a more extended period and is more reliable. Conversely, with higher water demand, there is a much higher power available for contribution initially, but this comes at the cost of a shorter time period of operation.

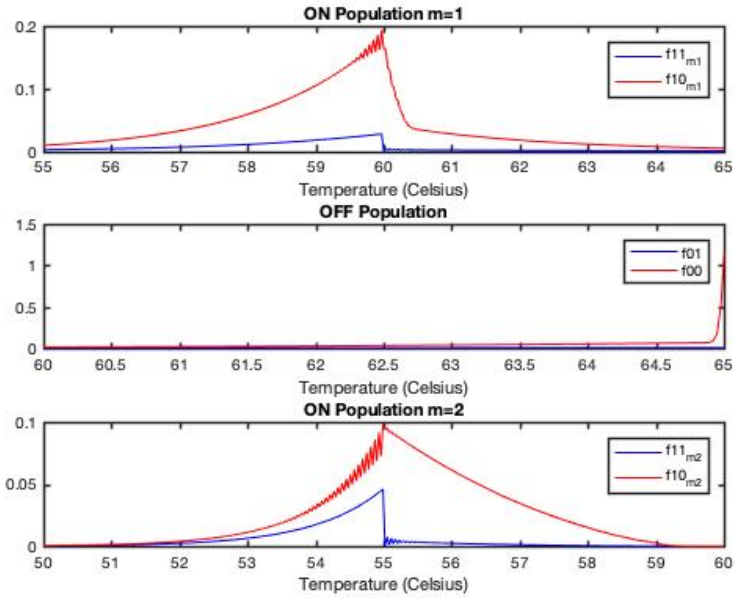


Figure 5.35 Illustration of the probability density functions updated by the Kolmogorov equations after 20 minutes of adjusting the EWHs setpoint temperature to $T_{sp} = 55°C$. The EWHs have fulfilled a shared energy demand, simulated by setting $A = 81\frac{°C}{min}$.

In order to ensure the reliability and validity of our findings, the EWHs discussed earlier have been implemented within the power system. Through the observations from these EWHs, one aims to validate the experimental outcomes, thus strengthening the credibility and trustworthiness of their efficiency. In this simulation, we introduce a +0.1 p.u. perturbation, which is three times the consumption of the EWHs under normal conditions. This perturbation has been set to mimic situations during cold load peaks, characterized by significant power surges throughout the system. During the occurrence of the perturbation, in one system, the EWHs are operated under normal temperature setpoint conditions and are not allowed to reduce their lower thermostatic dead-band. Where once they are unable to regulate the frequency deviations within ±0.1 Hz, the new setpoint change mechanism is activated, allowing the devices to decrease their lower thermostatic dead-band to $55°C$. On the other hand, we inject the same perturbation in the similar system, which in this scenario, the lower

thermostatic dead-band setpoint is not changed during the whole process.

As shown in Fig. 5.36, during the initial moment of the perturbation's occurrence, both systems exhibited similar behavior, as the frequency deviation was within ±0.1 Hz. Subsequently, after the frequency response reached 59.9 Hz, the new setpoint mechanism was activated in one of the systems. As previously analyzed, we expect the EWHs in this system to contribute more to regulation, as they have been allowed to reduce their power consumption to $\frac{R'}{10}$, which is one-tenth of the maximum power consumption of each EWH. This expectation aligns with the observed behavior.

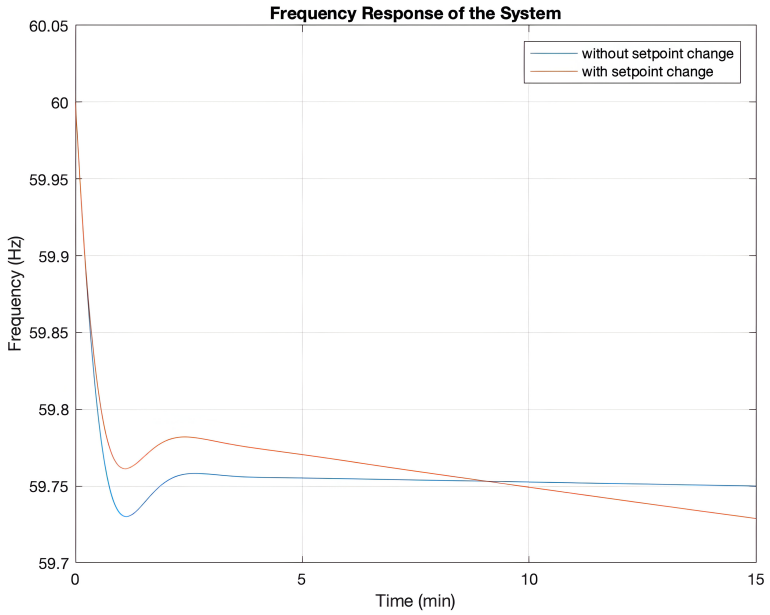


Figure 5.36 The frequency responses of two systems, one with and the other without the setpoint change control mechanism, are compared. The EWHs have satisfied a comparable energy demand, simulated by setting $A = 81\frac{^{\circ}C}{\text{min}}$. It is evident that during the initial moments of the perturbation, lowering the setpoint made the DR more effective in regulating the frequency. However, as time progresses, it gradually loses its effectiveness compared to the normal DR control mechanism.

Meanwhile, as time progresses, the water temperature of more devices reaches the new setpoint of 55°C, causing them to enter layer $m = 2$ of the ON state population, as depicted in Fig. 5.35. This results in the devices increasing their power consumption to bring back the water temperature within a comfortable range for customers. Consequently, there is a rise in the total power consumption of the EWHs, making them unable to contribute to DR. This can be observed in Fig. 5.37, where the aggregated power consumption of EWHs in both systems is initially similar until the frequency deviation exceeds the safe zone of ±0.1

Hz. Following this, the modification of the lower thermostatic dead-band setpoint resulted in significant efficiency gains. However, its effectiveness diminished over time. The initial efficiency observed gradually declined, indicating a diminishing impact of the setpoint change on system performance.

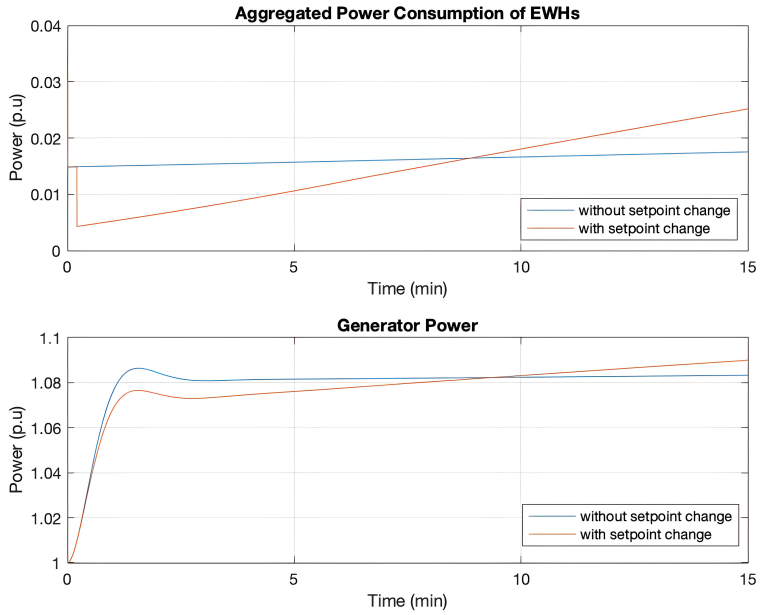


Figure 5.37 The setpoint change in lower thermostatic dead-band initially resulted in notable reduction in power consumption, but this effect gradually wears off over time. Upper figure: Power Consumption of EWHs. Lower figure: Power Generated in Generation Units.

It is interesting to note in Fig. 5.38 that the total fraction of ON devices is identical in both systems, making them challenging to distinguish. While the number of devices contributing to DR remains consistent over time, the total power consumption by EWHs differs based on their population in each ON state density layer.

And finally, in Fig. 5.39, the behavior of each individual EWHs and the droop mechanism can be observed, allowing validation of all the previously mentioned analyses.

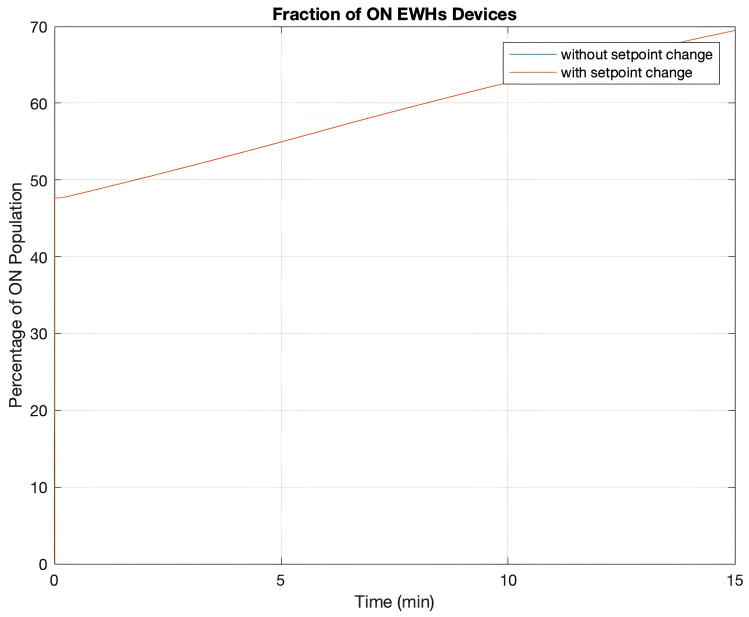


Figure 5.38 The total ON population of EWHs in two systems, one with and the other without the setpoint change control mechanism. Both systems are totally similar, making it difficult to disguise them.

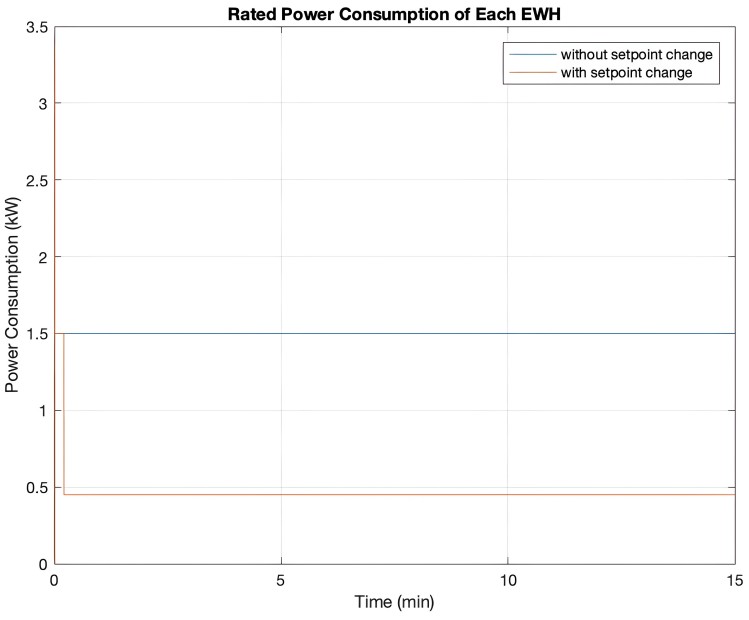


Figure 5.39 A figure showcasing the power consumption of each individual EWH, one with and the other without the setpoint change control mechanism when they are in density layer $m = 1$. A lower power consumption is indicated by the orange line for devices that benefit from the setpoint change mechanism.

# CHAPTER 6 CONCLUSION

This thesis explored the use of EWHs as a distributed DR resource for supporting frequency regulation in power systems. The research was motivated by the need for flexible, decentralized control mechanisms to manage frequency stability, especially in systems with high penetration of renewable energy sources. By focusing on the potential of EWHs to contribute to grid stability, this work builds on existing frequency control strategies and offers a novel approach to integrating residential loads into the power system's regulatory framework.

## 6.1 Summary of Research

The first phase of this research involved developing a detailed model of EWH behavior. This model accounted for the thermal dynamics of individual EWHs and the collective behavior of large populations of these devices. Using Kolmogorov partial differential equations, the model captured the stochastic variations in hot water consumption and temperature setpoints, providing a realistic depiction of how EWHs can respond to frequency deviations in real-time.

One of the key challenges addressed in this thesis was determining the appropriate droop control strategy for EWHs. Droop control, a common technique in generator frequency regulation, was adapted to the unique characteristics of EWHs. The droop constant was carefully tuned to ensure that EWHs could provide sufficient frequency support without compromising consumer comfort. This involved analyzing the relationship between temperature setpoints, power consumption, and system frequency, which was captured through extensive simulations.

### 6.1.1 Behavioral Analysis and Findings

The simulations conducted in this research demonstrated that EWHs, when controlled through droop-based demand response mechanisms, can significantly contribute to stabilizing grid frequency during disturbances. By adjusting their power consumption in response to frequency deviations, EWHs effectively mimic the behavior of conventional generation units in primary frequency control. The analysis revealed several key findings:

- EWHs can provide rapid and flexible frequency support, particularly in systems with high variability in supply and demand.

- The effectiveness of EWHs in frequency regulation depends heavily on the droop constant and the thermal inertia of the devices. A properly tuned droop constant ensures that EWHs respond proportionally to frequency deviations, maintaining system stability while preserving end-user comfort.
- Aggregated EWHs demonstrate a collective ability to mitigate frequency deviations, reducing the overall reliance on traditional generation units for frequency regulation.

In scenarios involving large frequency perturbations, such as sudden drops in generation, the integration of EWHs with droop control led to faster recovery of nominal frequency compared to systems relying solely on conventional generation. The ability of EWHs to quickly modulate their power consumption in response to frequency changes makes them a valuable resource for grid operators seeking to enhance system resilience.

## 6.2 Contributions of the Research

This thesis makes several important contributions to the field of power system stability and demand response:

### 6.2.1 Droop Control for Distributed Loads

One of the primary contributions of this research is the adaptation of droop control strategies for use with distributed loads like EWHs. Traditionally, droop control has been employed in large synchronous generators to manage frequency deviations. By extending this technique to residential loads, this work demonstrates the feasibility of using smaller, distributed devices to contribute to system-wide frequency regulation.

### 6.2.2 Modeling and Simulation of EWHs

Another significant contribution is the development of a comprehensive model for simulating the behavior of EWHs in a demand response context. The use of Kolmogorov partial differential equations allowed for a detailed representation of the thermal dynamics of EWHs, which was crucial in predicting their response to frequency deviations. This model provides a foundation for future work in this area, enabling further exploration of how different control strategies can optimize the performance of distributed energy resources.

### 6.2.3 Practical Applications and Grid Support

From a practical standpoint, this thesis offers a new perspective on the role of residential loads in supporting grid stability. The findings suggest that grid operators could leverage existing EWHs as part of a broader demand response strategy to enhance frequency control. By integrating EWHs into the control framework, utilities can improve the flexibility and reliability of power systems, particularly as the share of renewable energy sources increases.

## 6.3 Future Work and Recommendations

While this research has demonstrated the potential of EWHs in frequency regulation, there are several avenues for future exploration:

### 6.3.1 Optimization of Control Algorithms

Future work could focus on optimizing the control algorithms used to manage EWHs and other distributed loads. Machine learning and predictive control techniques could be employed to further refine the response of EWHs to grid conditions, ensuring that they provide the maximum possible support for frequency regulation while minimizing disruption to consumers.

### 6.3.2 Integration with Renewable Energy Sources

As renewable energy penetration continues to grow, the role of distributed loads in grid stability will become increasingly important. Future research should explore how EWHs and other residential loads can be integrated with renewable generation sources, such as solar and wind, to provide frequency support in systems with high levels of intermittency. This could involve developing hybrid control strategies that combine demand response with energy storage to smooth out fluctuations in supply and demand.

### 6.3.3 Field Trials and Real-World Implementation

Finally, while the simulations presented in this thesis provide valuable insights, the next step is to implement these strategies in real-world settings. Field trials involving large-scale deployment of droop-controlled EWHs could validate the findings of this research and provide additional data to refine the models and control algorithms. Collaboration between utilities, manufacturers, and regulatory bodies will be crucial in advancing this work from theory to practice.

## 6.4 Concluding Remarks

In conclusion, this thesis has demonstrated that Electric Water Heaters, when controlled through droop-based demand response mechanisms, can play a vital role in maintaining frequency stability in modern power systems. The novel application of droop control to distributed loads represents a significant advancement in the field of demand response, offering a scalable and flexible solution to the challenges posed by the increasing penetration of renewable energy. As the power system continues to evolve, the integration of distributed resources like EWHs will be essential to ensuring a reliable and resilient grid.

The findings of this research contribute to the broader goal of creating adaptive power systems capable of responding to the dynamic needs of modern electricity grids. By leveraging the inherent flexibility of residential loads, utilities can enhance system stability, reduce reliance on conventional generation, and support the transition to a more sustainable energy future.

# REFERENCES


[1] S. Kiani, K. Sheshyekani, and H. Dagdougui, "State space model of aggregated tcls for frequency regulation with a low communication requirement," in *2020 IEEE Power Energy Society General Meeting (PESGM)*, 2020, pp. 1–5.

[2] M. Wang *et al.*, "State space model of aggregated electric vehicles for frequency regulation," *IEEE Transactions on Smart Grid*, vol. 11, no. 2, pp. 981–994, 2020.

[3] A. Gholizadeh, "Simulation-based approach to impact analysis of electric water heater demand management based on consumer cost and comfort," Ph.D. dissertation, Wichita State University, 2016.

[4] K. Samarakoon, J. Ekanayake, and N. Jenkins, "Investigation of domestic load control to provide primary frequency response using smart meters," *IEEE Transactions on Smart Grid*, vol. 3, no. 1, pp. 282–292, 2012.

[5] T. Masuta and A. Yokoyama, "Supplementary load frequency control by use of a number of both electric vehicles and heat pump water heaters," *IEEE Transactions on Smart Grid*, vol. 3, no. 3, pp. 1253–1262, 2012.

[6] X. Kou *et al.*, "A comprehensive scheduling framework using sp-admm for residential demand response with weather and consumer uncertainties," *IEEE Transactions on Power Systems*, vol. PP, pp. 1–1, 12 2020.

[7] P. Kundur, *Power System Stability and Control*, 2nd ed. McGraw-Hill, 1994.

[8] J. Glover, M. Sarma, and T. Overbye, *Power System Analysis and Design*. Cengage Learning, 2011. [Online]. Available: https://books.google.ca/books?id=U77A2C37QesC

[9] authors, "P1 - policy 1: Load frequency control and performance," European Network of Transmission System Operators for Electricity, Report, 2009.

[10] Q. Shi *et al.*, "Dynamic demand control for system frequency regulation: Concept review, algorithm comparison, and future vision," *Electric Power Systems Research*, vol. 154, 1 2018. [Online]. Available: https://www.osti.gov/biblio/1549781

[11] M. Dulau and D. Bica, "Simulation of speed steam turbine control system," *Procedia Technology*, vol. 12, pp. 716–722, 2014. [Online]. Available: https://www.sciencedirect.com/science/article/pii/S2212017313007391

[12] E. Ela, M. Milligan, and B. Kirby, "Operating reserves and variable generation," *National Renewable Energy Laboratory*, 01 2011.

[13] Y. V. Makarov *et al.*, "Operational impacts of wind generation on california power systems," *IEEE Transactions on Power Systems*, vol. 24, no. 2, pp. 1039–1050, 2009.

[14] R. Diao *et al.*, "Electric water heater modeling and control strategies for demand response," *Power and Energy Society General Meeting, 2012 IEEE*, pp. 1–8, 01 2012.

[15] R. da Cunha Afonso and J. A. Peças Lopes, "Assessment of demand response impact on the frequency stability of low-inertia power systems," in *2023 IEEE Belgrade PowerTech*, 2023, pp. 1–6.

[16] H. Karbouj *et al.*, "Non-synchronous fast frequency reserves in renewable energy integrated power systems: A critical review," *International Journal of Electrical Power Energy Systems*, vol. 106, pp. 488–501, 03 2019.

[17] A. Molina-García, F. Bouffard, and D. S. Kirschen, "Decentralized demand-side contribution to primary frequency control," *IEEE Transactions on Power Systems*, vol. 26, no. 1, pp. 411–419, 2011.

[18] M. Nehrir *et al.*, "Power management of aggregate electric water heater loads by voltage control."

[19] J. Kondoh, N. Lu, and D. J. Hammerstrom, "An evaluation of the water heater load potential for providing regulation service," *IEEE Transactions on Power Systems*, vol. 26, no. 3, pp. 1309–1316, 2011.

[20] A. Sepulveda *et al.*, "A novel demand side management program using water heaters and particle swarm optimization," in *2010 IEEE Electrical Power Energy Conference*, 2010, pp. 1–5.

[21] S. Pourmousavi and M. Nehrir, "Demand response for smart microgrid: Initial results," in *ISGT 2011*, 2011, pp. 1–6.

[22] A. Haider, W. Stark, and T. K. Brekken, "Electric hot water heater primary frequency control," in *2018 IEEE Energy Conversion Congress and Exposition (ECCE)*, 2018, pp. 2670–2675.

[23] J. W. Shim *et al.*, "On droop control of energy-constrained battery energy storage systems for grid frequency regulation," *IEEE Access*, vol. 7, pp. 166 353–166 364, 2019.

[24] C.-Y. Chong and R. P. Malhami, "Statistical synthesis of physically based load models with applications to cold load pickup," *IEEE Transactions on Power Apparatus and Systems*, vol. PAS-103, no. 7, pp. 1621–1628, 1984.

[25] R. Malhame, "A markovian jump process-driven stochastic hybrid-state model, and its application for the prediction of the behavior of controlled electric water heating loads in power systems," in *1986 25th IEEE Conference on Decision and Control*, 1986, pp. 1228–1230.

[26] R. Malhamé, "A jump-driven markovian electric load model," *Advances in Applied Probability*, vol. 22, no. 3, pp. 564–586, 1990. [Online]. Available: http://www.jstor.org/stable/1427458

[27] J. Laurent and R. Malhame, "A physically-based computer model of aggregate electric water heating loads," *IEEE Transactions on Power Systems*, vol. 9, no. 3, pp. 1209–1217, 1994.

[28] G. A. Sod, "Numerical methods in fluid dynamics: Initial and initial boundary-value problems," Jan 1985.

[29] L. Pichler, A. Masud, and L. Bergman, *Numerical Solution of the Fokker–Planck Equation by Finite Difference and Finite Element Methods—A Comparative Study*, 01 2013, pp. 69–85.

[30] Z. Xu *et al.*, "Modeling of electric water heaters for demand response: A baseline pde model," *IEEE Transactions on Smart Grid*, vol. 5, no. 5, pp. 2203–2210, 2014.

[31] FNET/GridEye Consortium, University of Tennessee Knoxville, "Frequency recording of quebec interconnection during the disturbance of april 25th, 2023," 2023.

# APPENDIX A CODES

```
%% main.m

% Initializing parameters and variables
h=1;
a=0.193*10^(-4);
A=0.81;
R=0.2122;
alpha0=0.042;
alpha1=0.61;
xa=22;
xm=60;
xp=65;
T=20;
Nb=1;
xm_offset = 5; % How many degrees the EWHs are allowed to
   reduce their minimum temperature setpoint


% Defining the grids
dt=0.003;
dx=0.03;
xmin=xm-15;
xmax=xp+5;
fx=xmin:dx:xmax;
ft=0:dt:T;
tb=ft;
b = ones(1,length(ft));
ixm=1;
while (dx/2 < xm - fx(ixm))
    ixm=ixm+1;
end
ixp=1;
```

```
while (dx/2 < xp - fx(ixp))
   ixp=ixp+1;
end
ixm_offset=1;
while (dx/2 < xm-xm_offset - fx(ixm_offset))
    ixm_offset=ixm_offset+1;
end

% B matrix for numerical simulations of Kolmogorov equations
B=zeros(6,6);
B(1,1)=-alpha0;
B(1,2)=alpha1;
B(2,1)=alpha0;
B(2,2)=-alpha1;
B(3,3)=-alpha0;
B(3,4)=alpha1;
B(4,3)=alpha0;
B(4,4)=-alpha1;
B(5,5)=-alpha0;
B(5,6)=alpha1;
B(6,5)=alpha0;
B(6,6)=-alpha1;


% Kolmogorov initial parameters
MU = 63;
SIGMA = 0.5;
f00 = zeros(length(fx), length(ft));
f01 = zeros(length(fx), length(ft));
f10 = zeros(length(fx), length(ft));
f11 = zeros(length(fx), length(ft));
f00(:,1) = normpdf(fx,MU,SIGMA)';

% Generators initial parameters
df = zeros(1, length(ft));
dPg = zeros(1, length(ft));
```

```
dPm = zeros(1, length(ft));
dPl = zeros(1, length(ft));
P_EWH = zeros(1, length(ft));
dw = zeros(1, length(ft));
m = zeros(1, length(ft));
m2 = zeros(1, length(ft));
R_new = zeros(1, length(ft));

% Generators parameters
D = 1;
M = 13.1;
K = 0.05;
T_C = 0.3;
T_G = 0.2;
M = 12;
I=12;
H =5;
T_CH = 0.45/60;
T_G = 0.1/60;
T_R = 15/60;
M = 13.6/60;
FH = 0.3;

% New probability densities for the second layer m=2
f10_p = zeros(length(fx), length(ft));
f11_p = zeros(length(fx), length(ft));
f10_p(1:ixm_offset, 1) = f10(1:ixm_offset, 1);
f11_p(1:ixm_offset, 1) = f11(1:ixm_offset, 1);

%% System response
for i=1:length(ft)-1
    dPg(1, i+1) = dPg(1, i) - dt*(dPg(1, i)+df(1,i)/K)/T_G;
    dPm(1, i+1) = dPm(1, i) + dt*(dPg(1, i+1)-dPm(1, i))/T_C;

    % Ensuring the PFR is only caple of reducing or increaing
       generation
```

```
% power by 10%
if dPm(1, i+1) > 0.1
    dPm(1, i+1) = 0.1;
elseif dPm(1, i+1) < -0.1
    dPm(1, i+1) = -0.1;
end

% Setpoint mechansim is activated only when the frequecny
   has reached the threshold, here: 0.1 p.u
if abs(df(1, i)*60) > 0.1
    set_point_flag  = 1;
else
    set_point_flag = 0;
end

% The droop mechanism simulated in each EWH, get the
   frequency deviation and gives the corresponding power
   consumption for each EWH
R_new(1, i+1) = EWH_Power_Calculator(R, df(1, i), xm, xp,
   0.00001, set_point_flag);


% Fokker-Plank process using Lax_Wendroff function (Note:
   if you want to simulate the setpoint change algorithm you
    should set set_point_flag = 1, otherwise this function
   only calculate true values for ON density layer m=1 and
   the OFF density layer, the other values for the ON layer
   m=2 IS NOT VALID and!)
[f00, f01, f10, f11, f10_p, f11_p] = Lax_Wendroff(a,A,R_new
   (1, i+1),R,B,xa,ixm,ixm_offset,ixp,T,fx,ft, dt,dx, h, f11
   , f10, f01, f00, f11_p, f10_p, i, (R_new(1, i+1)-R_new(1,
    i))/dt, K, set_point_flag);

% Calculating the total fraction of ON devices in the first
    ON density layer m=1
m_1(1, i+1)= sum(f11(ixm_offset:ixp,i)+f10(ixm_offset:ixp,i
```

```
        ))*dx;

    % Calculating the total fraction of ON devices in the
       second ON density
    % layer m=2
    m_2(1, i+1)= sum(f11_p(1:ixm,i)+f10_p(1:ixm,i))*dx;

    % How much power have been consumed by the EWHs
    P_EWH(1, i+1) = 4.5/0.2122*R_new(1, i+1)*m_1(1, i+1)*0.021
       + 4.5*m_2(1, i+1)*0.021 - 0.0302; %A_81

    % Adding perturbations
    if ft(i) > 1
        dPl(1,i+1) = 0.1;
    end

    % Frequency response of the system
    df(1, i+1) = df(1, i) + dt*(dPm(1, i+1) - P_EWH(1, i+1) -
       dPl(1, i+1) - df(1, i)*D)/2/H;
end

%% Plotting the results
xlim_max = 20;

% Plot the frequency response of the system
figure
plot(ft, (df + 1) * 60)
xlabel('Time (min)')
ylabel('Frequency (Hz)')
grid on
ylim([59.9 60.1])
xlim([0 xlim_max])
title('Frequency Response of the System')

% Plot the rated power consumption of EWHs
figure
```

```
plot(ft, 4.5 * R_new(1, :) / 0.2122)
xlabel('Time (min)')
ylabel('Power Consumption (kW)')
grid on
title('Rated Power Consumption of Each EWH')
xlim([0 xlim_max])

% Plot the number of total ON EWHs devices in m=1
figure
plot(ft, (m1) * 100)
xlabel('Time (min)')
ylabel('Percentage of ON Population')
grid on
title('Fraction of ON EWHs Devices')
xlim([0 xlim_max])
ylim([13 17])

% Plot the number of total ON EWHs devices in m=2
figure
plot(ft, (m2) * 100)
xlabel('Time (min)')
ylabel('Percentage of ON Population')
grid on
title('Fraction of ON EWHs Devices')
xlim([0 xlim_max])
ylim([13 17])

% Plot the aggregated power consumption of EWHs and generator
   power
figure
subplot(2, 1, 1)
plot(ft, P_EWH + 0.03)
xlabel('Time (min)')
ylabel('Power (p.u)')
grid on
title('Aggregated Power Consumption of EWHs')
```

```
ylim([0 0.02])
xlim([0 xlim_max])
subplot(2, 1, 2)
plot(ft, dPm + 1)
title('Generator Power')
xlabel('Time (min)')
ylabel('Power (p.u)')
grid on
xlim([0 xlim_max])
% ylim([0.97 1.01])

%% Plotting the PDFs
t=i;
figure

% Subplot 1
subplot(3,1,1)
plot(fx, f11(:, t), 'b-', fx, f10(:, t), 'r-')
title('ON Population m=1')
xlabel('Temperature (Celsius)')
ylabel('')
xlim([50 65])
legend('f11_{m1}', 'f10_{m1}') % Add legend
set(gca, 'LineWidth', 1.5) % Increase line thickness
set(gca, 'FontSize', 10) % Adjust font size

% Subplot 2
subplot(3,1,2)
plot(fx, f01(:, t), 'b-', fx, f00(:,t), 'r-')
title('OFF Population')
xlabel('Temperature (Celsius)')
ylabel('')
xlim([60 64.5])
legend('f01', 'f00') % Add legend
set(gca, 'LineWidth', 1.5) % Increase line thickness
set(gca, 'FontSize', 10) % Adjust font size
```

```
% Subplot 3
subplot(3,1,3)
plot(fx, f11_p(:, t), 'b-', fx, f10_p(:, t), 'r-')
title('ON Population m=2')
xlabel('Temperature (Celsius)')
ylabel('')
xlim([50 65])
legend('f11_{m2}', 'f10_{m2}') % Add legend
set(gca, 'LineWidth', 1.5) % Increase line thickness
set(gca, 'FontSize', 10) % Adjust font size

%% Plotting a time lapse of the PDFs through time
plot_dist_space
-------------------------------------------------------------------

%% EWH_Power_Calculator.m
function P_EWH = EWH_Power_Calculator(R, dw, xm, xp, K,
   set_point_flag)
df = dw;

% Simulating the droop mechanism in each EWH
if df < -K
    P_EWH = R/3;
elseif df > K
    P_EWH = R;
else
    P_EWH = 2*R/3 + (df/K)*R/3;
end

% Checking the permission to change the setpoint, if applicable
    lower the
% power consumption
if set_point_flag == 1
    P_EWH = R/10;
else
```

```
    if P_EWH > R
        P_EWH = R;
    elseif P_EWH < R/3
        P_EWH = R/3;
    end
end
```

---

```
%% Lax_Wendroff.m
function [y1, y2, y3, y4, y5, y6] = Lax_Wendroff(a, A, R,
   R_full, B, xa, ixm, ixm_offset, ixp, T, fx, ft, dt, dx, h,
   f11, f10, f01, f00, f11_p, f10_p, t_index, dAdt, K,
   set_point_flag)
    % Initialize the time index
    i = t_index;

    % Iterate over the temperature domain
    for j = 2:(length(fx)) - 1
        % Calculate the A matrix (matrix of water cooling rates
           ) at current, previous, and next spatial points
        Ai = A_2cycle(fx(j), ft(i), a, A, xa, R, R_full);
        Ai_1 = A_2cycle(fx(j - 1), ft(i), a, A, xa, R, R_full);
        Ai1 = A_2cycle(fx(j + 1), ft(i), a, A, xa, R, R_full);

        % Construct the probability vectors at current, next,
           and previous spatial points
        f0 = [f00(j, i); f01(j, i); f10(j, i); f11(j, i); f10_p
           (j, i); f11_p(j, i)];
        f1 = [f00(j + 1, i); f01(j + 1, i); f10(j + 1, i); f11(
           j + 1, i); f10_p(j + 1, i); f11_p(j + 1, i)];
        f_1 = [f00(j - 1, i); f01(j - 1, i); f10(j - 1, i); f11
           (j - 1, i); f10_p(j - 1, i); f11_p(j - 1, i)];

        % Compute the first derivative using central difference
        D0 = (f1 - f_1) / (2 * dx);
```

```
% Compute the backward and forward differences
Dm0 = (f0 - f_1) / dx;
Dm1 = (f1 - f0) / dx;
% Compute the second derivative
Dp = (Dm1 - Dm0) / dx;

% Advection term
dAdx = a;

% Compute the next state using the Lax-Wendroff scheme
f = f0 + dt * Ai * D0 + dt * dAdx * f0 + h * 0.5 * (dt
   ^2) * ((Ai^2) * Dp + B * (B + 2 * dAdx) * f0 + ...
     (Ai * B + B * Ai) * D0 + 3 * Ai * dAdx * D0 + dAdt
        * D0 + (dAdx)^2 * D0) + dt * B * f0;

% Ensure non-negative values
f00(j, i + 1) = max(f(1), 0);
f01(j, i + 1) = max(f(2), 0);
f10(j, i + 1) = max(f(3), 0);
f11(j, i + 1) = max(f(4), 0);
f10_p(j, i + 1) = max(f(5), 0);
f11_p(j, i + 1) = max(f(6), 0);

% Update values based on the sign of Ai and probability
% conservation
if Ai(4, 4) <= 0
    if j == ixm
        f10(j, i + 1) = f10(j, i + 1) + Ai_1(1, 1) *
           f00(j - 1, i);
        f11(j, i + 1) = f11(j, i + 1) + Ai_1(2, 2) *
           f01(j - 1, i);
    end
    if j == ixp + 1
        f00(j - 1, i + 1) = f00(j - 1, i + 1) - Ai1(3,
           3) * f10(j, i);
        f01(j - 1, i + 1) = f01(j - 1, i + 1) - Ai1(4,
```

```
                4) * f11(j, i);
        end
    else
        if j == ixm
            f10(j, i + 1) = f10(j, i + 1) + Ai_1(1, 1) *
               f00(j - 1, i) - Ai1(5, 5) * f10_p(j + 1, i) *
                set_point_flag;
            f11(j - 1, i + 1) = f11(j - 1, i + 1) + Ai_1(2,
                2) * f01(j - 1, i) + Ai1(6, 6) * f11_p(j +
               1, i) * set_point_flag;
        end
        if j == ixm_offset
            f10_p(j, i + 1) = f10_p(j, i + 1) - Ai_1(3, 3)
               * f10(j - 1, i) * set_point_flag;
            f11_p(j, i + 1) = f11_p(j, i + 1) + Ai_1(4, 4)
               * f11(j - 1, i) * set_point_flag;
        end
        if j == ixp + 1
            f00(j - 1, i + 1) = f00(j - 1, i + 1) - Ai1(3,
               3) * f10(j, i);
        end
    end

    % Apply boundary conditions
    f10(1, i + 1) = 0;
    f11(1, i + 1) = 0;
    f10(2, i + 1) = 0;
    f11(2, i + 1) = 0;
end

% Enforce boundary conditions at the edges
f00(1, i + 1) = f00(2, i + 1);
f01(1, i + 1) = f01(2, i + 1);
f10(1, i + 1) = f10(2, i + 1);
f11(1, i + 1) = f11(2, i + 1);
f00(2, i + 1) = f00(2, i + 1);
```

```
f01(2, i + 1) = f01(2, i + 1);
f10(2, i + 1) = f10(2, i + 1);
f11(2, i + 1) = f11(2, i + 1);

f00(length(fx), i + 1) = 0;
f01(length(fx), i + 1) = 0;
f10(length(fx), i + 1) = 0;
f11(length(fx), i + 1) = 0;
f10_p(length(fx), i + 1) = 0;
f11_p(length(fx), i + 1) = 0;
f00(length(fx) - 1, i + 1) = 0;
f01(length(fx) - 1, i + 1) = 0;
f10(length(fx) - 1, i + 1) = 0;
f11(length(fx) - 1, i + 1) = 0;
f10_p(length(fx) - 1, i + 1) = 0;
f11_p(length(fx) - 1, i + 1) = 0;

% Normalize the sums to ensure conservation
somme = (sum(f10_p(1:ixm, i + 1)) + sum(f11_p(1:ixm, i + 1)
   ) + sum(f00(ixm:ixp, i + 1)) + ...
     sum(f01(ixm:ixp, i + 1)) + sum(f10(ixm_offset:ixp, i +
        1)) + sum(f11(ixm_offset:ixp, i + 1))) * dx;

% Normalize each state variable by the total sum
f00(:, i + 1) = f00(:, i + 1) / somme;
f01(:, i + 1) = f01(:, i + 1) / somme;
f10(:, i + 1) = f10(:, i + 1) / somme;
f11(:, i + 1) = f11(:, i + 1) / somme;
f10_p(:, i + 1) = f10_p(:, i + 1) / somme;
f11_p(:, i + 1) = f11_p(:, i + 1) / somme;

% Outputs
y1 = f00;
y2 = f01;
y3 = f10;
y4 = f11;
```

```
    y5 = f10_p;
    y6 = f11_p;
-----------------------------------------------------------------


%% A_2cycle.m
function y = A_2cycle(x, t, a, A, xa, R_control, R_full)
    % Calculate the state variables based on the inputs and
       parameters

    % Calculate r10, the difference between a*(x-xa) and
       R_control
    r10 = a * (x - xa) - R_control;

    % Calculate r11, which is r10 incremented by A (energy
       extraction coefficient)
    r11 = r10 + A;

    % Calculate r00, which is a*(x-xa)
    r00 = a * (x - xa);

    % Calculate r01, which is r00 incremented by A (energy
       extraction coefficient)
    r01 = r00 + A;

    % Calculate r10_p, the difference between a*(x-xa) and
       R_full
    r10_p = a * (x - xa) - R_full;

    % Calculate r11_p, which is r10_p incremented by A (energy
       extraction coefficient)
    r11_p = r10_p + A;

    % Initialize a 6x6 matrix with zeros
    y = zeros(6, 6);
```

```
    % Assign the calculated values to the diagonal elements of
       the matrix
    y(1, 1) = r00;
    y(2, 2) = r01;
    y(3, 3) = r10;
    y(4, 4) = r11;
    y(5, 5) = r10_p;
    y(6, 6) = r11_p;
end
```